



THE GEOLOGY AND GENESIS OF THE POLYMETALLIC

WAGGA TANK PROSPECT, MOUNT HOPE, N. S. W.

STEVEN J. RYAN B.Sc

Thesis submitted as partial fulfilment for
the Honours degree of Bachelor of Science.

November 1987

Department of Geology and Geophysics
The University of Adelaide

National Grid Reference: Mount Allen 8032 (1:100,000)

CONTENTS

ABSTRACT

1	INTRODUCTION	
	1.1 Location and Physiography	1
	1.2 History and Previous investigations	1
	1.3 Aims	2
	1.4 Methods of Study	2
2	GEOLOGY OF THE WAGGA TANK PROSPECT	
	2.1 Regional Geology	4
	2.2 Lithologies at the Wagga Tank Prospect	
	2.2.1 Introduction	5
	2.2.2 Conglomeratic Sandstone Sequence	5
	2.2.3 Flow Banded Rhyolite	7
	2.2.4 Amygdaloidal Rhyo-dacite	8
	2.2.5 Pyroclastics	8
	2.2.6 Volcaniclastic Sequence	10
	2.2.7 Siltstone - Slate Sequence	13
	2.2.8 Boolahbone Granite	14
3	MAJOR AND TRACE ELEMENT GEOCHEMISTRY OF THE VOLCANICS AND BOOLAHBONE GRANITE	16
4	STRUCTURE AND METAMORPHISM	
	4.1 Metamorphism	18
	4.2 Structure	19
5	MINERALIZATION	
	5.1 The Morphology of the Mineralization	21
	5.2 The Argillic Alteration Zone	22
	5.3 Petrography of the Mineralization	23
	5.3.1 Massive Type Mineralization	23
	5.3.2 Vein Type Mineralization	25
	5.4 Paragenetic Sequence	26
6	FLUID INCLUSION STUDY	
	6.1 Introduction	27
	6.2 Samples	27
	6.3 Microthermometry - Freezing	28
	6.4 Microthermometry - Homogenization	30
	6.5 The Influence of Pressure on Th	32
7	SULPHUR ISOTOPE ANALYSIS	
	7.1 Introduction	34
	7.2 Geothermometry	35
	7.3 Origin of the Sulphur	37
8	CHLORITE SOLID SOLUTION MODEL	40
9	THE CHEMISTRY OF THE MINERALIZING FLUID	41

10 GENESIS OF THE MINERALIZATION

10.1 Introduction	45
10.2 Metal / Ligand Source	45
10.3 Syngensis / Epigenesis	46
10.4 Heat Source	47
10.5 Position	49
10.6 Massive / Vein Type Sulphides	49
10.7 An Analogy	49

CONCLUSIONS

ACKNOWLEDGMENTS

BIBLIOGRAPHY

LIST OF APPENDICES

- 1 Selected thin section descriptions - host rocks
- 2 Whole rock analysis
- 3 Selected polished thin section descriptions
- mineralization
- 4 X.R.D. analysis - argillic alteration zone
- 5 Fluid inclusion analysis
- 6 Sulphur isotope analysis
- 7 Chlorite data
- 8 Electron microprobe analysis - sphalerite
- 9 Thermodynamic equations

LIST OF FIGURES

- 1 Location plan and regional geology
- 2 Reconnaissance map
- 3 1:2500 scale geological map (back pocket of thesis)
- 4 Interpretive cross-section (back pocket of thesis)
- 5 Discrimination diagrams
- 6 Mineralized zone - surface projection
- 7 Mineralized zone - cross-sections
- 8 Fluid inclusion - final melt temperatures
- 9 Fluid inclusion - first melt temperatures
- 10 Fluid inclusion - homogenization temperatures
- 11 Homogenization temperature vs salinity graph
- 12 Isochores for 5 wt% NaCl solution
- 13 Results of sulphur isotope measurements
- 14 Equilibrium isotopic fractionation factors
- 15 Contours of $\Delta = \delta^{34}\text{S H}_2\text{S} - \delta^{34}\text{S fluid}$
- 16 Log $f\text{O}_2$ - pH diagram
- 17 Log $\frac{\sum \text{SO}_4}{\sum \text{H}_2\text{S}}$ - T diagram
- 18 Mole % FeS in zoned sphalerite grains

LIST OF PLATES

- 1 Mt. Kennan rhyolite dome
- 2 Flow banded rhyolite
- 3 Tuff / rhyolite interbeds
- 4 Quartz pebble conglomerate
- 5 Polymict conglomerate
- 6 Carbonaceous turbidite

- 7 Framboidal pyrite lenses
- 8 Pyrite framboid
- 9 Graphitic siltstone - slate
- 10 Carbonaceous knotted slate
- 11 Vitric - crystal - lithic tuff
- 12 Glass shards
- 13 Amygdaloidal rhyo-dacite
- 14 Boolahbone Granite
- 15 Massive type sulphide, drill - core
- 16 Porous massive sulphide
- 17 Colloform texture
- 18 Pyrite aggregates
- 19 Cyclically zoned sphalerite
- 20 Chlorite and sericite gangue
- 21 Vein type sulphide, drill - core
- 22 Chalcopyrite replacing sphalerite
- 23 Fractured pyrite grains
- 24 Galena replacing pyrite
- 25 Cubanite exsolution in chalcopyrite
- 26 Curved cleavage traces in galena
- 27 Zoned sphalerite
- 28 Quartz primary fluid inclusions
- 29 Sphalerite secondary fluid inclusions

ABSTRACT

The Wagga Tank Prospect is located in Central Western N. S. W., 125 km south of Cobar. The prospect is hosted by the Lower Devonian Mount Hope Group, a complex succession of sedimentary, felsic volcanic and comagmatic intrusive rocks representing the oldest division of the Cobar Supergroup in the Mount Hope area.

The prospect is primarily a Pb and Zn deposit with minor Cu, Ag and significant Au. Gold values are highest within steeply dipping gossan shoots in the oxidised zone, while Pb and Zn values are highest in subvertical shoots of massive sulphide within the primary zone. Cu is concentrated as chalcocite, digenite and malachite at a zone of supergene enrichment.

The primary mineralization occurs within a zone of intense tectonic brecciation and argillic alteration at a pronounced flexure along the steeply dipping contact between the volcanoclastic sequence and siltstone - slate sequence.

The mineralization can be divided into two categories on the basis of textural relationships, ie. fine grained, crudely banded massive type sulphides and coarser grained vein type sulphides. The vein type sulphides are represented by varying proportions of pyrite, chalcopyrite, sphalerite and galena with rare inclusions of cubanite and pyrrhotite. The massive type sulphides show mineral abundances of pyrite > sphalerite > galena >> chalcopyrite.

Fluid inclusion and chlorite data indicate that the mineralizing fluid reached temperatures of about 325°C. Sulphur isotope compositions of the sulphide minerals ($\delta^{34}\text{S} = 10$ per mil) suggest that the sulphur originated from seawater SO_4^{2-} . Reduction of seawater SO_4^{2-} to H_2S was primarily by an inorganic process at elevated temperatures in a heated rock pile. Thermodynamic

calculations suggest possible $\log fO_2$ - pH constraints of about $\log fO_2 = -29.5$ to -31.7 and $pH = 3$ to 4.5 for the mineralizing fluid.

The mineralization is considered to be of epigenetic - hydrothermal origin. The hydrothermal fluid was probably derived from dewatering of the rock pile during metamorphism accompanying the major deformation. Sulphide precipitation occurred along a plane of high permeability produced by folding of adjacent beds with a contrasting competency.

The prospect bears many similarities to the principal deposits in the Cobar area. Those deposits are typically narrow steeply plunging elongate bodies occurring along sheared or brecciated contacts between cleaved turbiditic siltstones and coarser clastic beds or felsic volcanics.



1.1 LOCATION AND PHYSIOGRAPHY

The Wagga Tank Prospect is located in central - western New South Wales 125 km south of Cobar and 27 km north - west of the small township of Mount Hope at latitude $145^{\circ}42'20''$, longitude $32^{\circ}38'46''$ on the Mount Allen 1:100,000 geological sheet. The field area lies on both Coan Downs and Boolahbone stations. Access to the prospect can be gained from the Cobar to Roto road 300 metres north of Wagga Tank.

The prospect is surrounded by grass covered alluvium to the west and low hills cut by soil filled valleys containing drainage channels to the east. The hills support a dense cover of grass, clusters of native pines and sparse eucalypts. Exposure is poor and is generally confined to the ridges.

1.2 HISTORY AND PREVIOUS INVESTIGATIONS

The Wagga Tank Prospect was discovered in 1968 when property owner A. H. Loyd dislodged a fragment of gossan while cutting fire breaks.

Past exploration licence holders include Kennecott Exploration in joint venture with Newmont and Texas Gulf (1972 - 1976) which conducted a mapping and geochemistry program, a magnetic survey and put down one diamond drill hole which recorded significant but low grade Pb and Zn. Noranda (1980 - 1982) evaluated the prospect using magnetic surveys and geological mapping. Amoco Minerals (1983-) intersected anomalous Cu and Au in drill holes.

Homestake Australia Limited in a joint venture with Amoco Minerals (now the Cyprus Minerals Australia Company) have been the licence holders since 1984, and which extensive drilling has been

undertaken, defining the anomalous near surface chemistry and the morphology of the mineralization at depth.

Previous investigations relevant to the field area include those of Suppel [1982] documenting the geology and mineral occurrences, Scheibner and Barron [1982] on the volcanics and intrusions and Glen et al. [1985] summarising the geology and controls of mineralization in the Cobar Region.

1.3 AIMS OF THE STUDY

- (1) To map and interpret the geology of the area.
- (2) To investigate the mineralization using data obtained from mineralogical and petrographic studies, geochemistry, fluid inclusion measurements and sulphur isotope analyses.
- (3) To determine the controls responsible for the positioning of the mineralized body.
- (4) To use the combined data to propose a genetic model for the mineralization.

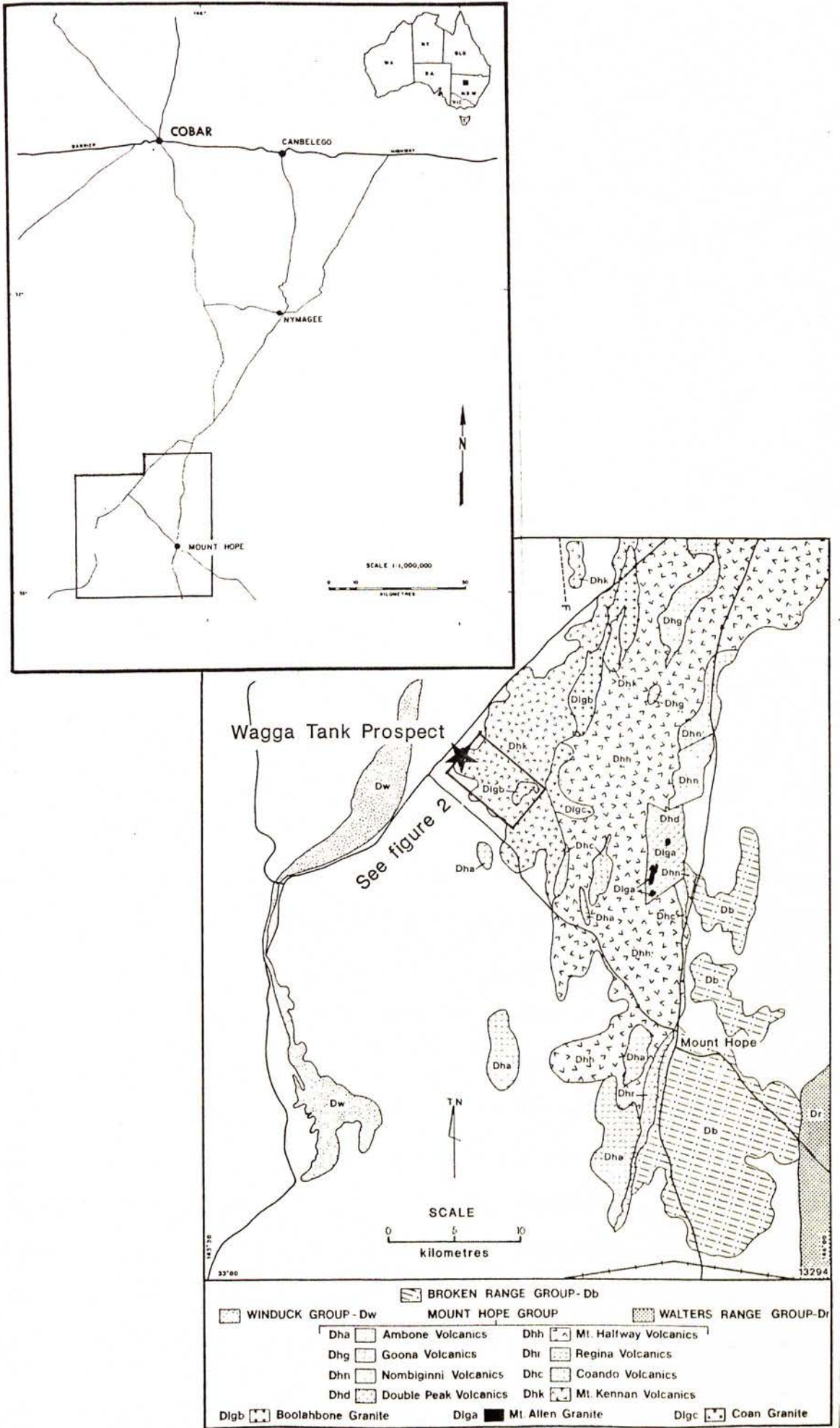
1.4 METHODS OF STUDY

- (1) Field mapping was undertaken using 1:5000 scale aerial photographs to produce a reconnaissance geological map. A grid was then surveyed over an 1700 by 1100 metre area in order to produce a detailed 1:2500 scale geological map.
- (2) Petrographic examination of approximately 120 thin and polished thin sections.
- (3) Re-appraisal of core logs and assay data.
- (4) 7 igneous rock samples were analysed for major and trace element compositions.
- (5) Electron microprobe analysis of 17 polished thin sections to determine the elemental composition of sphalerite, pyrite,

chalcopyrite and galena. The composition of chlorite was determined for the purpose of using the chlorite solid solution model of Walshe [1986] to calculate T and fO_2 of the hydrothermal fluid.

- (6) Fluid inclusion measurements using quartz and sphalerite samples taken throughout the mineralized body.
- (7) Sulphur isotope analysis of 26 samples of pyrite, sphalerite, galena and chalcopyrite.
- (8) X-ray diffraction analysis of 12 samples from the argillic alteration zone surrounding the mineralization.

FIGURE 1 LOCATION PLAN AND REGIONAL GEOLOGY - Mt. Allen Sheet



CHAPTER 2 GEOLOGY OF THE WAGGA TANK PROSPECT

2.1 REGIONAL GEOLOGY

The Wagga Tank Prospect is hosted by the Lower Devonian Mount Kennan Volcanics, tentatively accepted as the oldest formation of the Mount Hope Group [Suppel, 1982]. The Mount Kennan Volcanics are overlain by the Coando Volcanics and fault emplaced adjacent to the younger Mount Halfway Volcanics to the east. The Mt. Kennan Volcanics have been intruded by the co-magmatic Boolahbone Granite. No basement lithology has been recognized in the area.

The Mount Hope Group is a complex succession of sedimentary, felsic volcanic and co-magmatic granitic intrusive rocks deposited in the north - south trending Mount Hope Trough. It represents the oldest division of the Cobar Supergroup in the area [Glen et al., 1985]. The stratigraphic relationships within the Cobar Supergroup are poorly understood.

A tectonic model for the evolution of the Cobar Region that has aided interpretation of stratigraphic relationships is the concept of the Cobar and Mineral Hill Synclinal Zones proposed by Gilligan [1974] and refined by Pogson [1983] and Glen et al. [1985]. This concept considers the Cobar Region as a site of back-arc rifting that originated in the Ordovician and continued into the earliest Devonian by the reactivation of old basement faults and ensuing ensialic trough and basin development [Pogson, 1983]. Marine sedimentation and volcanism, representing both shallow water shelf facies or deeper water trough facies form composite structural zones consisting of two north - south trending belts that merge forty km north-east of Cobar [Gilligan, 1974]. The Cobar Supergroup has subsequently been affected by both the Tabberabberan and Kanimblan Orogenies.

Stratigraphic and structural relationships combined with

Landsat lineament studies and geophysical data indicate extensive block faulting throughout the Mount Hope Area [Schiebner and Barron, 1982].

2.2 LITHOLOGIES WITHIN THE WAGGA TANK AREA

2.2.1 Introduction

This section presents the field descriptions and petrography of the lithologies from the map area as well as the nearby Mount Kennan rhyolite dome and Boolahbone Granite. Detailed hand specimen and thin section descriptions along with sample locations are given in Appendix 1. The distribution of the Mount Kennan Volcanics is shown on the regional geology and locality map (figure 1) and on the reconnaissance geological map of the Wagga Tank area (figure 2). The 1:2500 scale field map (figure 3) and interpretive cross-section (figure 4) are included in the back pocket of the thesis. Stratigraphic correlation and structural interpretation was limited by the poor outcrop in much of the area mapped.

2.2.2 Conglomeratic sandstone sequence

The conglomeratic sandstone lithology forms the basal sequence of the Mount Kennan Volcanics [Glen et al., 1985; Scheibner and Barron, 1982]. Good exposure of the coarser horizons on top of the ridge 1km east of the prospect shows the beds to be composed of 5 belts of a dark brown and purple, poorly sorted sub rounded polymict cobble - pebble conglomerate and grit in a muddy arenite matrix. Clasts are up to 150mm in diameter and consist of massive quartz (70%), fine grained sandstone (20%) and siltstone (10%). The south dipping beds display doubly graded bedding. The five 5-10 m thick conglomerate beds, graded on a 10 cm scale, each grade

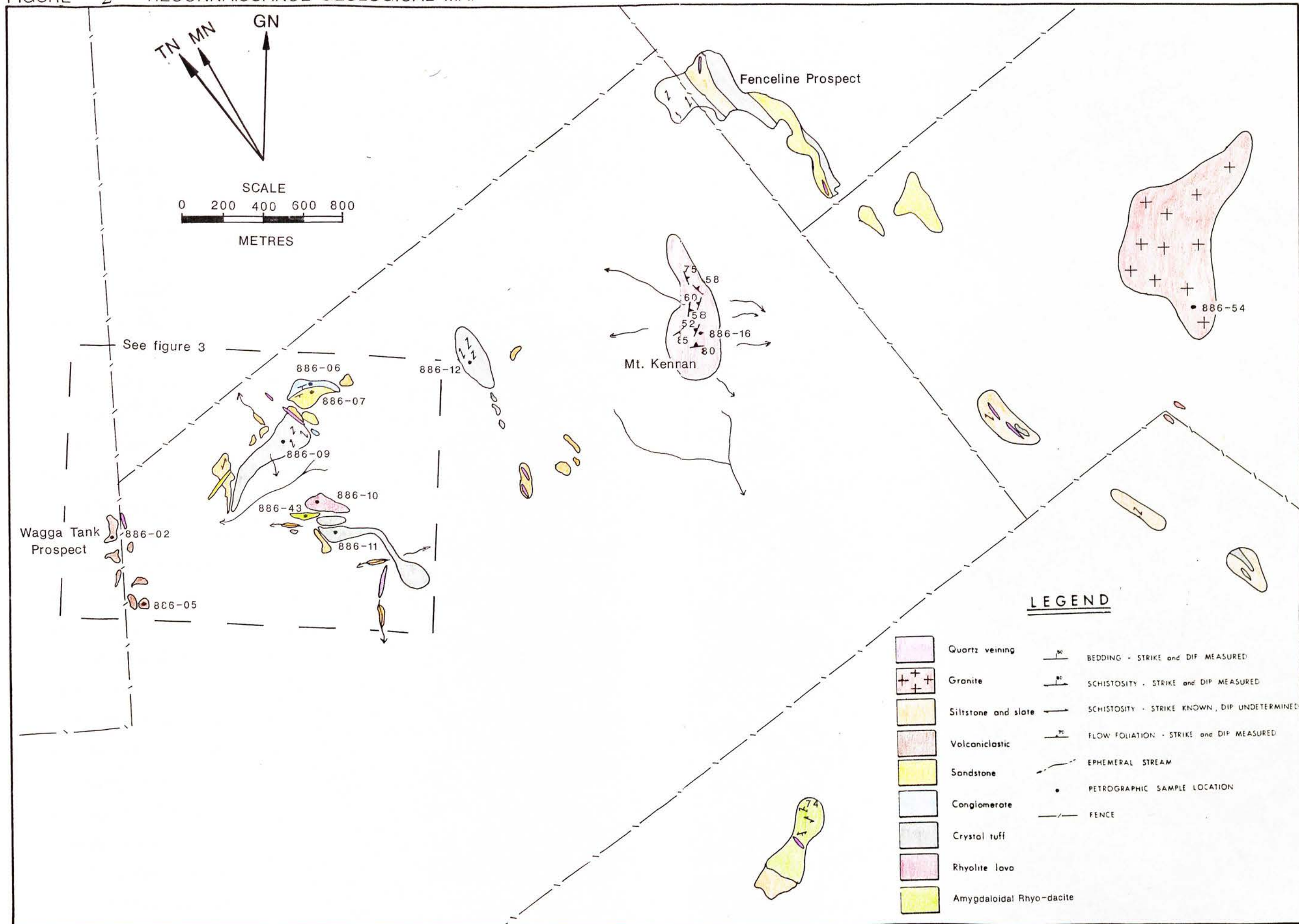
SAMPLE LOCATIONS

-Surface sample locations are depicted on the reconnaissance map (figure 2).

SAMPLE NO. / DRILL-CORE / DEPTH

886-21	HD 12	228.7 m
886-22	HD 12	230.7 m
886-25	HD 12	238.4 m
886-26	HD 12	260.0 m
886-27	HD 13	241.4 m
886-28	HD 13	237.0 m
886-32	HD 6	139.9 m
886-33	FLHD 6	(Fenceline prospect)
886-45	HD 14	224.6 m
886-46	HD 10	400.5 m
886-47	HD 12	229.1 m
886-48	HD 15	207.2 m
886-49	HD 10	401.0 m
886-62	HD 10	400.0 m
886-64	HD 14	169.5 m
886-67	HD 14	191.1 m
886-68	HD 14	217.3 m
886-69	HD 14	222.9 m
886-70	HD 14	224.8 m
886-73	HD 13	244.3 m
886-74	HD 12	228.4 m
886-76	HD 12	221.9 m
886-77	HD 10	365.9 m
886-79	HD 10	406.2 m
886-81	HD 10	400.5 m
886-82	HD 10	402.5 m
886-83	HD 10	112.3 m
886-88	HD 11	181.7 m
886-99	HD 6	238.3 m
886-101	HD 10	531.8 m

FIGURE 2 RECONNAISSANCE GEOLOGICAL MAP



into approximately 10 m of massive, clast free muddy arenite. Further up sequence the muddy arenite lithology predominates and contains minor thin grit horizons and rare solitary well rounded quartz and sandstone pebbles. This lithology then grades into siltstone and shale. The abrupt termination of the conglomeratic beds to the west can probably be attributed to fault displacement. The two belts of unbedded conglomeratic sandstone to the east are probably stratigraphically lower beds exposed on a westerly plunging syncline.

The sandstone component is composed of rounded quartz grains (0.50 - 0.75 mm), sericitized siltstone and silty fine grained sandstone fragments and minor primary mica in a sericitized matrix. Detrital opaques can form up to 20% of the sample. Zircon is a common accessory.

The quartz clasts from the coarser sandstone fraction are of two types. Large (2 mm) polycrystalline aggregates of amoeboid interlocking quartz grains form up to 10% of the sample. The remaining quartz clasts are equant, slightly strained grains (0.5 - 1 mm) exhibiting shadowy extinction and micro-fracturing. The two types of quartz clasts suggest a dual provenance with the polycrystalline aggregates originating from a metamorphic terrain. Other quartz aggregates exhibit a complex shape and grain regrowth representing incipient recrystallization.

The conglomeratic sandstone sequence represents deposition in a shallow water fluvial or alluvial fan environment. Analogous sequences are found as basal units of the Cobar Supergroup throughout the Cobar Region [Pogson and Felton, 1978]. The provenance can be traced to the metamorphosed Giralambone basement and Silurian intrusions upon which the basal conglomerates unconformably rest.

2.2.3 Flow banded rhyolite

Flow banded rhyolite outcrops at two localities on the reconnaissance geological map [figure 2]. The largest outcrop (700 x 250 m) is found at Mount Kennan trig station, the highest point in the map area.

The rhyolite is an A - type and is of nearly identical chemical composition to the nearby Boolahbone Granite, suggesting that these rocks are comagmatic [Scheibner and Barron, 1985].

Variable orientation of the flow banding around Mount Kennan was used by Braithwaite [1975] to suggest that the feature represents a rhyolite dome. The flow fabric, which is only visible on the weathered surfaces, occurs as both planar and highly convoluted banding 1 to 5 mm thick (plate 2).

A smaller (260 by 70 m) outcrop of rhyolite occurs stratigraphically below and interbedded with purple amygdaloidal lava flows of rhyo-dacitic composition. The flow banding at this locality is planar and unidirectional. A single thin bed (20 mm) of flow banded rhyolite in a coarse grained sandstone is exposed in a drainage channel.

The rhyolite is a massive dark grey, generally aphanitic rock composed of primary quartz, K-feldspar and plagioclase and secondary sericite and chlorite. K-feldspar (20%) and plagioclase (10%) occur in the very fine grained groundmass and as pervasively sericitized remnant phenocrysts (2 mm). Quartz displaying undulose extinction occurs as 2 mm equant phenocrysts (5%). Decussate chlorite (25%) and sericite (25%) alteration is pervasive throughout the fine K-feldspar and acicular plagioclase groundmass. Minor disseminated opaques occur throughout.

Secondary quartz, carbonate and hematite occur as fracture

filling.

2.2.4 Amygdaloidal rhyo-dacite

The highly weathered red amygdaloidal lava flow of probable rhyo-dacitic composition [Scheibner, 1987] outcrops poorly on the northern face of the ridge 900 m south - south east of the prospect. The lava flow sits conformably above the rhyolite and is interbedded with it for approximately 10 m. The interbeds, ranging from 15 cm to 2 m in thickness, form sharp contacts. The total thickness exceeds 30 m. The upper sections are interbedded with pyroclastics of the overlying lithology.

The amygdales are oblate to rod - like with axial ratios of 1:2:3 to 1:1:12 and range from 5 mm to 60 mm in length. The amygdales are composed of radially oriented, inward pointing prismatic quartz crystals that increase in size from <0.1 mm to 1 mm towards the core. The larger and less elongate amygdales are hollow and filled with an acicular hematite network produced during weathering.

The groundmass mineralogy is intensely hematized and therefore indistinguishable except for small (0.2 mm) corroded quartz grains. The amygdales are oriented at high angles, but never quite perpendicular, to bedding. This feature and the extreme elongation of the 'pipe amygdales' can be attributed to the extrusion of lava onto a wet substrate resulting in rapid devolatilization and ascending vesicles.

Between 30 to 60 percent of the rock consists of vesicles, suggesting a highly scoriaceous lava flow. Quartz infilling occurred soon after vesiculation as no deformation of the voids resulted from the accreting volcanic pile.

2.2.5 Pyroclastics

Three highly weathered and altered but petrographically

distinct lithic- and crystal - lithic - tuffs occur in the map area. These are the outcrops of aphanitic tuff on the ridge 1100 metres south - south east of the prospect, the porphyritic crystal - lithic tuff on the ridge 600 metres east of the prospect and the tuffs and tuffaceous sandstones and siltstones hosting the mineralization (described in 2.2.6).

The tuff on the southern ridge rests conformably on the amygdaloidal rhyodacite and on the flow banded rhyolite towards the east. The exposure is moderate but highly weathered. The rock is a pink aphanitic tuff displaying a north - south trending sericite defined tectonic fabric. The lithology represents a pyroclastic deposit of limited strike extent as it appears to lens out into sandstone and siltstone to both the east and west. Outcrop shape and bedding delineates a broad syncline plunging at a moderate angle to the south.

The volcanic on the east ridge is a highly weathered light purple crystal - lithic tuff. The tuff is porphyritic to the west where small (1mm) altered white phenocrysts give the pyroclastic a speckled appearance. A weak north-south sericite fabric is evident. Bedding, seen only at one locality is of variable orientation. The eastern margin of the outcrop terminates against an inferred fault while the lack of outcrop to the west prevents an appraisal of strike extent.

In both tuffs, quartz, sericite and hematite are the only minerals that can be identified. Quartz (up to 60%) occurs as 0.5 to 2 mm equant inclusion free phenocrysts displaying undulose extinction and deformation lamellae. The bipyramidal form of the quartz is evident in most sections. Minor aggregates up to 2 mm of sutured interlobate fine grained quartz occur. Pelitic fragments exhibit pervasive sericitization. Quartz existing as fine (<0.2

mm) corroded and typically polygonal grains is the only primary mineral identified in the groundmass.

The porphyritic tuff contains sericite pseudomorphs of inferred feldspar forming subhedral laths up to 2 mm found as phenoclasts interstitial to lithic fragments. Anhedral sericite pseudomorphs (10 - 30%) with diffuse boundaries and surrounded by abundant fine euhedral opaque grains represent an original mafic mineral, or altered lithic fragments.

Opaques are disseminated throughout the groundmass and include hematite pseudomorphs of cubic pyrite. Voids (<1 - 5%) up to 5 mm and pervasive hematite staining of the groundmass can probably be attributed to the weathering of disseminated sulphides.

The tuff horizon between the prospect and Mount Kennan depicted on the reconnaissance geological map is a light purple aphanitic tuff containing up to 10 percent voids after inferred sulphide. Flattened pumice fragments (fiamme), up to 10 mm long form up to 60% of the tuff. The pumice fragments are generally randomly oriented which may indicate slumping of the pyroclastic.

2.2.6 Volcaniclastic sequence

The volcaniclastic sequence is a very poorly outcropping and complex succession that partially hosts the mineralization. Extensive drilling has defined a vertical to steeply west dipping open antiformal structure facing to the west. The outcropping beds display a westward progression of silicified tuffaceous sandstone, polymict conglomerate then tuffaceous siltstone. Drill-cores reveal a more complicated sequence of interbedded tuffaceous sandstone, siltstone, polymict conglomerate, crystal - lithic tuff and crystal - lithic - vitric tuff. All lithologies display considerable lateral and vertical variation in grain and clast

size, degree of sorting and rounding, and bed thickness. The volcanoclastic sequence is intensely silicified and sericitized, contains disseminated sulphides, and exhibits zones of moderate to intense brecciation. At least two phases of quartz veining cross-cut the sequence.

The tuffaceous sandstone is a highly variable facies composed of poorly to well sorted, moderately rounded coarse grained equant quartz grains (50 - 75%) that are typically recrystallized. Sericitized clasts (5 - 10%) were probably original feldspar or lithics. Recognised phenocrasts of inclusion free, bipyramidal equant quartz and sericitized subhedral feldspar can form up to 10% of the sample. Sphene, rutile and primary muscovite are accessory. Both disseminated and vein sulphides occur throughout.

The conglomeratic facies appears as lenses stratigraphically above and interbedded with the sandstone facies. The facies is composed of a moderately sorted pebble conglomerate composed of angular to subrounded clasts (up to 40 mm) of fine grained sericitic sandstone, sericitic slate and minor tuff in a highly silicified silty matrix. The sandstone clasts contain strained quartz, sericitized siltstone fragments and rutile in a sericite matrix. Rare tuffaceous clasts contain sericitized but recognisable phenocrysts or phenocrasts of feldspar. Angular quartz clasts (1 mm) displaying bipyramidal refraction patterns indicative of low pressure crystallization represent further volcanic input. Disseminated pyrite occurs in the matrix. Quartz and sulphide veins cross-cut both clasts and matrix. Another apparently sulphide - free quartz veining event can be recognized.

The siltstone facies consists of thick to thinly bedded sericitic slate containing carbonaceous material and fine grained

tuffaceous sandstone interbeds hosting quartz and sericitized feldspar phenocrysts. This facies is complexly interbedded with the tuffaceous sandstone facies. The fine sandstone beds consists of equant bipyramidal quartz grains to 0.2mm, recrystallized aggregates (up to 2 mm) of polygonal quartz grains, granular sphene aggregates and minor sericitized and chloritized clasts, primary muscovite and subhedral pyrite grains (up to 0.1 mm). The siltstone beds consists of 0.02 mm quartz grains, rare sphene aggregates, fine disseminated cubic pyrite and trace carbonate in a sericite matrix. A single occurrence in drill-core of a knotted slate produced by the deviation of the graphitic fabric around ghost porphyroblasts of andalusite is enigmatic (plate 10).

The pyroclastic facies, defined in drill - core, consists of lithic tuff, lithic - crystal tuff and vitric - lithic - crystal tuff. Lithic fragments include subrounded clasts of crystal and vitric - crystal tuff, pumice and rhyolite up to 40 mm in size. Variable abundances of non-volcanic clasts of siltstone and fine grained sandstone are incorporated in the tuffs. Phenocrasts of quartz to 2 mm occur. Tabular and prismatic phenocrasts (1 - 2 mm) of inferred feldspar and mafic silicates have been pseudomorphed by sericite and chlorite. The formerly vitroclastic groundmass consists of fine K-feldspar or sericite, chlorite and quartz. Sericitized unwelded cusped vitric shards (0.2 - 0.5 mm) are common in the groundmass. Disseminated, aggregate and vein sulphides are ubiquitous.

Sedimentary structures in the volcanoclastic sequence are uncommon. Parallel bedding laminations are present in some slate units and rare graded bedding occurs in some of the sandstone beds.

The extent of chloritization, sericitization, silicification and siderite veining in the volcanoclastic sequence increases proximal to the mineralized body.

The volcanoclastic sequence grades conformably into the siltstone - slate sequence.

The massive nature of the sequence and the rare graded bedding and parallel laminated siltstone are compatible with the criteria indicative of the A, B and D subdivisions of the Bouma turbidite model [1962]. This would imply that the volcanoclastic sequence was deposited in a submarine basin proximal to a volcanic terrain.

2.2.7 Siltstone - slate sequence

The siltstone-slate sequence lies to the west of, and conformably above, the volcanoclastic sequence but does not outcrop. The weathered foliated siltstone and minor sandstone horizons that outcrop sporadically over much of the 1:2500 geological map (figure 3) east of the prospect may be a facies equivalent of the siltstone - slate above the volcanoclastic sequence. However, the stratigraphic relationship with the volcanics and volcanoclastic sequence is unclear.

The siltstone - slate sequence is defined in drill-core as a thinly bedded slaty siltstone containing occasional thin interbeds of fine grained silty sandstone. Alternating medium grey and dark grey beds range from 5 to 100 mm in thickness. Intensely pyritic horizons up to 3 mm thick occur parallel to bedding (plate 6). Pyrite also occurs as veins associated with quartz and as concretions. Rare clusters of pyritized crinoid and rugose coral fragments have been identified. The cleavage surface, developed to varying degrees, is highly graphitic. Minor siderite veining cross - cuts the bedding.

The dark grey beds are composed of silt fraction quartz,

sericite and abundant carbonaceous or graphitic material. Lenses (1-5 mm in length) of framboidal pyrite lie parallel to bedding and can form up to 6% of the sample. The framboids are seen under the scanning electron microscope (SEM) as spherical aggregates (0.01 - 0.04 mm) of 1 - 2 micron sized octahedral pyrite crystals.

The medium grey beds are composed almost entirely of sericite with some fine disseminated pyrite and minor quartz. Carbonaceous material is less abundant.

Minor fine sand sized quartz grains (0.2 mm), carbonate grains (0.2 mm), detrital muscovite and trace rutile are scattered through both the medium and darker grey beds. SEM study of the non-framboidal disseminated pyrite grains showed them to be of octahedral and sometimes cubic crystal form. Continuous pyritic bands greater than 0.5 mm in thickness that run parallel to the bedding are composed of octahedral crystals (0.005 - 0.01 mm) that may have been recrystallized from original framboids. Fine anhedral corroded grains of sphalerite found in sandy horizons appear to be of detrital origin.

Sedimentary structures are common and well preserved. They include small scale graded bedding, parallel bedding lamination, disrupted bedding, flame and load structures.

The sedimentary structures in the siltstone - slate sequence are compatible with the criteria indicative of the D and E subdivisions of the Bouma turbidite model [1962]. This would imply that the siltstone - slate sequence formed either as a distal turbidite deposit, or as a more proximal deposit if the fine grained detritus was derived from a low lying, erosionally mature hinterland. The euxinic submarine basin was the site of syn-sedimentary or syn-diagenetic Fe sulphide precipitation.

2.2.8 Boolahbone Granite

The Boolahbone Granite outcrops 6km south-east of the prospect, as a large tor strewn hill. A possible apophyse or subsurface extension has been found in drill core at the Fenceline Prospect 3km east of the Wagga Tank mineralization.

The granite is a dark green, coarse grained holocrystalline rock composed of quartz, K-feldspar, plagioclase, sericite and chlorite. The feldspars occur as anhedral phenocrysts of sericitized K-feldspar up to 15 mm and medium grained (2 mm) subhedral plagioclase. Sericitization is prevalent in both feldspars with remnants usually confined to the cores. Quartz occurs as equant fractured grains to 4 mm with corroded and complex boundaries. Granophyric intergrowth is ubiquitous. Extensive sericitization and chloritization attests to a metamorphic influence. Opaques are closely associated with subhedral chlorite pseudomorphs of probable biotite. Zircon sphene and rutile are accessory.

The granite from the Fenceline Prospect drill-core appears to be a slightly finer grained equivalent of the Boolahbone Granite, but with some unaltered mica remaining.

Plate 1

Mt. Kennan rhyolite dome.

Plate 2

Highly convoluted flow banding in rhyolite - Mt Kennan.

Plate 3

Crystal tuff interbedded with flow banded rhyolite - 1100 metres S. E. of the prospect.

Plate 4

Quartz pebble conglomerate displaying graded bedding (conglomeratic sandstone).

Plate 5

Polymict conglomerate from the volcanoclastic sequence. Contains clasts of siltstone and fine grained sandstone in a highly silicified siltstone matrix. The fracture running parallel to the core axis is filled with sphalerite and galena. The bar scale is 2cm. (sample no. 886-50)

Plate 6

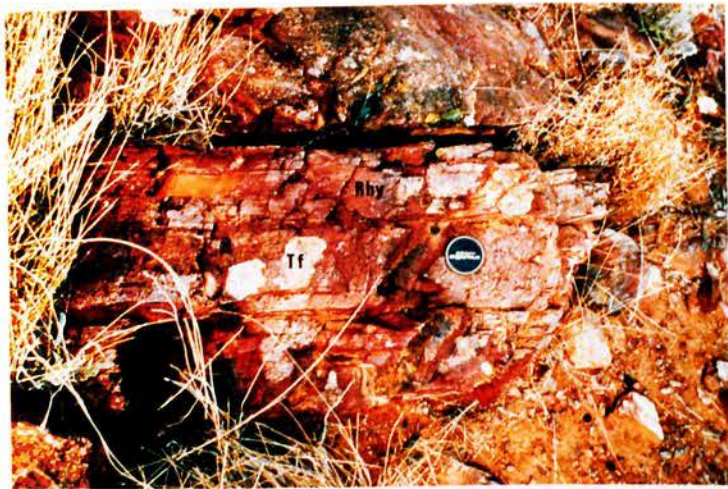
Pyritic and carbonaceous turbidite from the siltstone - slate sequence. B = Bedding parallel pyrite band 3mm thick. C = pyrite concretion. The scale is 1cm. (sample no. 886-82)



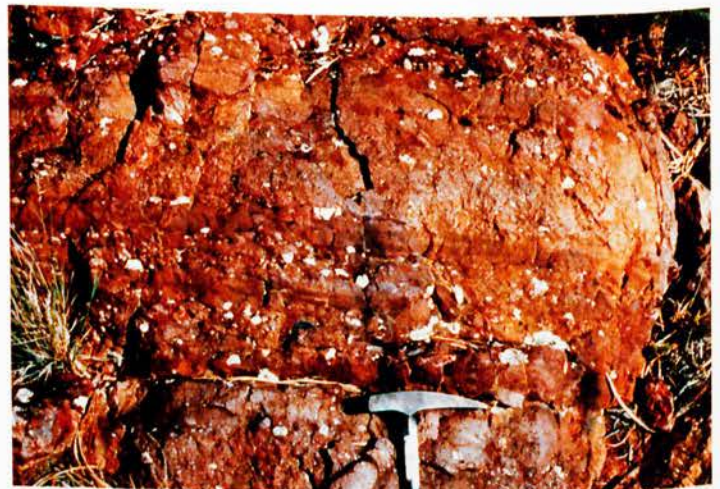
1



2



3



4



5



6

Plate 7

Lenses of framboidal pyrite hosted by the carbonaceous turbidite beds of the siltstone - slate sequence. The field of view is 1mm. (sample no. 886-32, reflected light)

Plate 8

A pyrite framboid composed of 1 - 2 micron sized octahedral pyrite, from the siltstone - slate sequence. The field of view is 0.25mm. (sample no. 886-32, reflected light)

Plate 9

Very thin beds of turbiditic siltstone and very fine grained sandstone cut by a sericite - graphite fabric at 45°. - Siltstone - slate sequence. The field of view is 2.5mm. (sample no. 886-77, transmitted light - plane polarised)

Plate 10

Carbonaceous knotted slate from the volcanoclastic sequence. The augen contain cores of clay pseudomorphs of andalusite. The field of view is 15mm. (sample no. 886-48, transmitted light - plane polarised)

Plate 11

Vitric - crystal - lithic tuff from the volcanoclastic sequence. Quartz (Q) and K-feldspar (K) phenocrysts occur in a vitroclastic sericite, quartz and K-feldspar matrix. The field of view is 2.5mm. (sample no. 886-101, transmitted light - crossed polars)

Plate 12

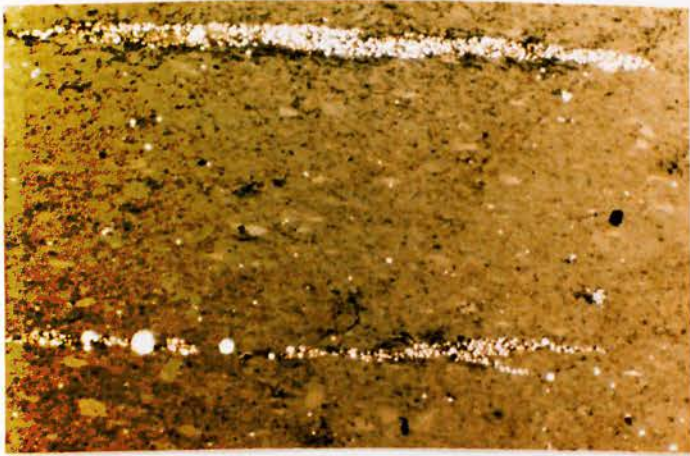
Vitric - crystal - lithic tuff from the volcanoclastic sequence showing unwelded glass shards. Note relict euhedral crystal in centre of plate. The field of view is 2.5mm. (sample no. 886-101, transmitted light - plane polarised)

Plate 13

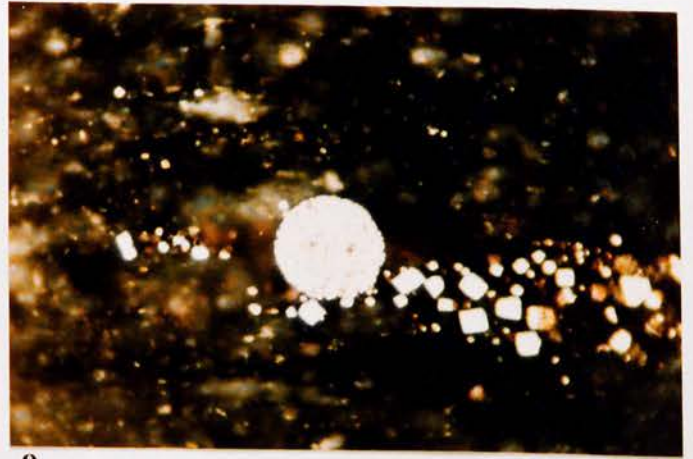
Amygdaloidal rhyo-dacite: The section is cut across the shortest axes of the quartz amygdales. Fine grained quartz is the only primary mineral remaining in the hematite stained groundmass. The field of view is 15mm. (sample no. 886-43, transmitted light - plane polarised)

Plate 14

Boolahbone Granite: Composed of corroded quartz (Q), plagioclase (P), sericitized K-feldspar phenocrysts (K), granophyre (G), chlorite and secondary carbonate (C). The field of view is 2.5mm. (sample no. 886-54, transmitted light - crossed polars)



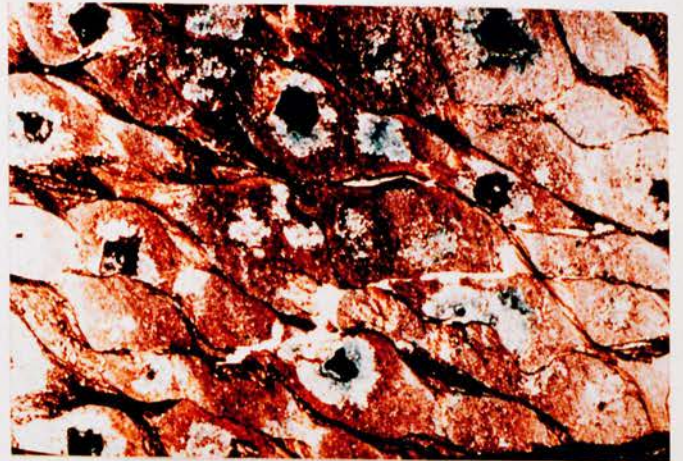
7



8



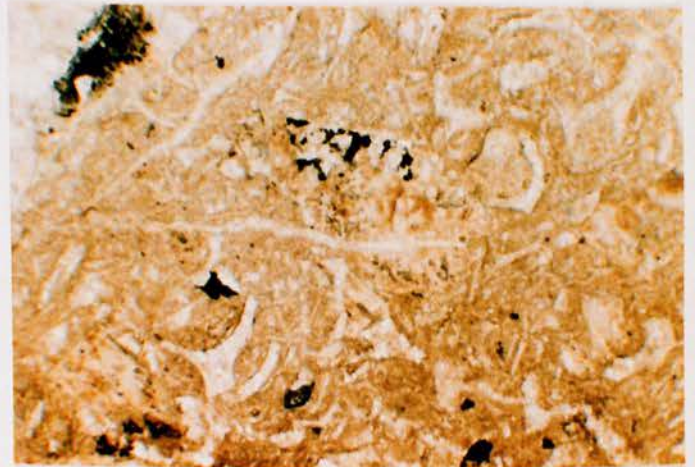
9



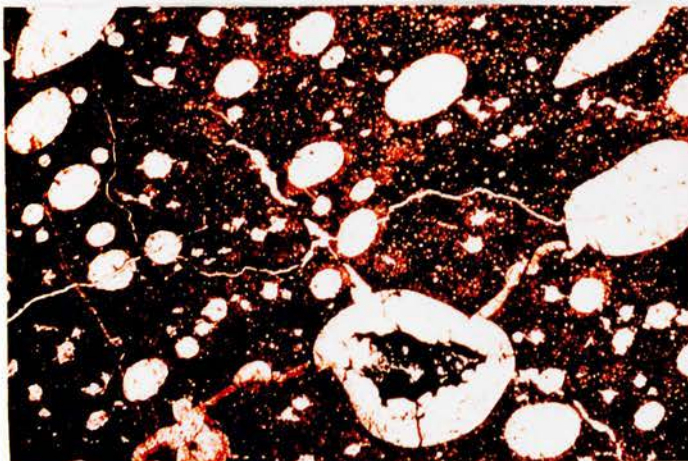
10



11



12



13



14

CHAPTER 3 MAJOR AND TRACE ELEMENT GEOCHEMISTRY OF THE VOLCANICS
AND BOOLAHBONE GRANITE.

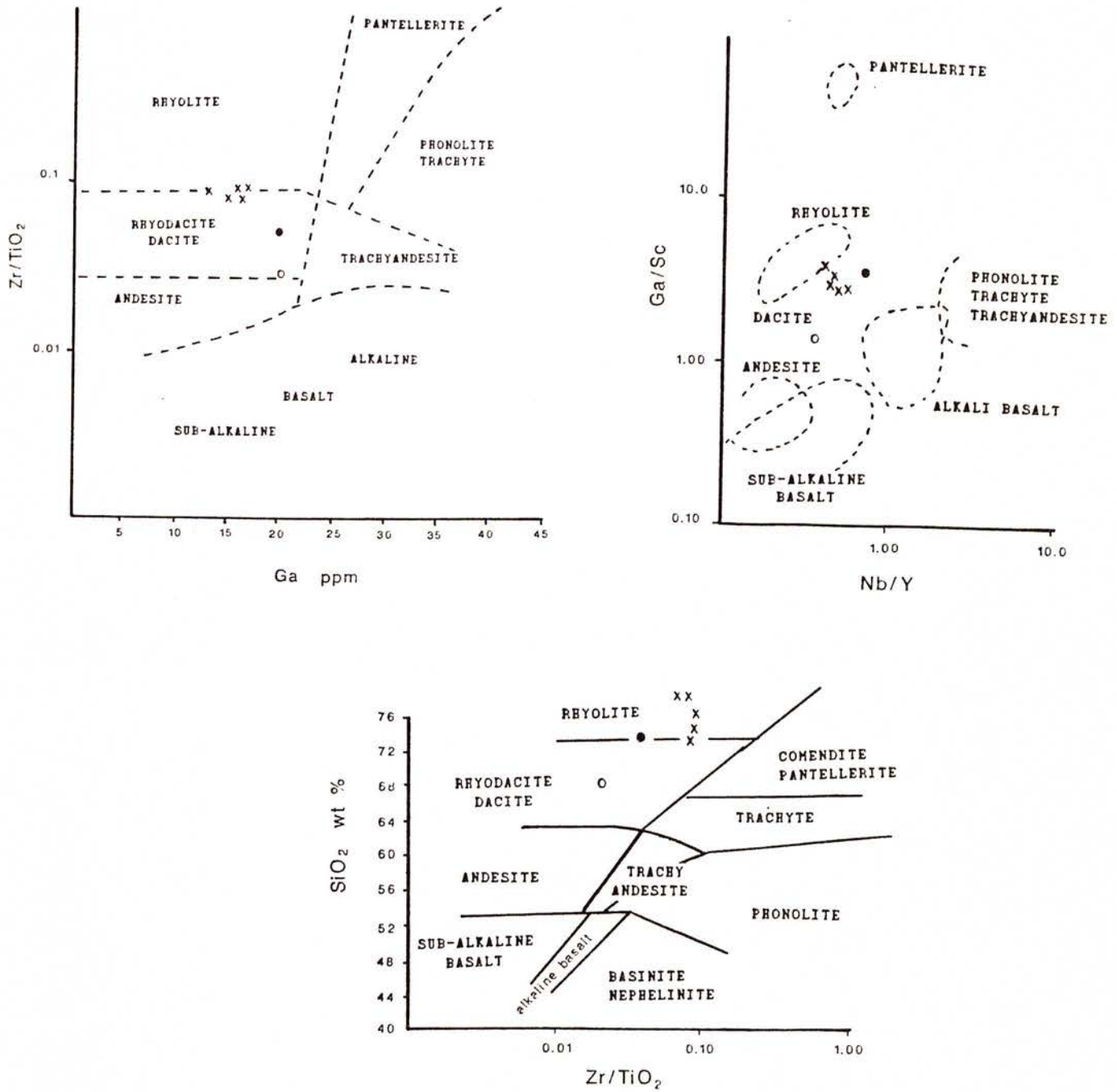
Seven samples were analysed for major and trace element chemistry (appendix 2). No fresh rock could be collected from the Wagga Tank area. Samples 886-43, 49, 10, and 11 are highly weathered, samples 886-54 and 886-16 are moderately weathered and sample 886-33 is fresh granitic rock recovered from drill-core at the nearby Fenceline Prospect, 3.5 km east of the Wagga Tank Prospect. The granite is mineralogically similar to the Boolahbone Granite and is possibly an apophyse or concealed extension of the main intrusion. All samples exhibit pervasive chlorite and sericite metamorphic alteration.

Due to the degree of weathering, most of the major element abundances are considered unsuitable for comparisons. Analyses of less weathered intrusive and extrusive rocks from the Mount Hope Group conducted by Scheibner and Barron [1982] plot in Kunos' [1969] calc-alkaline field on an A.F.M diagram. The Mount Kennan Volcanics and Boolahbone Granite plot at the high alkaline, final fractionation end of the trend.

Due to an almost total obliteration of the original mineralogy (except quartz) by alteration and/or weathering, some ambiguity exists as to rock classification. In order to distinguish the volcanic rock type, abundances of minor and trace elements Ti, Zr, Y, Nb, Ga and Sc have been plotted on established discrimination diagrams [Winchester and Floyd, 1977]. These elements are relatively immobile during metamorphism and may also be less influenced during weathering processes.

The discrimination diagrams (figure 5) show that the lavas and pyroclastics plot together near the rhyolite - rhyo-dacite boundary. The Boolahbone Granite and its subsurface equivalent

FIGURE 5



- x Volcanics
- o Boolahbone Granite
- Fenceline Granite

Winchester and Floyd, 1977

plot within the rhyo-dacite field and therefore should probably be referred to as an adamellite. The spread of the two granite plots away from the volcanics is either a weathering effect or an indication of separate intervals of liquid removal from a fractionating melt.

4.1

METAMORPHISM

The rocks in the Wagga Tank area away from the obvious hydrothermal alteration of the mineralized zone contain sericite and chlorite. This metamorphic mineral assemblage implies that the Mount Kennan Volcanics have been altered to greenschist metamorphic grade. However, the absence of clinozoisite also indicates very low grade (blue schist) metamorphism [Winkler 1979].

A problem in the Wagga Tank area is that most rocks, notably the sediments, display intense multiphase quartz veining and sporadic disseminated and vein sulphides remote from the known prospect. This implies a regional hydrothermal influence that may have possibly masked metamorphic assemblages in the area. Conversely, the fact that the metamorphic mineral assemblage, chlorite and sericite, reach the greatest development proximal to the mineralized body could suggest that metamorphism and the sulphides are related to the same fluid event.

Higher grade metamorphism may have occurred locally, related to the intrusion of the Boolahbone Granite. A bedded siltstone adjacent to the granophyric granite (probably an apophyse of the Boolahbone granite) recovered in drill-core at the Fenceline Prospect, contained sericite nodules (1 - 2 mm in diameter) which Barron [1977] suggested could have been cordierite prior to alteration. At the Wagga Tank Prospect a knotted slate from the volcanoclastic sequence (HD 15, 207 m) contains euhedral relict porphyroblasts that appear to have been andalusite. This may be indicative of a slightly higher grade of metamorphism, although andalusite can still occur within greenschist facies.

Structural interpretation of the Wagga Tank area is considerably complicated by the poor outcrop. This poses a major problem in understanding the possible structural control of the mineralized body.

The only well defined structural feature in the map area is the vertical to steeply west plunging open antiformal structure hosting the mineralization. Parasitic folds on the limbs of the major fold (rapid changes in bedding to cleavage angles in drill-core) and a slight overturning of the beds have been revealed by extensive drilling. This implies at least a moderate folding influence.

A syncline plunging at moderate angles to the south has been inferred for the outcropping volcanics in the 1:2500 map area (figure 3). An east - west striking syncline suggested for the conglomeratic sandstone beds east of a north - south trending fault is highly tentative.

Apparent small scale folding seen only in the rhyo-dacite and thin pyroclastic interbeds is a flow feature.

Low grade regional metamorphism and deformation produced a north - south trending cleavage and schistosity across the Wagga Tank area. The orientation is roughly axial planar to the major syncline inferred for the area east of the prospect. No other fabric indicative of a second deformation event can be defined.

The regional structure of the Cobar Supergroup sediments incorporates two deformations [Glen et al., 1985]. The stronger D1 structural elements consist of generally north to north - west trending folds and cleavage and high angle reverse faults. D2 effects are generally minor except in areas of less intense D1 influence where F2 folds overprint F1 folds. Glen [1982, 1985]

provided several lines of evidence suggesting that the major deformation took place in the Early Carboniferous, correlated with the Kanimblan Orogeny. Previous authors attributed the major deformation to the Middle Devonian Tabberabberan Orogeny [Gilligan, 1974].

5.1 THE MORPHOLOGY OF THE MINERALIZATION

The prospect contains significant concentrations of lead and zinc with minor copper, silver and gold. Gold values are highest within the steeply dipping gossan in the oxidized zone, while lead and zinc values are highest within subvertical elongate shoots of primary sulphide. Copper is concentrated as chalcocite, digenite and malachite at a zone of supergene enrichment. A near surface As, Pb and Au geochemical anomaly broadly outlines the surface projection of the mineralized zone.

The tonnage potential is probably less than 100,000 tonnes of oxidized mineralization with an estimated 2 to 3 grams/tonne Au, and around 200,000 tonnes of primary base metal mineralization, estimated as greater than 10% combined base metals [Homestake, 1987].

The sulphide mineralization occurs within a zone of intense tectonic brecciation and argillic hydrothermal alteration at a pronounced flexure along the contact between the volcanoclastic sequence and the stratigraphically higher siltstone - slate sequence (figures 6 and 7). Away from the zone of tectonic brecciation and sulphide mineralization the contact is seen to be conformable and gradational over one metre.

The primary sulphide body is very poddy. Correlations between drill-cores are ambiguous, so the sub-surface definition is poor.

The geometry of the zone of tectonic brecciation is complex. The most intense brecciation forms two subparallel, steeply dipping zones approximately 35 m apart which roughly follow the folded contact for 550 m along strike. The western zone separates the two lithologic units and diverges into the volcanoclastic

sequence while the eastern zone is confined to the volcanoclastic sequence. Both zones are narrow and continuous at depth. Other zones of less intense tectonic brecciation have been defined. These may be separate structures or branches off the major zones, or part of an en-echelon fracture system. [Rabone, 1987].

The contact between the volcanoclastic sequence and siltstone - slate sequence delineates a broad antiformal structure which dips steeply to the east at the point of flexure and subvertically to steeply west dipping on both limbs. Turbiditic sedimentary structures in the siltstone-slate sequence indicates a facing direction to the west.

A sericite regional schistosity is pervasive throughout the mineralized zone. The relationship between cleavage and tectonic brecciation is unclear although drill-core and surface excavation evidence suggests that it is of a parallel or low angle character.

5.2 THE ARGILLIC ALTERATION ZONE

Argillic alteration occurs pervasively throughout, and restricted to, the zone of tectonic brecciation hosting the mineralization. Although alteration is associated with unmineralized fracture zones and the vein type sulphides, it appears to be most extensively developed enveloping the massive type sulphide pods. Samples from drill-core consist of friable clay containing fragments of host rock and sulphide, or completely argillized siltstone - slate still displaying a cleavage.

An X-ray diffraction study of the argillic alteration zone (appendix 4) revealed the presence of illite, kaolinite, chlorite, hidalgite ($\text{PbAl}_3\text{AsO}_4\text{SO}_4(\text{OH})_6$) and a single occurrence of siderite and talc. The surface gossan contains goethite, illite, hidalgite and jarosite ($3[\text{KFe}^{3+}(\text{OH})_3(\text{SO}_4)_2]$). The jarosite structure did not

FIGURE 6

MINERALIZED ZONE - SURFACE PROJECTION

(Adapted from Rabone, 1987)



Zone of 1.00 g/tonne Au cutoff



Zone of low grade mineralization

MOUNT KENNAN VOLCANICS



Siltstone - slate sequence



Volcanoclastic sequence

DRILLING

○ HD = Diamond drill-hole - Homestake

○ ND = Diamond drill-hole - Newmont

● HP = Percussion drill-hole - Homestake

FIGURE 6

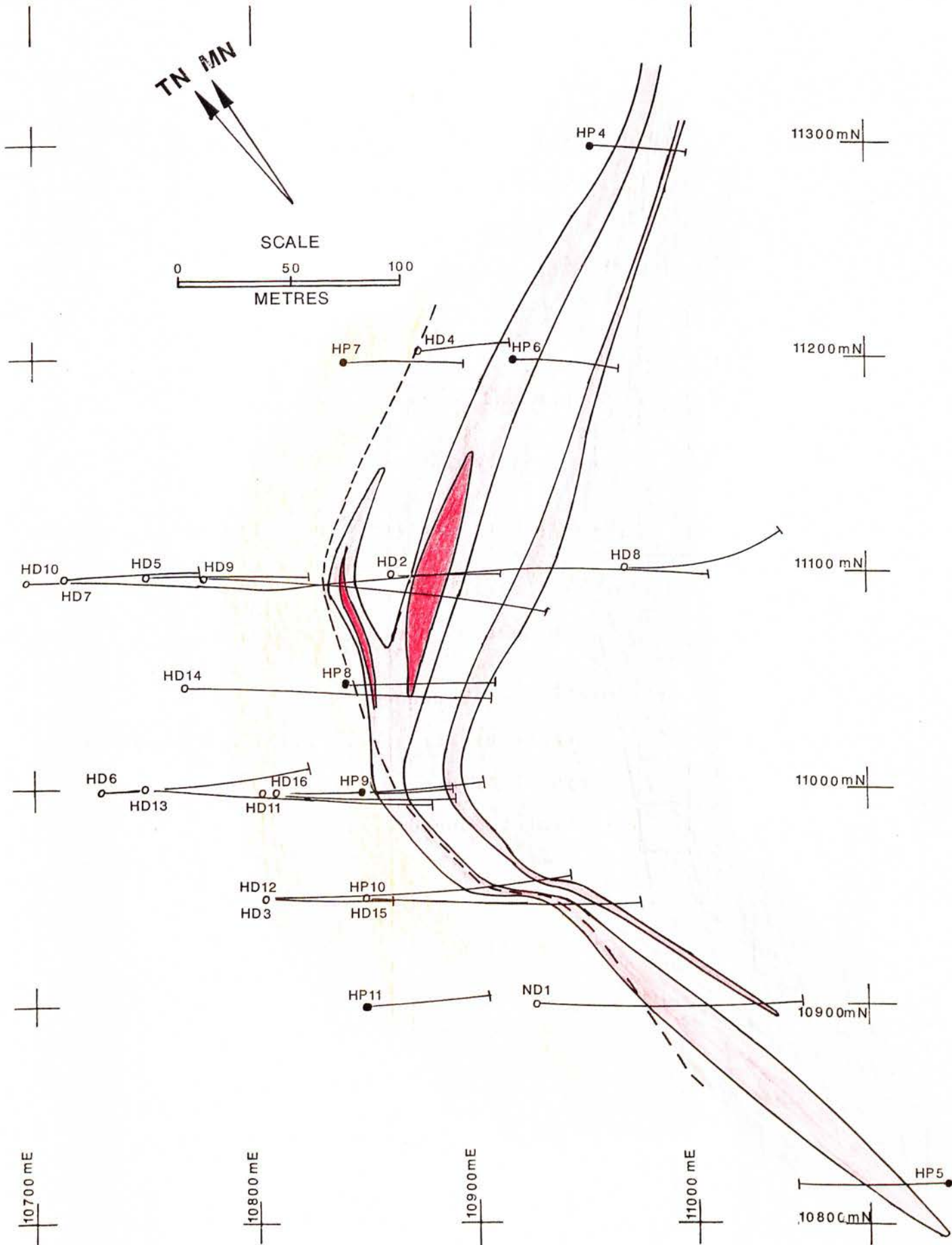


FIGURE 7

MINERALIZED ZONE - CROSS-SECTIONS

(Adapted from Rabone, 1987)

MOUNT KENNAN VOLCANICS



Soil and rubble overburden



Gossan and massive type sulphide



Vein type sulphide



Argillic alteration zone - kaolinite, sericite

Siltstone - slate sequence



-carbonaceous pyritic turbidite

Volcaniclastic sequence



-tuffaceous siltstone, shale and sandstone



-crystal-lithic (-vitric) tuff



-polymict conglomerate

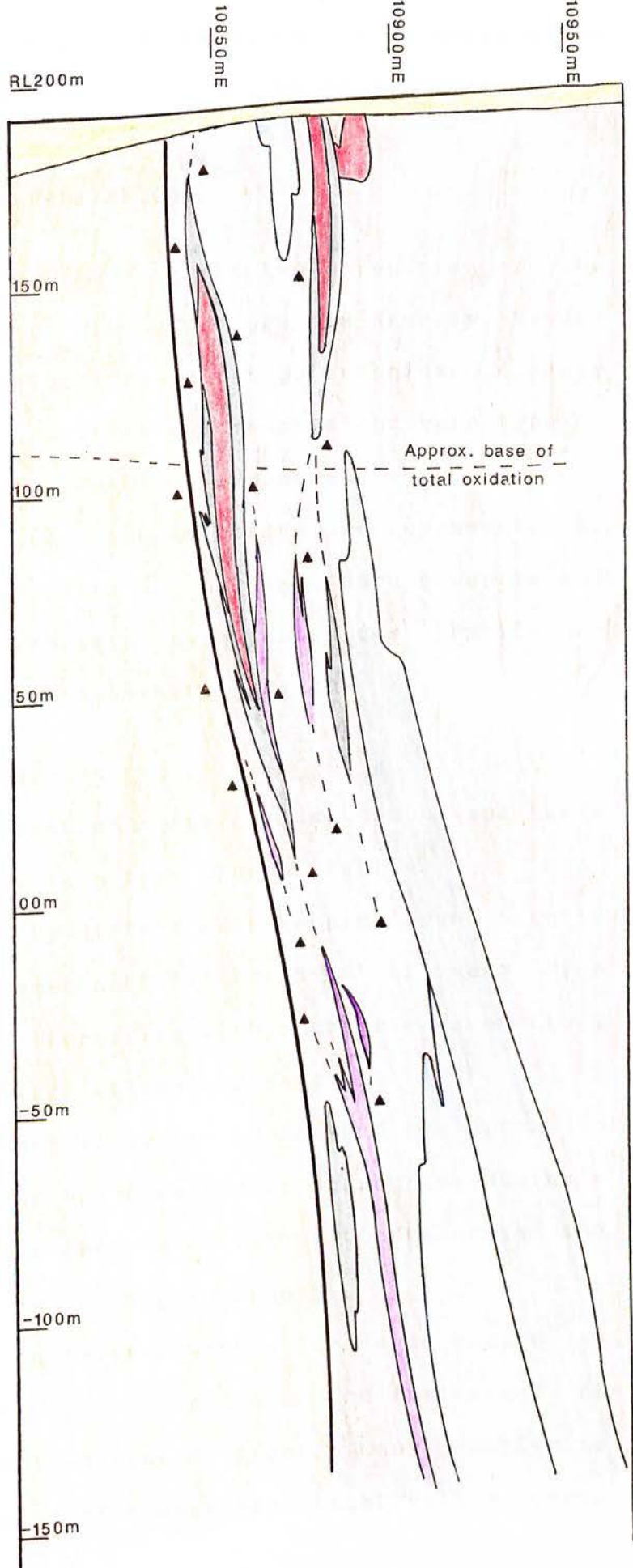
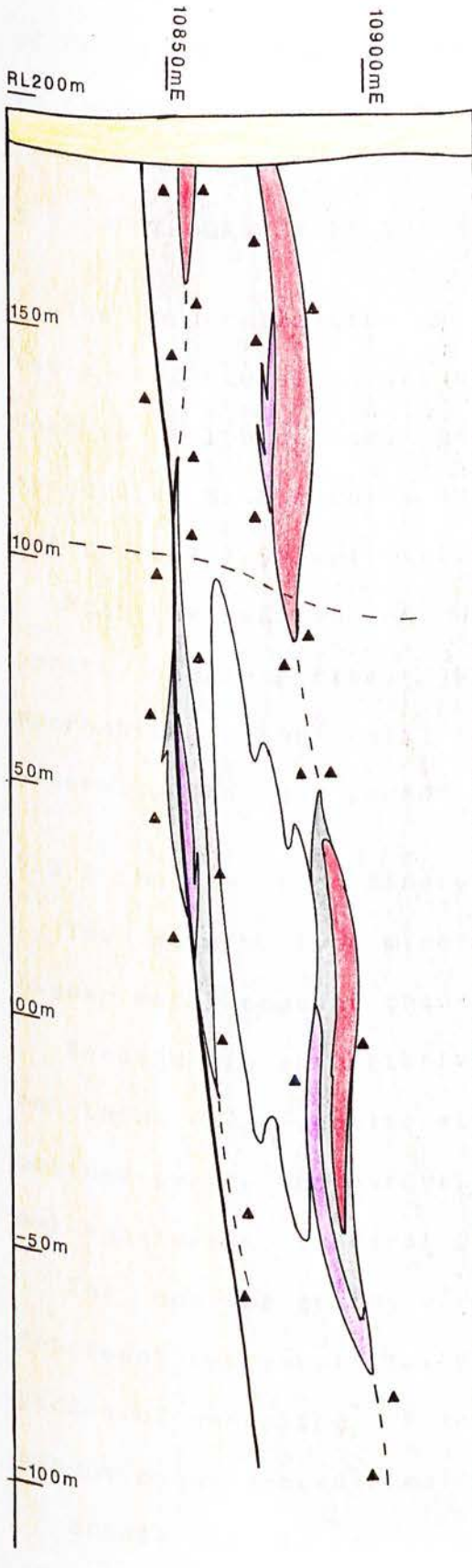


-Brecciation

FIGURE 7

11050mN

11100mN



show a shift in the d - spacings, that could indicate the presence of Pb in the jarosite structure, suggesting that hidalgoite alone is responsible for the anomalous Pb recorded in gossan assays.

5.3 PETROGRAPHY OF THE MINERALIZATION

The mineralization can be divided into two categories on the basis of textural relationships viz. fine grained crudely banded massive sulphides and coarse grained vein type sulphides closely associated with massive quartz. The terms massive and vein type do not present any implications as to mineral genesis.

Both the massive and the vein type sulphides are represented by pyrite, chalcopyrite, sphalerite and galena. Rare cubanite and pyrrhotite occur only in the vein type sulphides. Pyrite is generally the most common sulphide mineral present.

5.3.1 Massive type mineralization

The massive type mineralization contains less gangue and has a higher metal content than the vein type mineralization.

Banding is characterized by diffuse macroscopic layers 5 to 10 mm thick of irregular aggregates (0.01 - 0.25 mm) of very fine grained pyrite and gangue, alternating with coarser grained (to 1 mm) sphalerite, euhedral pyrite, galena and gangue.

The coarser grains of euhedral pyrite (0.25 - 0.5 mm) appear to represent recrystallization of the fine pyrite aggregates during a period of annealing. Pressure shadows of galena, sphalerite and gangue occur around some of the pyrite aggregates.

Sphalerite is closely associated with galena and occurs as elongate masses hosting euhedral pyrite grains and inclusions of chalcopyrite (0.05 mm). In transmitted light, many sphalerite grains are seen to be composed of translucent light yellow cores

devoid of chalcopyrite inclusions, becoming dark brown and containing an increasing abundance of chalcopyrite inclusions towards the rims, to produce a texture that resembles the "chalcopyrite disease" described by Eldridge et al. [1983] for the Kuroko ores. Chalcopyrite appears to be replacing sphalerite rather than exsolving from it, as the abundant inclusions display little affinity for cleavage traces. This could imply an increase in temperature of the mineralizing fluid after sphalerite precipitation.

Under transmitted light, some of the largest sphalerite grains are seen to be composed of dark and light cyclically zoned sphalerite fragments enclosed in an unzoned lighter translucent sphalerite host. Fractures cutting the zonation are also filled with the lighter sphalerite. This fragmentation and recementation of sphalerite is interpreted as a hydrothermal brecciation feature.

Colloform banding is found in the massive mineralization. The banding is characterized by concentric bands 0.02 to 0.75 mm thick of alternating very fine grained sphalerite, pyrite and gangue around a core of coarser pyrite, sphalerite, galena and gangue. The texture probably represents cyclic changes in fluid chemistry with sequential precipitation of pyrite and sphalerite on a coarser nucleus in an open space.

The massive type sulphide mineral ratios are less variable than that found for the vein type mineralization and the relationship: Pyrite > sphalerite > galena >> chalcopyrite holds for all samples described [py = 25-40%, sphal = 14-20%, gn = 5-10%, cpy = <2% and gangue = 30-50%].

The gangue mineralogy consists of fine grained chlorite and sericite with or without strained quartz and minor carbonate

(mostly siderite) intercalated with the sulphides.

5.3.2 Vein type mineralization

Vein type mineralization consists of coarse grained (up to 20 mm) pyrite, chalcopyrite, sphalerite and galena. Sections of the vein type mineralization can be either pyrite, chalcopyrite, sphalerite or galena dominant, but all four sulphide phases were observed in any sample even if only as rare inclusions.

Pyrite occurs as euhedral to subhedral grains (0.1 - 1 mm) commonly exhibiting pervasive chalcopyrite and galena filled fractures. Pyrite contains abundant inclusions of galena, especially near grain boundaries. All pyrite - galena contacts are ragged and complexly amoeboid. This texture is indicative of pyrite replacement by galena. Probe analysis of pyrite reveals an arsenic content of up to 2.35 atom %.

Galena occurs as large enveloping grains typically displaying tightly curved cleavage traces indicative of post mineralization deformation.

Sphalerite occurs either as translucent honey coloured, dark brown or opaque anhedral grains. The darker the sphalerite the greater the abundance of chalcopyrite inclusions. As in the massive mineralization the inclusions represent a replacement of sphalerite by chalcopyrite rather than exsolution.

Chalcopyrite occurs as large, moderately fractured grains commonly hosting euhedral pyrite. Minor cubanite inclusions occur as exsolution bodies within chalcopyrite.

A single specimen of vein type mineralization composed almost entirely of sphalerite displays minor small (0.01 - 0.05 mm) inclusions of pyrrhotite within the sphalerite host.

The gangue mineralogy consists predominantly of coarse grained

strained quartz and minor fine grained chlorite.

5.4 PARAGENESIS

From the observed textural relationships it appears that the pyrite was precipitated before, and partially replaced by galena, and that a phase of sphalerite precipitation occurred before chalcopyrite. Evidence for this is independent of any interpretations based on the degree of mineral idiomorphism.

Evidence for possible solid state mobilization of sulphide phases in the hydrothermal solution suggested by the enclosure of randomly oriented zoned sphalerite fragments within unzoned sphalerite complicates any interpretation of paragenesis. The mineralization has experienced a period of deformation as indicated by curved cleavage traces in galena, fracturing of pyrite, and pressure shadow development. However, the deformation influence must have been minor as the delicate colloform textures would not survive appreciable metamorphism.

Plate 15

Massive type sulphide, drill-core sample composed of fine grained pyrite, sphalerite, galena and minor chalcopyrite. Crude banding and colloform textures are visible. The scale is 2cm. (sample no. 886-99)

Plate 16

Highly porous fine grained massive sulphide. The scale is 2cm. (sample no. 886-102)

Plate 17

Colloform texture in massive sulphide consisting of concentric bands of very fine grained pyrite, sphalerite and gangue around a nucleus of coarser pyrite, sphalerite, minor galena and gangue. The field of view is 2.5mm. (sample no. 886-102, reflected light)

Plate 18

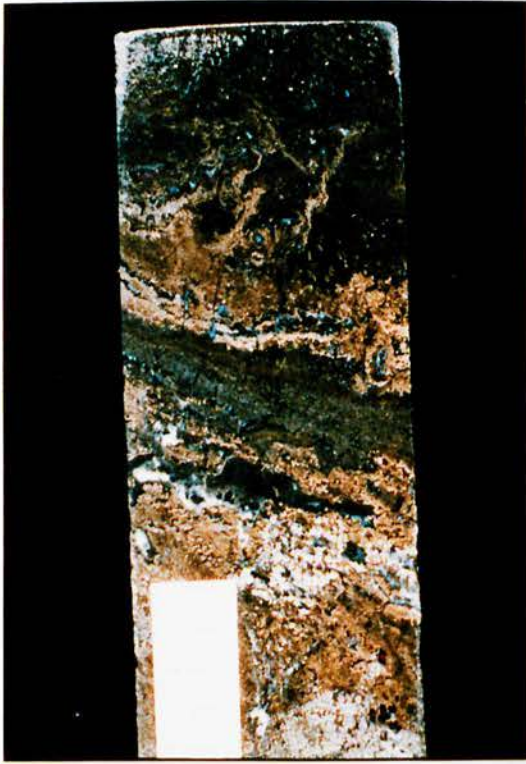
Aggregates of very fine grained euhedral pyrite in chlorite, sericite and quartz gangue - Massive type sulphide. The field of view is 0.4mm. (sample no. 886-81, reflected light)

Plate 19

Cyclically zoned sphalerite fragments hosted by lighter, unzoned translucent sphalerite. The field of view is 2.5mm. (sample no. 886-81, transmitted light - plane polarised)

Plate 20

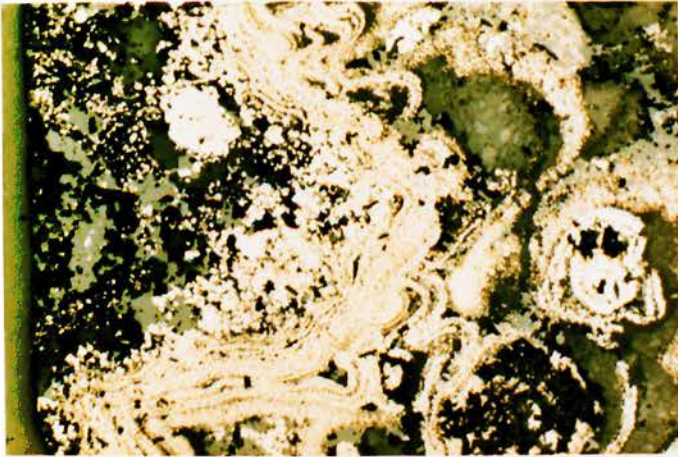
Chlorite and sericite gangue from the massive type sulphide. The field of view is 1mm. (sample no. 886-45, transmitted light - cross polars)



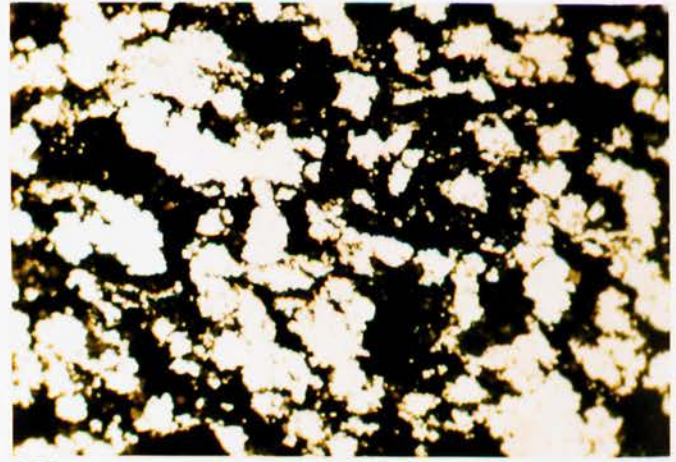
15



16



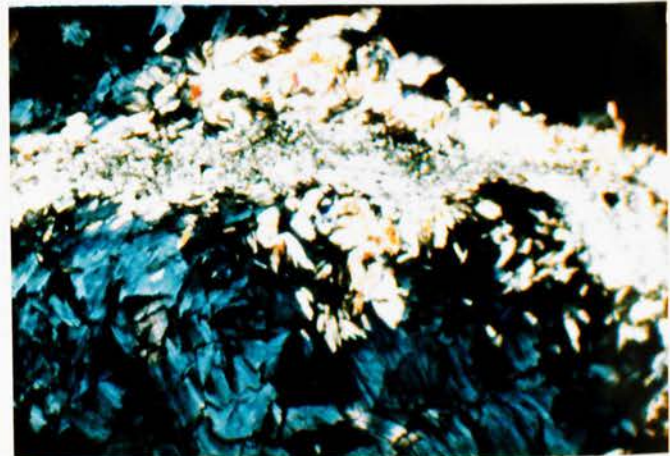
17



18



19



20

Plate 21

Vein type sulphide, drill-core sample composed of coarse grained pyrite, sphalerite, galena, chalcopyrite and quartz. The scale is 2cm. (sample no. 886-47)

Plate 22

Vein type sulphide - Chalcopyrite is seen to be replacing sphalerite. P = pyrite S = sphalerite G = galena C = chalcopyrite. The field of view is 2.5mm. (sample no. 886-47, reflected light)

Plate 23

Fractured pyrite grains in chalcopyrite - Vein type sulphide. Galena can be seen filling some of the fractures. The field of view is 2.5mm. (sample no. 886-21, reflected light)

Plate 24

Galena replacing euhedral pyrite along grain boundaries - vein type sulphide. P = pyrite G = galena C = chalcopyrite. The field of view is 0.64mm. (sample no. 886-21, reflected light)

Plate 25

Cubanite exsolution in chalcopyrite - Vein type sulphide. The field of view is 0.4mm (sample no. 886-28, reflected light)

Plate 26

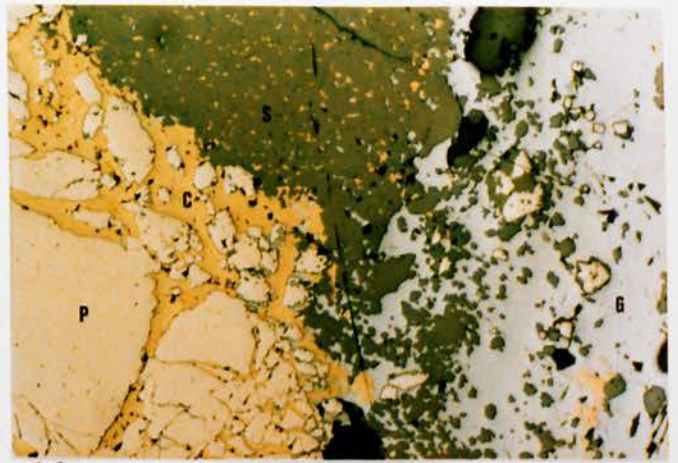
Curved cleavage traces in galena - Vein type sulphide. The field of view is 2.5mm (sample 886-28, reflected light)

Plate 27

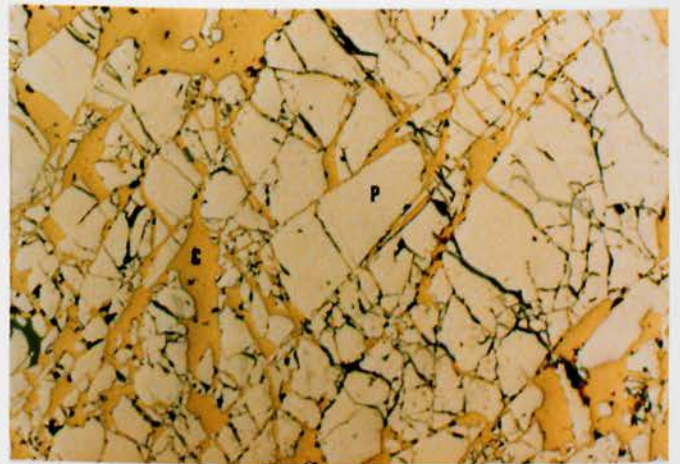
Zoned sphalerite surrounded by galena and quartz - sericite - chlorite gangue - Massive type sulphide. The field of view is 2.5mm. (sample 886-99, transmitted light - plane polarized)



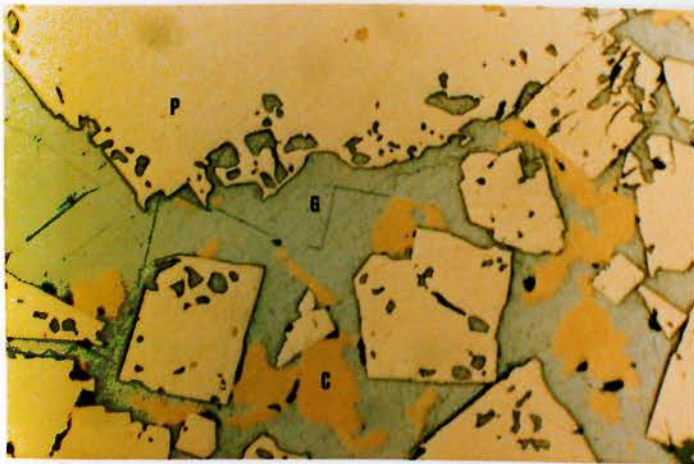
21



22



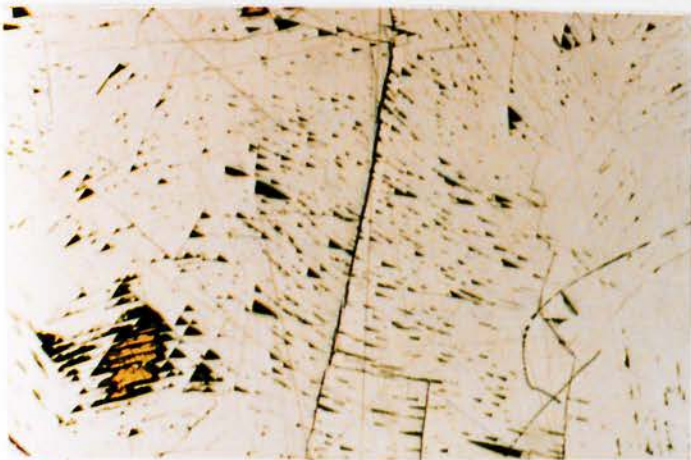
23



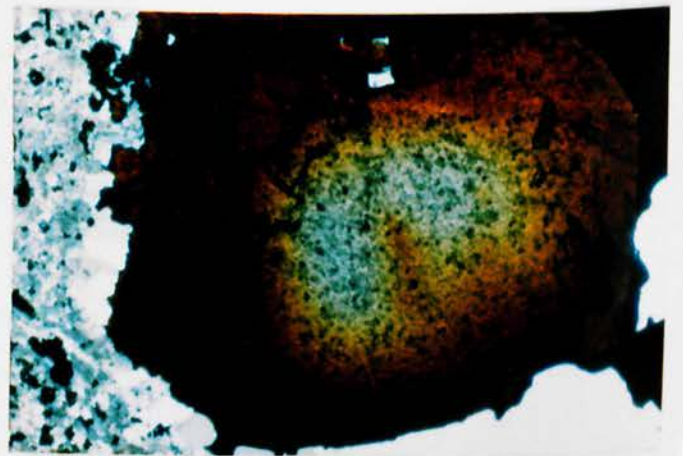
24



25



26



27

6.1 INTRODUCTION

The use of fluid inclusions is now an accepted technique in providing a reliable estimate of the temperature, pressure, salinity and composition of the fluids that formed or traversed the rock. Fluid inclusions have proved particularly useful in the field of ore genesis as many mineral deposit studies envisage the involvement of a fluid phase in ore formation.

Fluid inclusions are crystal defects representing trapped portions of the liquid, gases and melts from which the crystal has grown [Shepherd et al., 1985]. Without fluid inclusion analysis, studies of the physio-chemical nature of the ore forming phase can only assume that the fluids or gases contained only those constituents now present in the deposit. However, most ore forming fluids contained, in addition to the ore elements deposited, large amounts of volatile constituents and soluble salts that passed through the deposit leaving no trace, except in the fluid inclusions [Roedder, 1984].

6.2 SAMPLES

The fluid inclusions studied were found in quartz and translucent sphalerite. Measurements of siderite hosted fluid inclusions were unsuccessful due to poor light transmission through the doubly polished thin sections.

Quartz samples closely associated with sulphide minerals were taken throughout the vein type mineralized zone. No suitable quartz samples could be found in the massive type mineralization due to the fine disseminated nature of the gangue.

Fluid inclusions analysed in quartz were of two types, vis.

rare larger, slightly faceted fluid inclusions between 50 and 75 microns across the largest dimension, tentatively considered to be primary, and smaller irregular oblate to ellipsoidal fluid inclusions between 10 and 30 microns, also considered to be primary. In general, a large range of fluid inclusion abundances exist, with the abundance of fluid inclusions being inversely proportional to size. Secondary fluid inclusions in quartz are distributed throughout specific planes and are too small for analysis.

Although translucent sphalerite is common throughout both the vein and massive type mineralization, only one sample contained liquid / vapour fluid inclusions suitable for analysis. The inclusions were of two types, viz. complex, flat, multifaceted fluid inclusions with negative crystal faces, between 20 and 40 microns across the largest dimension, considered to be secondary, and sporadically occurring irregular fluid inclusions less than 10 microns, considered to be primary. Many inclusions in sphalerite lack a vapour phase, are solid filled or have been decrepitated.

All fluid inclusions examined were two phase, brine and vapour filled, with vapour / liquid ratios between 10 and 20% by volume. In general, the larger the inclusion the slightly greater the vapour/liquid ratio. The absence of daughter minerals implies an undersaturated saline solution. No immiscible phases such as CO₂ or CH₄ were detected optically. The comparative consistency of the vapour - liquid ratios suggests that the trapping of the liquid was homogeneous and no fluid boiling occurred at the site of quartz and sphalerite precipitation.

6.3 MICROTHERMOMETRY - FREEZING

Microthermometry is the technique employed to measure phase

transition temperatures in fluid inclusions. These are then compared to experimentally determined phase transitions in known systems.

The freezing temperature range provides an estimate of the salinity and composition of fluid within the inclusion. On reheating a frozen fluid inclusion, the first melt temperature (T_{fm}) corresponds to the eutectic, which is determined by the composition of the liquid phase. The final melt temperature (T_m) is proportional to the amount of salt in solution and the composition. Due to the difficulty in obtaining a qualitative analysis of a probably multicomponent fluid, salinities derived from final melt temperatures are expressed in terms of weight % NaCl equivalent if T_m is between -0.015°C and -21.1°C or weight % CaCl_2 equivalent if T_m is between -21.2°C (the NaCl - H_2O eutectic) and -49.5°C [Shepherd et al., 1985].

The final melting temperatures from which the salinities were obtained are depicted on a histogram in figure 8. Detailed results are listed in Appendix 5.

The final melt temperature for quartz primary fluid inclusions form a roughly symmetrical distribution with a range between -1.3°C and -5.5°C , corresponding to salinities of 2.2 to 8.5 weight % NaCl equivalent. The distribution mode is -3.0°C corresponding to 5.0 weight % NaCl equivalent. The final melt temperatures and mode for sphalerite primary inclusions fall within the temperature range found in quartz - hosted fluid inclusions; the temperature range of -1.4°C to -5.4°C corresponds to a salinity of 2.4 to 8.4 weight % NaCl equivalent.

The first melt temperatures of quartz primary fluid inclusions range between -10°C and -32°C , and form a reasonably symmetrical distribution around a mode of -20°C to -22°C (figure 9). The

FIGURE 8 Final Melt Temperature

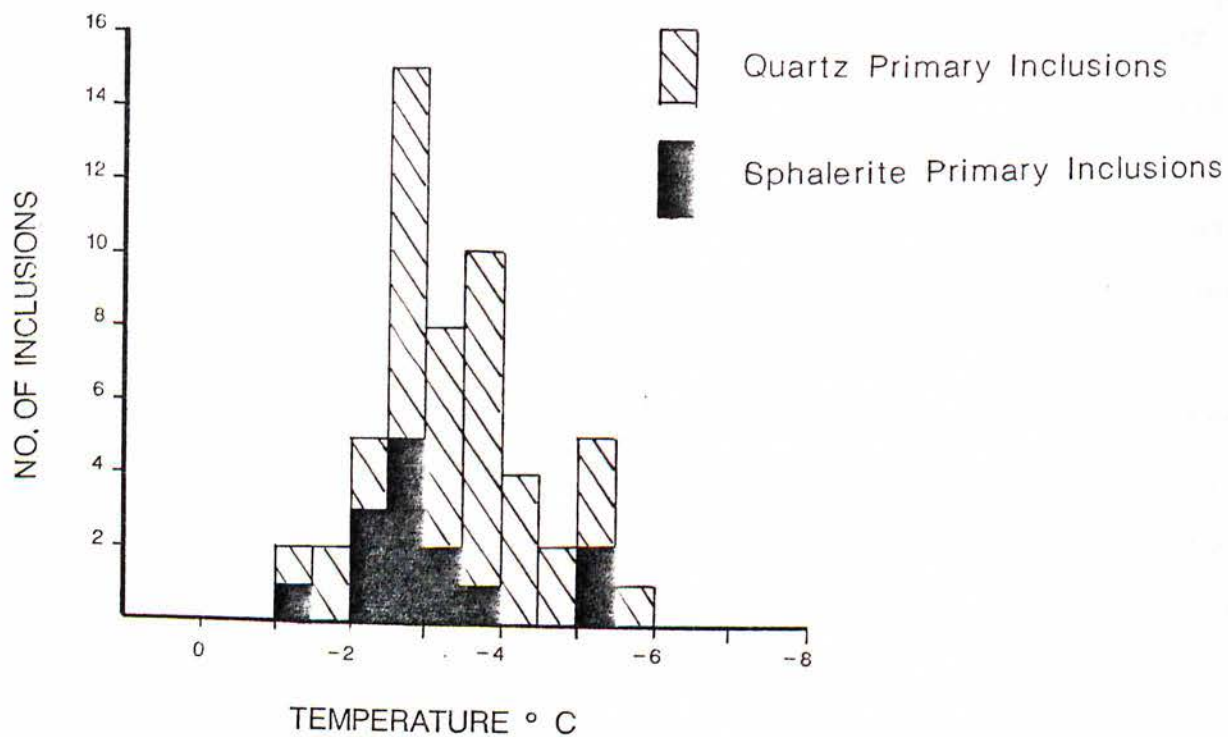


FIGURE 9 First Melt Temperature

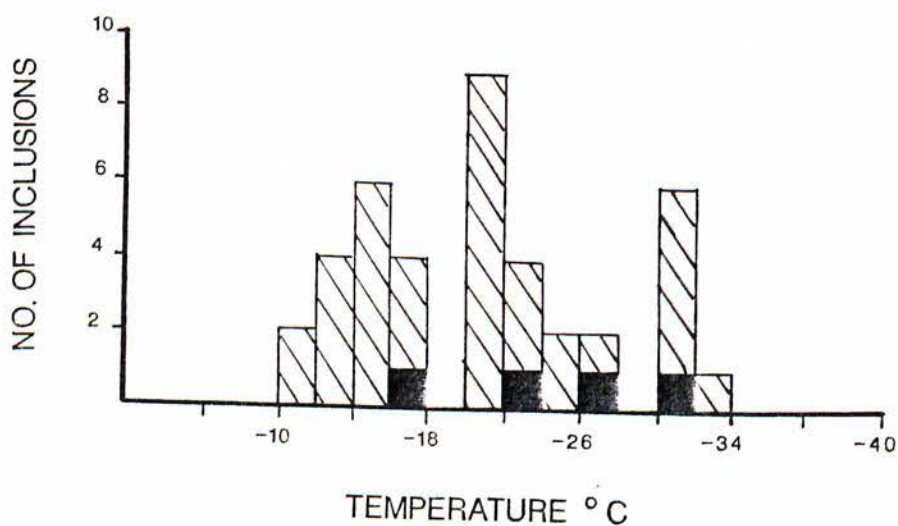
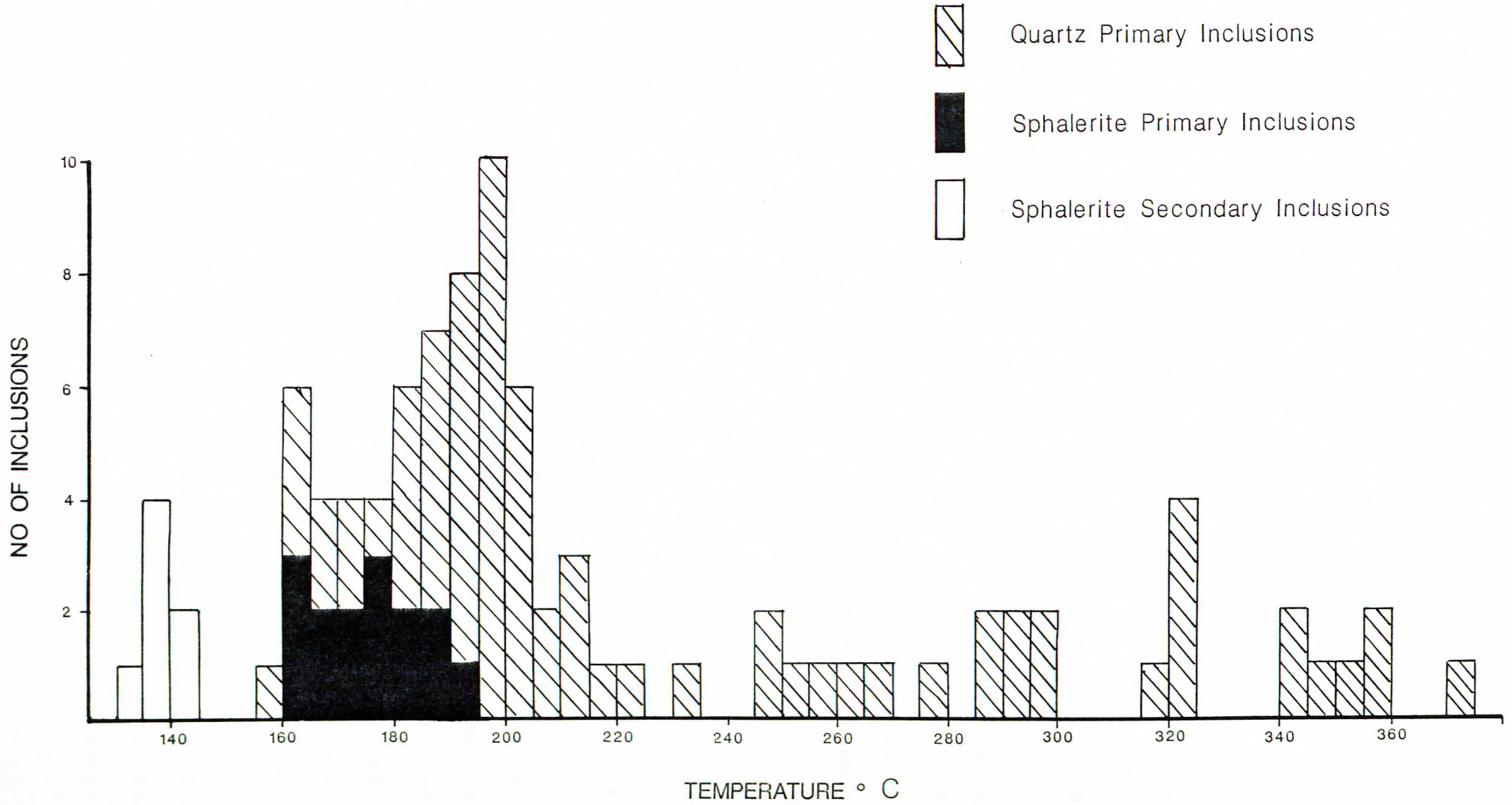


FIGURE 10

Homogenization Temperatures



depression of the first melting temperatures below that of the NaCl - H₂O eutectic (T_e = -21.2°C) indicate the presence of other soluble salts such as CaCl₂ (T_e = -49.5°C) or MgCl₂ (T_e = -33.6°C) or a multicomponent solution [Ypma, 1979].

Due to poor light transmission through the sphalerite sample, phase transitions were difficult to observe. Measurement of first melt temperatures for sphalerite could only be achieved for four primary fluid inclusions. T_{fm} ranged from -18°C to -31°C and the sphalerite, therefore, appears to be associated with the same fluid event as the quartz.

Qualitative analyses of the fluid inclusions were attempted, using the electron microprobe method of Bone and Griffin [1984] and the SEM method of Metzger et al. [1977], but both approaches were unsuccessful. The former failed because the electron beam did not burst the inclusions and the latter did not locate any evaporite associated with opened inclusions.

6.4 MICROTHERMOMETRY - HOMOGENIZATION

The use of fluid inclusions for geothermometry relies on the differential shrinkage of host mineral and inclusion fluid on cooling from the temperature of trapping to that of observation [Roedder, 1984]. In the simplest case, after entrapment and isolation in the crystal, the fluid shrinks more than the host, resulting in the formation of a near vacuum bubble. A reversal of this process, by heating until the bubble disappears (homogenization) allows a minimum temperature of formation to be obtained.

At least two measurements of homogenization temperature (T_h) were run for each fluid inclusion. T_h for fluid inclusions that did not regain their vapour phase upon cooling were not recorded.

This problem occurred particularly with sphalerite secondary fluid inclusions.

The homogenization temperatures are depicted on a histogram in figure 10. Detailed results are listed in Appendix 5.

T_h measured on a number of fluid inclusions in a sample generally fall within a narrow range. It is the measurements between different samples that account for the overall spread of T_h . The histogram shows that the quartz primary fluid inclusion homogenization temperatures form a roughly bimodal, but probably overlapping distribution. The lower temperature group ranges from 159°C up to about 235°C with a mode of approximately 200°C. The higher temperature group ranges from about 235°C to 372°C with a mode of approximately 325°C.

An apparent bimodality of the temperature distribution is related to the size and abundance of the fluid inclusions in the quartz host. The lower temperature distribution is found in the larger faceted and irregular fluid inclusions in clear euhedral quartz. The higher temperature distribution is found in cloudy white quartz samples containing a high concentration of smaller irregular, equidimensional fluid inclusions.

Sphalerite secondary fluid inclusions fall within a narrow T_h range between 133°C and 141°C. The temperatures are lower than that found in any quartz samples.

T_h for sphalerite primary fluid inclusions range between 163°C and 191°C. These temperatures correlate remarkably well with quartz fluid inclusions from the same core sample (temperature range between 159°C and 205°C).

The salinity versus homogenization temperature graph (figure 11) defines two different trends:

- (1) T_h between 160°C and 210°C with variable salinities.

FIGURE 11

Salinity vs Homogenization Temperature

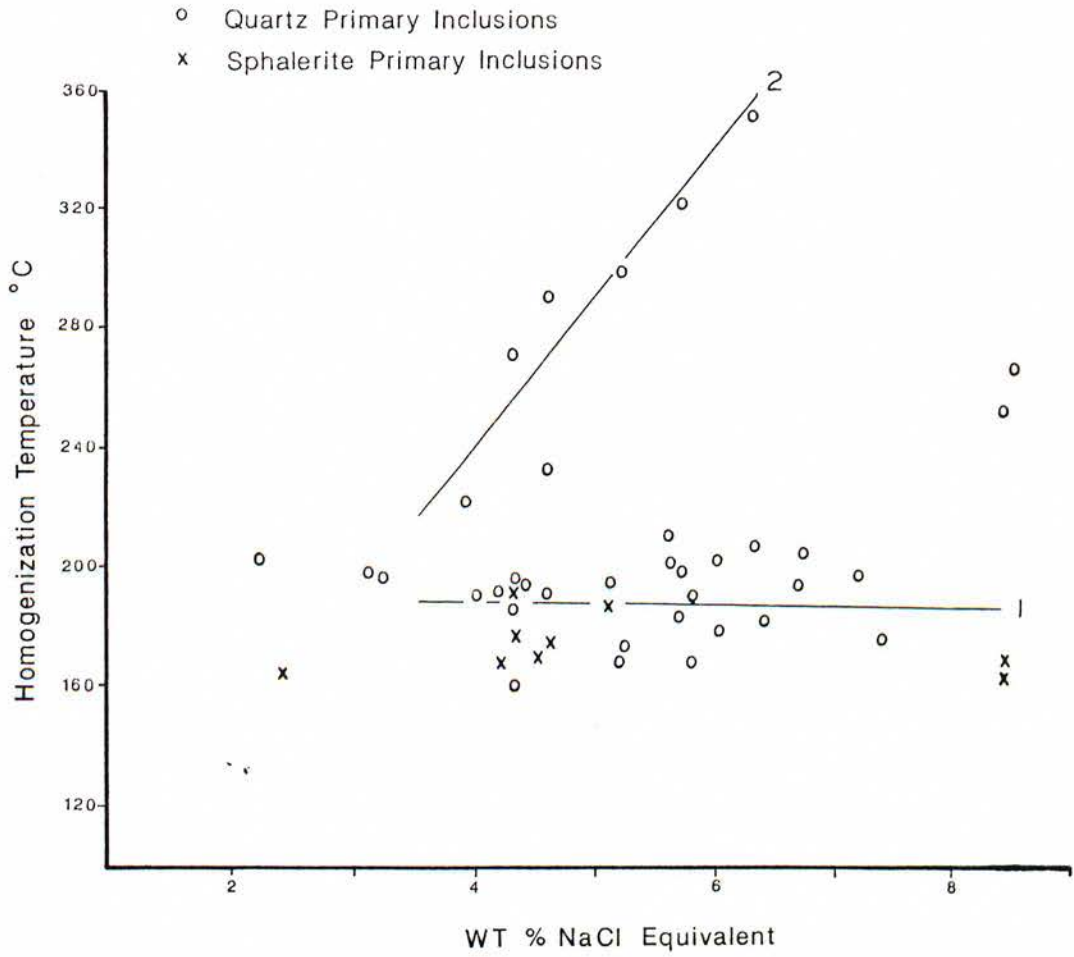
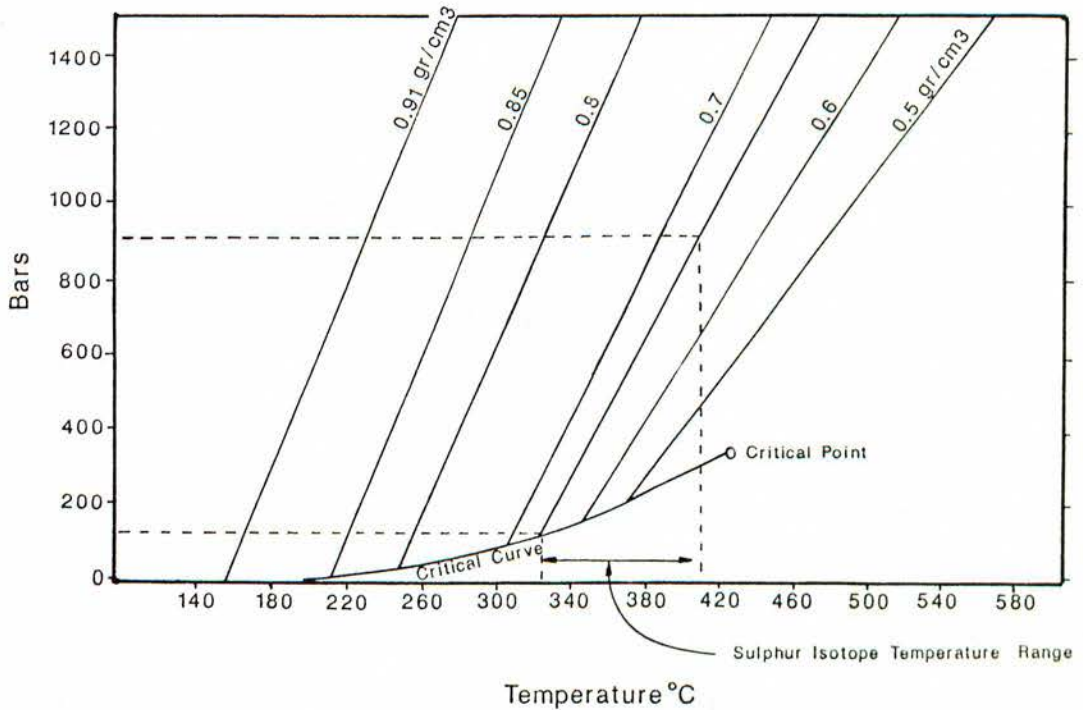


FIGURE 12 ISOCHORES FOR 5 WT% NaCl SOLUTION



(2) T_h decrease with decreasing salinity.

Trend (2) indicates a mixing of the fluid with another that is cooler and less saline. Trend (1) could be due to isothermal mixing of fluids with contrasting salinity. A further possibility is that only line (2) really exists. The apparent spread towards higher salinities on the isothermal trend could also be due to the presence of CO_2 in the fluid. CO_2 disrupts salinity measurements by depressing the final melting temperature of a saline solution, thus indicating an incorrectly high salinity.

If two separate trends actually exist then two quartz precipitating fluid phases have influenced the mineralized zone. As no relationship between T_h - salinity and the position of the sample in the mineralized zone is evident, the graph represents a temporal rather than spatial variation in the state of the fluid.

6.5 THE INFLUENCE OF PRESSURE ON T_h .

The homogenization temperature equals the fluid temperature only if the inclusion is trapped along the critical curve (ie, boiling) (figure 12). If the fluid is trapped at a pressure and temperature combination above the critical curve, a bubble will not form in it on cooling until the pressure has dropped to the critical curve. Therefore, T_h is only a minimum temperature of fluid trapping. The actual temperature is related to pressure, which defines the position along the isochore (line of constant density) and to fluid density, a function of salinity and composition, which defines the slope of the isochore.

An independent geothermometer can be used to calculate the pressure of fluid entrapment. In figure 12 the sulphur isotope temperature range (324 to 408°C - chapter 7) intersects the isochore at a pressure of between 100 and 900 bars. The isochore

is plotted for a 5% weight percent NaCl equivalent solution originating at 325°C on the critical curve.

Any pressure correction for fluid entrapment is considered to be minimal for the Wagga Tank mineralization. Precipitation of the sulphides and quartz appears to have occurred in open fractures in which hydrostatic rather than lithostatic pressure prevailed. However, the fact that fluid inclusions show no evidence of boiling and the fluid reached temperatures of at least 325°C, indicates that some pressure influence existed.

Plate 28

Primary fluid inclusions in quartz. Field of view is 0.4mm.

Plate 29

Secondary fluid inclusions displaying negative crystal faces in sphalerite. The field of view is 0.4mm.

28



29



7.1 INTRODUCTION

Sulphur isotope ratios were measured on 24 samples of sphalerite, galena, pyrite and chalcopyrite taken throughout the mineralization, from both vein and massive type sulphides. In addition, two samples of pyrite from the siltstone - slate sequence, were analysed. Sample 886-83 B represents a 3mm thick bedding parallel pyrite band in slate consisting of octahedral pyrite (10 microns) closely associated with pyrite framboids (plate 6). Sample 886-83 C represents a pyrite concretion closely associated with the pyrite band. The pyrite band is thought to have formed as a volcanogenic submarine, sedimentary or diagenetic precipitate.

The object of the sulphur isotope study was to supplement the petrology and fluid inclusion data in establishing the temperature of the mineralizing fluid and in defining the chemical conditions and mechanisms of sulphide deposition. Sulphur isotope ratios may also reveal the source of the sulphur. This information is based on the observation that the major factors which control the sulphur isotope composition of hydrothermal minerals are: (1) the temperature, which determines the fractionation between sulphur bearing species; (2) $\delta^{34}\text{S}$ fluid which is controlled by the source of the sulphur; and (3) the proportions of oxidized and reduced sulphur species in solution, which are a function of temperature, pH and $f\text{O}_2$ of the hydrothermal fluid [Ohmoto and Rye, 1979].

Fractionation of sulphur isotopes may occur in a variety of situations during the history of the mineralizing fluid, eg. (1) at the source of sulphur, such as during separation of the fluids from a magma or during leaching of sulphides; (2) during reduction of seawater sulphate; (3) during cooling of hydrothermal fluids;

FIGURE 13

Results Of Sulphur Isotope Measurements

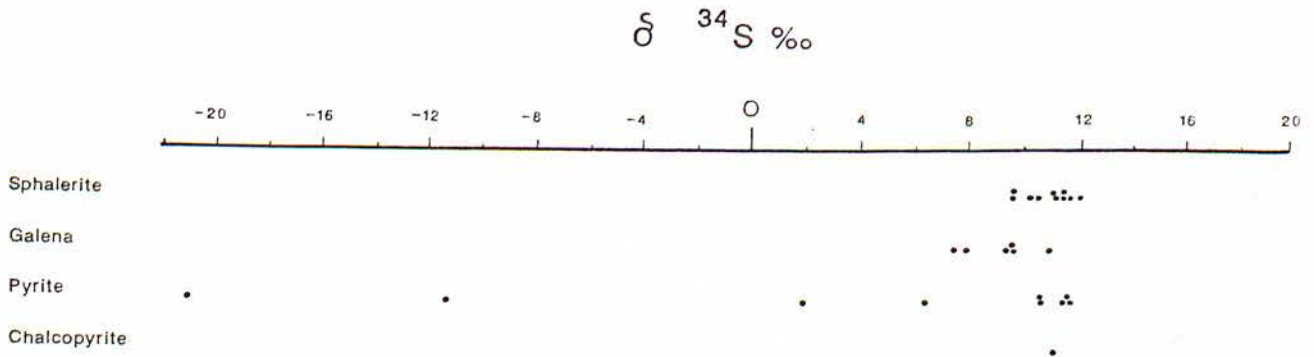
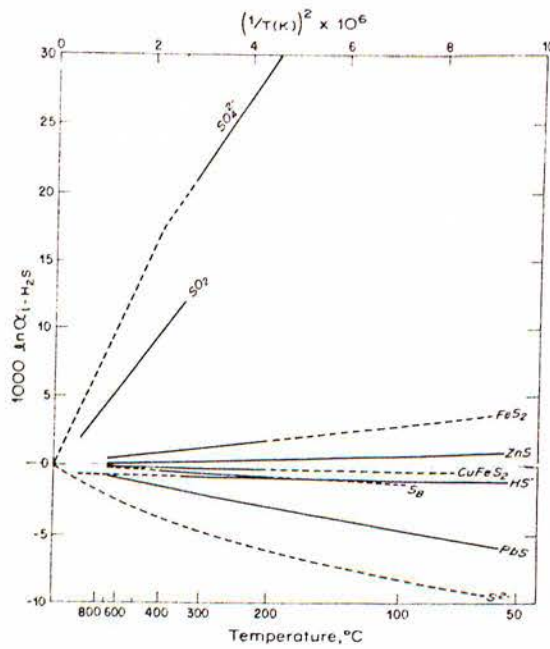


FIGURE 14



Equilibrium isotopic fractionation factors among sulfur compounds relative to H_2S . Solid lines—experimentally determined. Dashed lines—extrapolated or theoretically calculated. (From Ohmoto and Rye, 1979)

(4) during precipitation or replacement of minerals [Ohmoto and Rye, 1979].

7.2 GEOTHERMOMETRY

Sulphur isotope geothermometry is based on the equilibrium isotope fractionation between co-existing sulphur bearing compounds. The equilibrium isotopic fractionation factors for sulphide species are inversely proportional to temperature (figure 14). Pairs of sulphur compounds in which the fractionation factors have the steepest slope versus temperature are the most sensitive geothermometers.

The successful application of sulphur isotope geothermometry depends on:

- (1) Both mineral phases having formed in isotopic equilibrium.
- (2) No isotopic exchange having taken place between the mineral phases, or between a mineral phase and a fluid phase after formation of the mineral, ie. re-equilibration during metamorphism.
- (3) The availability of pure mineral phases separated for isotopic analysis.

The question of isotopic equilibrium between mineral pairs is difficult to resolve. The selection of sulphide pairs that have grown in contact with each other is a criterion that cannot be relied upon to imply equilibrium. Equilibrium is unlikely to have been achieved in non-contemporaneous phases, especially if the physical and chemical conditions of the fluids were highly variable during paragenesis.

The best method available in determining the nature of equilibrium between minerals, if isotopic exchange occurred, or the purity of mineral phases sampled, is by a comparison of

isotopic temperatures with those estimated by other means, eg. fluid inclusions.

The results of the sulphur isotope study are provided in appendix 6. The most reasonable isotopic temperatures were obtained from sphalerite - galena coexisting pairs using the relationship provided by Ohmoto and Rye [1979].

$$\Delta^{34}\text{S} = \delta^{34}\text{S}_{\text{sp}} - \delta^{34}\text{S}_{\text{gn}} \quad T^{\circ}\text{K} = \frac{(0.85 \pm 0.03) \times 10^3}{\Delta^{0.5}}$$

The experimental error factor of 0.03 is in addition to an analytical error of +/- 0.2 per mil.

Only mineral pairs from the vein type mineralization provided reasonable isotopic temperatures. Isotopic temperatures derived for the massive type sulphides have proved to be unreliable. This is probably due to contamination by other sulphide phases resulting from the difficulty in separation of the fine grained mineralization. The $\delta^{34}\text{S}_{\text{sp}} - \text{gn}$ ratios and isotopic temperatures derived for the vein type sulphide samples are given below.

Sample No.	$\delta^{34}\text{S}_{\text{sp}} - \text{gn}$	T [°] C
886-21	2.03	324
886-46	1.56	408
886-47	1.59	401
886-68	1.75	370
	Average	$\overline{\overline{376}}$

Sulphur isotopic temperatures were determined for three pyrite - galena pairs but their reliability is likely to be lower than the sphalerite - galena isotopic temperatures. The petrographic study indicates that pyrite may have precipitated at different times or during a much longer period of the paragenesis than galena. The $\delta^{34}\text{S}_{\text{py}} - \text{gn}$ isotopic temperatures were derived using

the relationship (Ohmoto and Rye, 1979):

$$\Delta^{34}\text{S} = \delta^{34}\text{S}_{\text{py}} - \delta^{34}\text{S}_{\text{gn}} \quad T^{\circ}\text{K} = \frac{(1.01 \pm 0.04) \times 10^3}{\Delta^{0.5}}$$

Sample No.	$\delta^{34}\text{S}_{\text{py}} - \text{gn}$	$T^{\circ}\text{C}$
886-21	1.88	464
886-46	2.13	419
886-47	2.22	405
	Average	$\overline{\overline{429}}$

The $\delta^{34}\text{S}_{\text{sp}} - \text{gn}$ isotopic temperature range falls around the upper limits of the homogenization temperatures found for quartz fluid inclusions and extends to 50°C above the maximum Th. Considering Th represents a minimum crystallization temperature of the quartz host, isotope temperatures for the sulphides correlate well with the fluid inclusion data. It can, therefore, be concluded that equilibrium between sphalerite and galena prevailed.

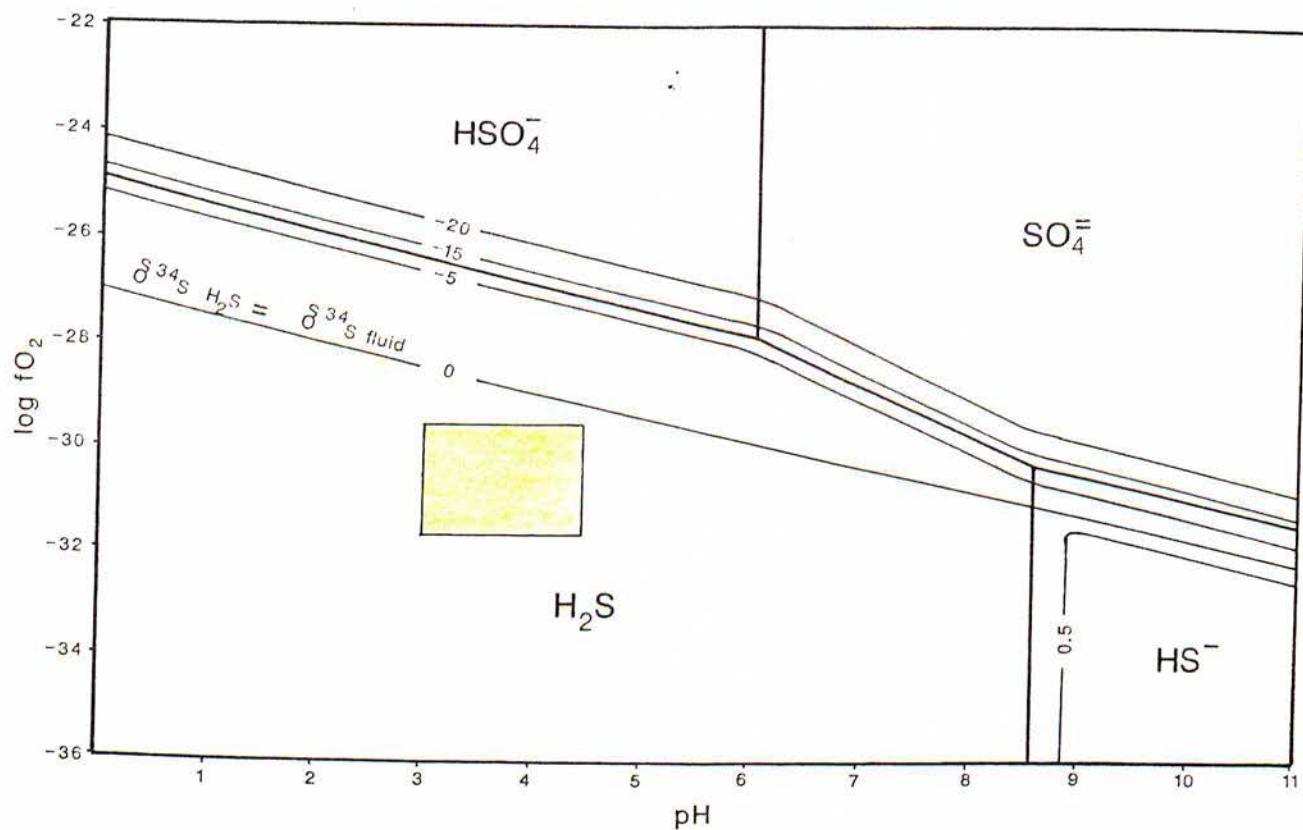
7.3 ORIGIN OF THE SULPHUR

Sulphur in hydrothermal ore deposits has originated ultimately from either an igneous source, including sulphur carried in magmatic fluids or sulphur obtained by leaching of igneous rocks, and/or a seawater source [Ohmoto and Rye 1979].

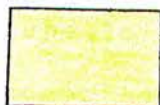
Sulphur is present in seawater as aqueous sulphates which along with sulphate bearing connate or meteoric waters can evolve into sulphide bearing hydrothermal fluids by: (1) the in situ reduction of sulphate to H_2S by sulphur reducing bacteria to form sedimentary sulphides, or (2) reduction of aqueous sulphates to aqueous sulphides inorganically at elevated temperatures.

Contours for $\delta^{34}\text{S}_{\text{H}_2\text{S}} - \delta^{34}\text{S}_{\text{fluid}}$ have been plotted on a log

FIGURE 15



CONTOURS OF $\Delta = \delta^{34}S_{H_2S} - \delta^{34}S_{fluid}$ AT 325°C UNDER EQUILIBRIUM CONDITIONS.

- Sulphur species stability fields
- -10 — $\Delta = \delta^{34}S_{H_2S} - \delta^{34}S_{fluid}$ contour in permil
-  Proposed $\log fO_2$ - pH conditions for mineralization

fO₂ - pH diagram (figure 15) at 325°C and on a $\log \frac{\sum \text{SO}_4}{\sum \text{H}_2\text{S}}$ - temperature diagram at pH 4 (figure 17). Both diagrams have been calculated for S = 0.01 M.

Under the suggested fO₂ - pH conditions (chapter 9), the dominant sulphur species in the mineralizing fluid would be H₂S. Figures 15 and 17 show that the 0 per mil contour lies in the H₂S field close to the proposed fluid conditions and therefore, $\delta^{34}\text{S}_{\text{H}_2\text{S}} = \delta^{34}\text{S}_{\text{fluid}}$.

Figure 13 shows the $\delta^{34}\text{S}$ values for the various sulphide minerals. As the sulphides formed from a fluid under conditions of isotopic equilibrium and $\delta^{34}\text{S}_{\text{H}_2\text{S}} = \delta^{34}\text{S}_{\text{fluid}}$, the average $\delta^{34}\text{S}$ values for sphalerite, galena, pyrite and chalcopyrite, allowing for the isotopic fractionation factor for each mineral ($\delta^{34}\text{S}_{\text{mineral}} - \delta^{34}\text{S}_{\text{H}_2\text{S}}$) at 325°C, indicates that the $\delta^{34}\text{S}_{\text{fluid}}$ equals about 10 per mil. This value implies that a likely source for most of the sulphur is from sea-water. Reduction of seawater SO₄²⁻ to H₂S was primarily by an inorganic process at elevated temperatures, probably by convection through a heated rock pile. The $\delta^{34}\text{S}$ value for coeval Lower Devonian sea-water is approximately 18 per mil [Claypool et al., 1980]. It is possible that the observed $\delta^{34}\text{S}$ value deviates from the coeval seawater value due to a mixing of isotopically lighter sulphur from a magmatic or biogenically reduced sulphur source. However, sulphur isotope studies of massive sulphide deposits [Sangster, 1968] and modern submarine exhalative systems [Styrt et al., 1981] have demonstrated that the isotopic composition of H₂S may be as much as 15 per mil lighter than the coeval seawater sulphate following inorganic reduction during convective crustal circulation.

The two syngenetic or diagenetic pyrite samples from the siltstone - slate sequence possess isotopically light $\delta^{34}\text{S}$ values

($\delta^{34}\text{S} = -11.1$ and -20.9) indicative of low temperature bacterial reduction of seawater sulphate to sulphide in a euxinic environment. The two pyrite samples with $\delta^{34}\text{S}$ values of 2.2 and 6.7 per mil taken from the mineralized zone proper, indicate some mixing of both biogenically reduced sulphur and high temperature reduced seawater sulphate. The spread of $\delta^{34}\text{S}$ to lighter values only occurs in pyrite.

The use of chlorite to define the physico-chemical conditions of hydrothermal ore deposit formation is a recently developed technique that has not been fully appraised. The method, devised by Walshe [1986], uses the non-stoichiometry of chlorite as the basis of a six - component chlorite solid solution model. The model uses electron microprobe analyses of chlorite to calculate the temperature, redox state and chemical activity (fS_2) parameters of the mineralizing fluid. Microprobe data of chlorite gangue from the Wagga Tank Prospect was processed on computer by Dr. J. Walshe at the Australian National University.

The results of the analysis are shown in appendix 7. 10 samples were analysed from 4 different polished thin sections. Chlorite is only associated with the massive sulphides, thus providing the only temperature estimate for this type of mineralization. The temperature range of 228°C to 302°C, with most values occurring at the higher temperature region, correlates well with the fluid inclusion and sulphur isotope geothermometers of the vein type mineralization. The $\log fO_2$ range is between -31.9 to -42.5 with most of the values around the higher region. An estimate of $\log fS_2$ given by the model ranges from -10.1 to -15.9.

CHAPTER 9 THE CHEMISTRY OF THE MINERALIZING FLUID

Thermodynamic data combined with petrographic, geochemical, fluid inclusion and sulphur isotope data have been used to define the possible fO_2 - pH conditions of the mineralizing fluid. Figure 16 has been calculated for $325^\circ C$ on the basis of the modal value for the higher distribution homogenization temperature range for quartz fluid inclusions and on the reasonable agreement provided by the sulphur isotope, and chlorite model temperatures. A total sulphur content of the fluid of 0.01 M has been used in the construction of figures 16 and 17, as lower $\sum S$ values result in a magnetite field separating the pyrite and pyrrhotite stability fields. Both pyrite and minor pyrrhotite occur but magnetite has not been detected in the primary sulphide zone. An $a_{Cl^-} = 1.0$ M has been used for calculating Zn and Cu solubility contours; this is based on fluid inclusion final melting temperatures indicating a 5 wt% NaCl equivalent fluid.

The fO_2 - pH constraints shown in figure 16 are made on the basis of the sulphide mineralogy, the hydrothermal alteration mineralogy and sphalerite geochemistry. Pyrite and chalcocopyrite are the primary minerals present in the Cu - Fe - S - O system, which coexist over a large range of fO_2 - pH conditions at $325^\circ C$. The presence of minor pyrrhotite inclusions in sphalerite is indicative of a change in the fO_2 and/or temperature conditions.

Only a broad pH constraint can be made on the nature of the mineralizing fluid. The presence of both sericite and kaolinite and the absence of K-feldspar in the hydrothermal alteration zone indicates that the fluid pH was below 5.9 and at some time crossed the sericite / kaolinite stability field boundary to a pH below 3.8. These constraints are based on an $a_{K^+} = 0.01$. A higher a_{K^+} value pushes the sericite / kaolinite stability field boundary to

FIGURE 16

LOG fO_2 - pH CONSTRAINTS ON MINERALIZATION

-Calculated for $T = 325^\circ C$

———— Sulphur species boundaries

———— Fe - S - O mineral boundaries for
 $\sum S = 0.01 M$

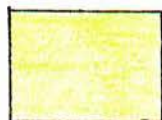
— — — — Bornite / Chalcopyrite boundary

- - - - - Cu solubilities (ppm) calculated for
 $a_{Cl^-} = 1.0$

— . — . — . Zn solubilities (ppm) calculated for
 $a_{Cl^-} = 1.0$

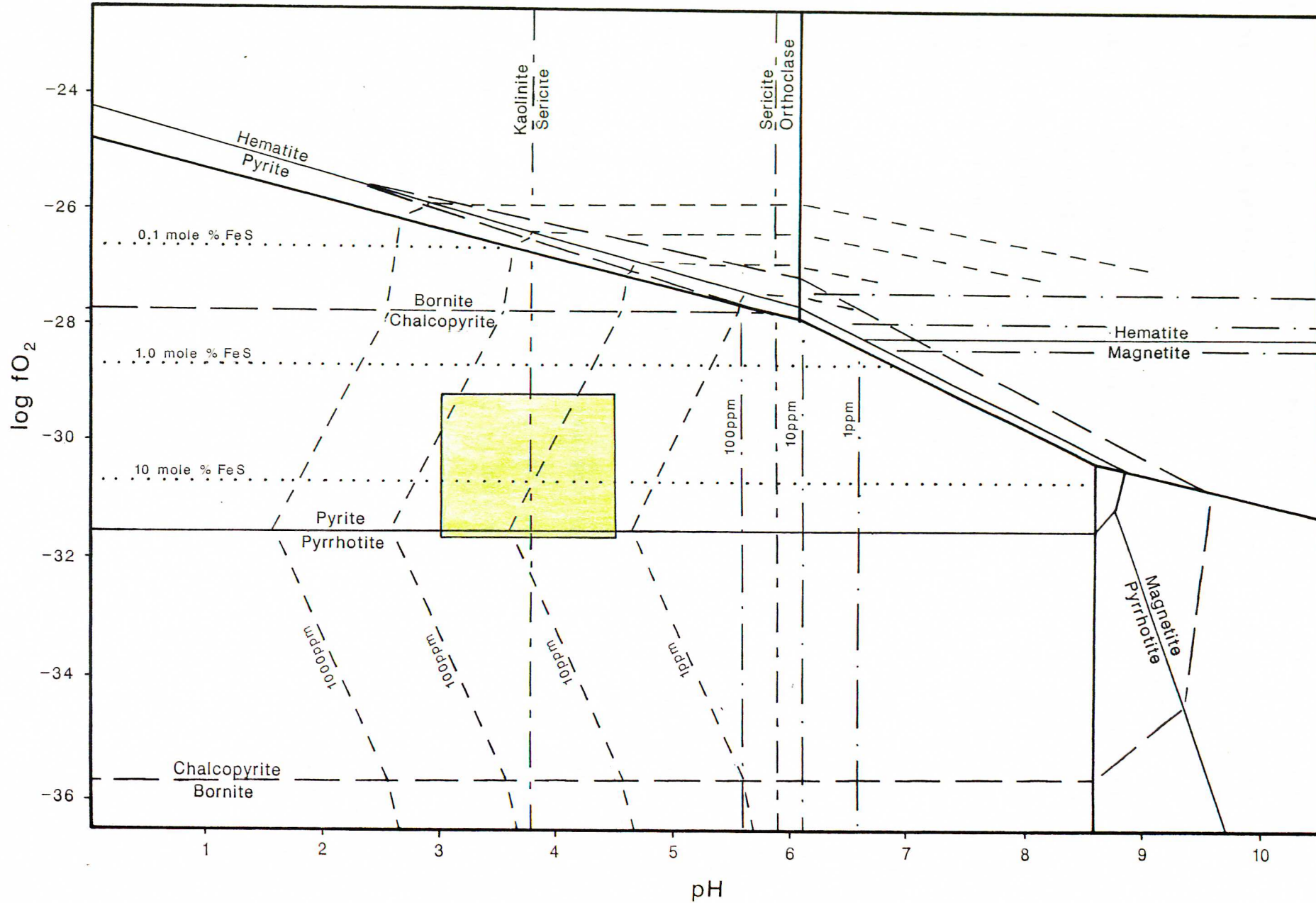
..... Mole % FeS in Sphalerite

— - - - - Kaolinite / sericite / orthoclase
boundaries for $a_{K^+} = 0.01$



Proposed log fO_2 - pH conditions for
mineralization

FIGURE 16



lower pH values and high Cu solubilities considered unrealistic for a hydrothermal system that produced only relatively minor copper mineralization. The pH region between pH 3 and pH 4.5 defined on figure 16 is based on a realistic Cu solubility limit of between 1 and 100 ppm Cu in solution. Neutrality at 325°C occurs at approximately pH = 5.6.

Constraints on the fO_2 of the mineralizing fluid are defined by the FeS content of sphalerite. The fO_2 - pH diagram has been contoured for mole % FeS content of sphalerite in the pyrite field. Electron microprobe analysis of sphalerite shows the FeS content ranges between 2.4 and 14.7 mole % (Appendix 8) indicating a log fO_2 of between -29.5 and -31.7. This value is just higher than the independent fO_2 estimate given by the chlorite solid solution model (for somewhat lower temperatures).

Of considerable note is the fact that samples of sphalerite containing pyrrhotite inclusions (the only way pyrrhotite occurs) have FeS contents greater than 12 mole %. The pyrrhotite / pyrite field boundary occurs at exactly 12 mole % on the fO_2 - pH diagram indicating the suitability of the constraints used, and the application of the diagram to the mineralization.

The spread of FeS contents for sphalerite is the same for both the vein and massive type sulphides. Microprobe traverses of zoned sphalerite shows that the FeS content gradually increases (along with the abundance of chalcopyrite inclusions) from the lighter coloured cores to the darker rims (figure 18). According to figure 17, the increase in FeS content can be attributed to either decreasing fO_2 and/or increasing temperature.

Fluid inclusion data indicate that a variation in fluid temperature occurred during sulphide precipitation. At least one phase of sphalerite precipitation is known to have occurred at

FIGURE 17

LOG $\Sigma \text{SO}_4 / \Sigma \text{H}_2\text{S}$ - TEMPERATURE CONSTRAINTS ON MINERALIZATION

-Calculated for pH = 4

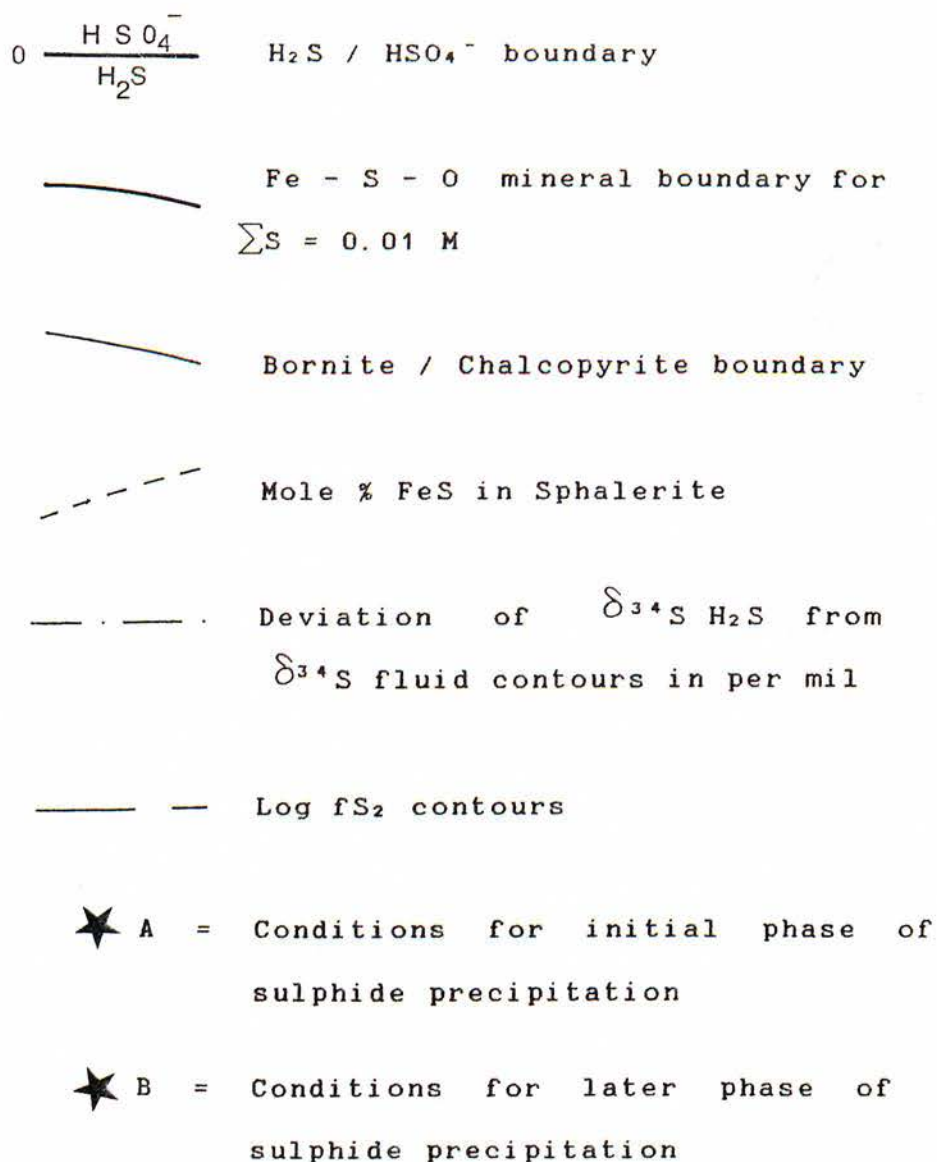


FIGURE 17

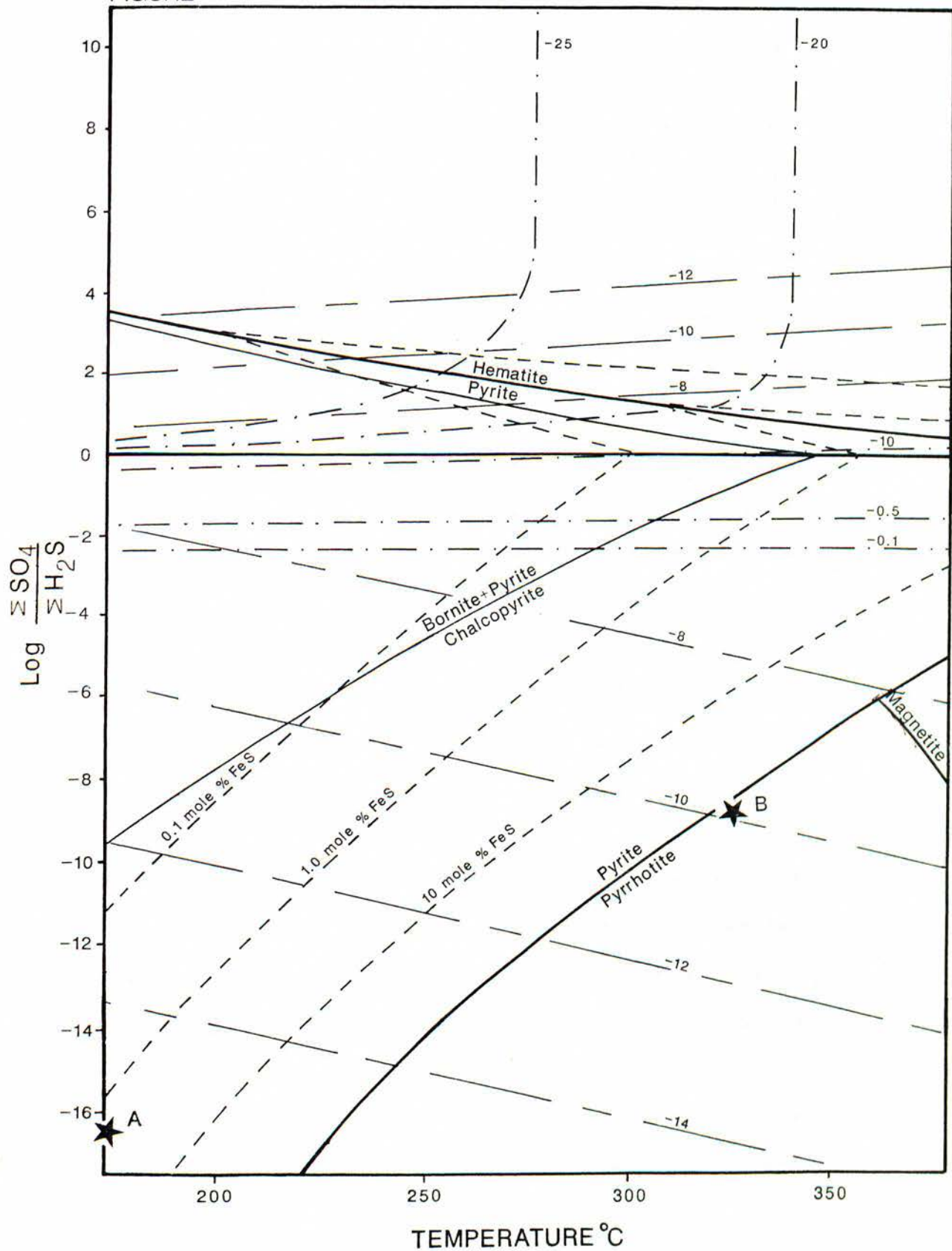
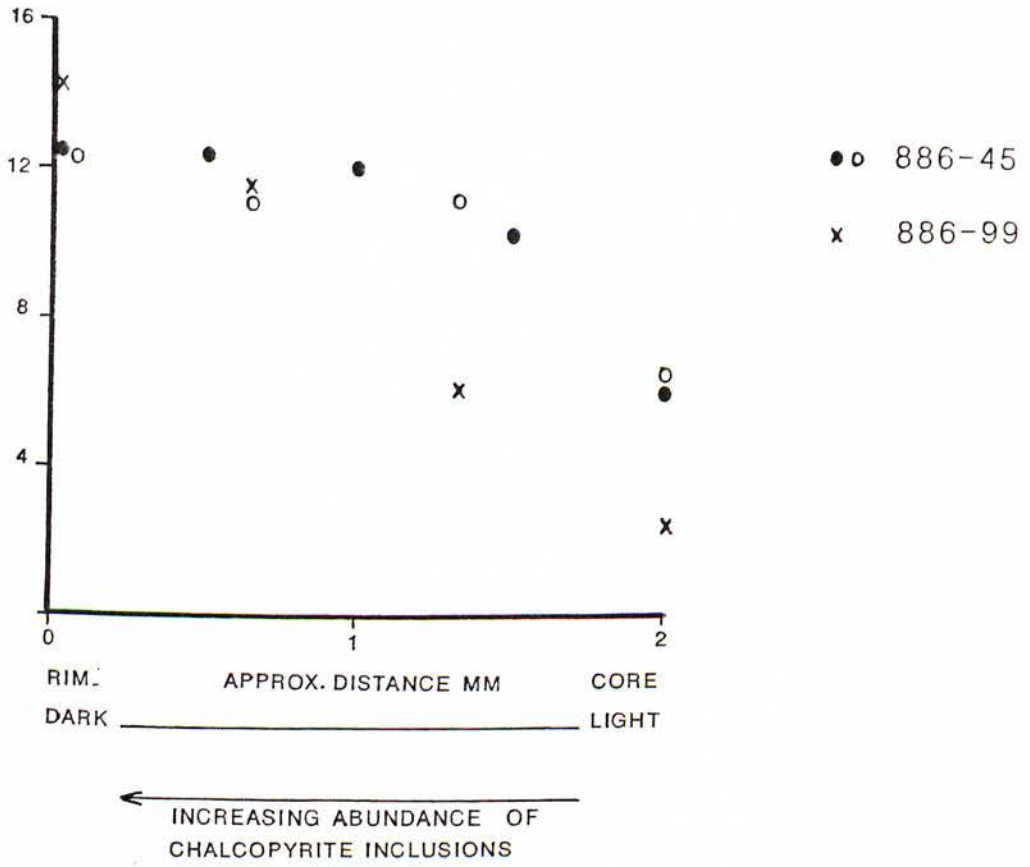


FIGURE 18

Mole % FeS in Zoned Sphalerite
- Massive Type Sulphide -



about 170 °C. The FeS content of the 170°C sphalerite is 2.6 mole % (represented by point A on figure 17). The higher homogenization temperature quartz hosts dark coloured, higher FeS content sphalerite (point B on figure 17 - assuming T = 325°C for the darkest sphalerite). These observations and the fact that chalcopyrite is replacing sphalerite, indicate that sphalerite precipitated during an early, low temperature (about 170°C) phase of mineralization and that the Fe and Cu contents of the fluid subsequently increased with an increase in temperature (to about 325°C) resulting in the precipitation of chalcopyrite and pyrrhotite. Precipitation of the mineralization could have been due to an increase in pH, which decreases the solubility of both Cu and Zn, a decrease in temperature (even if the temperature of the hydrothermal system was increasing) or by a change in the redox state. The actual mechanism is difficult to ascertain, although the Th versus salinity graph (figure 11) suggests a mixing with another cooler less saline fluid. It is likely that this fluid would have had a pH closer neutral, so deposition may have been due to a change in T, pH and possibly fO₂ if the other fluid was less reduced. Figures 16 and 17 show that an increase in pH or a decrease in T is the most efficient mechanism for dropping Cu, Pb and Zn out of solution. Such conditions would prevail if the hydrothermal fluid came into contact with ground water.

Fluid inclusions show no evidence of fluid boiling so this mechanism is not responsible for precipitation. Precipitation may also have been induced when the metals, transported as chloride complexes, encountered a source of reduced sulphur (syngenetic) in the siltstone - slate sequence.

The high concentration of Pb and Zn compared to the low gold concentration in the primary mineralization (< 0.5 ppm), can be

attributed to the chemistry of the hydrothermal fluid. At a pH of 4 the efficiency of gold transport as the two major complexes, $\text{Au}(\text{HS}^-)_2$ and AuCl_2^- , is at a minimum. Transport of gold as $\text{Au}(\text{HS}^-)_2$ is favoured in solutions of neutral to alkaline pH and high H_2S . Transport of gold as AuCl_2^- is favoured in solutions of low pH, low H_2S and a high salinity ($> 5\%$ wt% NaCl) [Seward, 1982., Large, 1987]. The efficiency of Zn - Pb solubility and transport for the fluid conditions proposed (figure 16) is great enough to achieve the concentration of these metals present at the Wagga Tank Prospect.

10.1 INTRODUCTION

The questions involved in considering the genesis of the mineralization at the Wagga Tank Prospect include:

- (1) The source of the metals and the metal complexing ligands.
- (2) The timing of the mineralization (ie. synsedimentary or epigenetic).
- (3) The heat source.
- (4) The controls on deposit formation, including both vein and massive type sulphides.

10.2 METAL / LIGAND SOURCE

The ultimate source of the metals deposited in the Wagga Tank Prospect is most likely to be the volcanics or sub-volcanic intrusions of the Mount Kennan Formation. The metal source may have been the trace concentrations in the siltstone-slate sequence, which was probably derived from weathering of the nearby volcanic centres. The metal source is unlikely to be the pre - Devonian metamorphics and Silurian intrusions that form the basement below much of the Cobar Supergroup. No significant massive sulphide mineralization in the basement owes its origin to a pre - Lower Devonian event [Glen et al., 1985].

As the sulphur originated from seawater it is reasonable to assume that this was the source of most of the metal complexing ligands. A 5 wt% NaCl equivalent solution would be formed by less than a 2 fold concentration of seawater, assuming a salinity similar to the present day (3.5 wt% dissolved solids, [Krauskopf, 1967]). This could be achieved through a heated rock pile from which further metal complexing agents are leached.

10.3 SYNGENESIS / EPIGENESIS

Characteristics of the prospect that could be used to imply a syn-sedimentary (syngenetic or diagenetic) origin include:

- The banded massive sulphides as a sea-floor deposit and the vein type mineralization as a stringer zone.
- The apparent conformity of the massive sulphide to bedding.
- The proximity of the mineralization to a deep-water marine euxinic basin containing obvious exhalative syn-sedimentary Fe sulphides.

The observations that imply an epigenetic origin include:

- (1) The argillic alteration zone was apparently produced by the same hydrothermal event as sulphide precipitation and indicates that the mineralization is epigenetic rather than syngenetic. The argillic alteration zone enveloping the massive and vein type sulphides is only found in a narrow but vertically extensive plane of high permeability. Alteration is not found away from the mineralization into the volcanoclastic sequence. Therefore the mineralizing fluids rose upwards from depth when the beds were in, or near, the present orientation and not from the stratigraphically lower volcanoclastic sequence while the beds were horizontal, as would be required in a syn-sedimentary model.
- (2) Much of the mineralization lies in the volcanoclastic sequence. The sequence was deposited from turbidity currents that contained sufficient energy to transport clasts up to 4cm in diameter. The environment is unlikely to have been conducive to the precipitation of finely banded syngenetic sulphides but could provide the host for diagenetic mineralization. However, a 5% wt% NaCl equivalent fluid at

325°C that is not boiling must be at a minimum pressure of 100 bars which is equivalent to 1500m water depth [Haas, 1971]. This depth occurs in off-shelf basins that do not contain coarse clastic sediments.

- (3) Fragments of the siltstone-slate sequence have been incorporated into the sulphides, indicating that the host rocks were lithified prior to mineralization (It is possible that the fragments were incorporated into the sulphides during plastic deformation). Quartz and sulphide filled fractures in the volcanoclastic sequence imply post lithification mineralization.
- (4) The presence of sulphide banding is no criterion for syngensis as it is found in known epigenetic deposits [Guilbert and Park, 1986]. The banding was probably formed by cyclic precipitation of various sulphide phases on the wall-rock in large fractures (parallel banding) or onto a coarse grained sulphide nucleus (colloform banding).

10.4 HEAT SOURCE

Volcanism and sub-volcanic intrusive activity is considered unlikely to have been the heat source. As the mineralization is envisaged as syn- or post-major deformation for the reasons detailed in 10.3, back - arc basin sedimentation and volcanism in the Cobar Region had ceased.

The heat required to set up the hydrothermal system was possibly provided by the energy sources which also produced the regional deformation and low grade metamorphism. Fluids containing seawater sulphur, trapped as connate water in the rock pile since sedimentation, would have been released during metamorphism. As the regional metamorphic influence must have occurred at reasonable depths, an over - pressured fluid is envisaged as

having travelled up a zone of high permeability to reach a gradient in terms of fO_2 / pH / T / dilution or a reduced sulphur source, inducing metal precipitation. Disseminated sulphides and sericite and chlorite alteration, ubiquitous throughout the Mt. Kennan Volcanics, reach the greatest development in the mineralized zone as wallrock alteration, where open fractures apparently concentrated the metamorphic fluid. Active circulation of ocean water into a convective cell, as in the model proposed by Scott [1983], could not occur if the driving force was metamorphism. Minor solid state deformation of the sulphides implies precipitation before the end of deformation or a mild, post mineralization deformation event.

The importance of faulting as a heat source and localizing influence is difficult to ascertain. Extensive block faulting is known to occur throughout the Mount Hope area [Scheibner and Barron, 1982]. Studies of aerial photographs do not define any linear feature near the Wagga Tank Prospect.

Glen [1987] attributes a syndeformational epigenetic origin to the copper and gold deposits in the Cobar mining field. The conclusion is based on a study of the orientation of growth fibres in fibrous veins hosting the sulphide mineralization, which indicate that the veins developed from hydraulic fracturing syntectonic to the D1 deformation. Binns et al. [1986] came to a similar conclusion by studying the relationships between wall rock alteration, cleavage and vein development and the mineralization at the C. S. A. mine, Cobar. The mineralization appears to have been emplaced during the early stages of a deformational - metamorphic episode that continued after subsequent ore deposition.

10.5 POSITION

The factors responsible for the position of the deposit is the zone of tectonic brecciation produced by the effect of the fold flexure on a competency contrast between the siltstone - slate and volcanoclastic sequences during the major deformation.

10.6 MASSIVE / VEIN TYPE SULPHIDES

The formation of both massive and vein type sulphide, if a primary feature, may be due to a variability in the rate of metal precipitation from the mineralizing fluid. According to this model the vein type sulphide precipitates deeper in the conduit where a lower gradient in terms of pH / fO_2 / T / fS_2 or dilution allows for a slower rate of sulphide precipitation and the formation of coarser grains. The massive type sulphide would precipitate rapidly from solution under conditions of a higher gradient or interface in terms of pH / fO_2 / T / fS_2 or dilution resulting in the formation of only fine grained sulphides. The mechanism for this would be analagous to the melt freezing rate factor in igneous rock grain size [Carmichael et al., 1974].

10.7 AN ANALOGY

The Wagga Tank Prospect has a number of features that are common to many of the principal deposits of the Cobar mining field [Gilligan, 1974; Suppel, 1982; Glen et al., 1985; O'Connor, 1980; Rayner, 1969; Russell and Lewis, 1965; Sangster, 1979].

- (1) An affinity for steeply dipping lithological contacts that have been sheared or brecciated.
- (2) Typically occurring in flexures or folds along such contacts.
- (3) Tendency to be narrow steeply plunging elongate bodies.
- (4) The contact tends to be between a thinly bedded and cleaved turbiditic siltstone, and coarser clastic beds or felsic volcanics of the Cobar Supergroup.

- (5) The sulphide mineralogy is predominantly pyrite, chalcopyrite, sphalerite and galena and is often banded
- (6) The mineralization is commonly within a silicified and chloritized envelope.



CONCLUSIONS

- (1) The primary mineralization consists of pyrite, sphalerite, galena and chalcopyrite with rare pyrrhotite and cubanite. The gangue consists of quartz in the vein type sulphide and chlorite and sericite in the massive type sulphide.
- (2) The mineralization is located in a zone of tectonic brecciation and hydrothermal alteration along a folded contact.
- (3) A fluid inclusion study indicates:
 - (i) A salinity of about 5 wt% NaCl equivalent for the mineralizing fluid.
 - (ii) Two distinct temperatures of significant mineralization precipitation as determined by homogenization temperatures, at about 200°C and 325°C.
 - (iii) Sulphide precipitation may have been due to a mixing with cooler less saline fluid (probably ground water).
- (4) Sulphur isotope studies indicate:
 - (i) That the sulphide phases approached isotopic equilibrium.
 - (ii) The temperature of sulphide precipitation determined from isotope fractionation between sphalerite and galena was within the range 324°C to 408°C.
 - (iii) Most of the sulphur was derived from sea-water.
- (5) Chlorite analyses indicate:
 - (i) A temperature of the massive type mineralization of 228°C - 302°C.
 - (ii) A log f_{O_2} of -31.9 - -42.5.
 - (iii) A log f_{S_2} of -10.1 - -15.9
- (6) Thermodynamic calculations based on fluid inclusion, sulphur isotope and petrographic data indicate:
 - (i) pH of between about 3 and 4.5.
 - (ii) Log f_{O_2} values of about -29.5 to -31.7

- (iii) The evolution of the hydrothermal fluid involved an increase in temperature and an increase in Cu - Fe content.
- (7) The hydrothermal fluid was probably derived from dewatering of the rock pile during metamorphism accompanying the major deformation.

ACKNOWLEDGEMENTS

I wish to thank Homestake Australia Limited for allowing me the opportunity to work on such a project, and for the logistic support provided throughout the year. I am greatly indebted to Mr. Graeme Rabone of Homestake for his inspiration and assistance .

I would particularly like to express my gratitude to Dr. Ross Both for his enthusiastic supervision and invaluable advice provided during the year.

I also convey my appreciation to Dr. Keith Turnbull for his help with sulphur isotope work, Dr. J. Walshe (Australian National University) for processing the chlorite data, and to Dr. Yvonne Bone and Mr. Evert Bley for advice with fluid inclusions.

Acknowledgement is made to; Wayne Mussared, Geoff Trevellyan, John Stanley, Phil McDuie, John Willoughby, Rick Barrett, Chris Badcock and Fleur Delaine for their help over the year, and to Bev Otte from Homestake for drafting of the field map.

BIBLIOGRAPHY

- Barron, L. M. 1977: Some sediments and porphyries from the Mount Hope area. New South Wales Geol. Surv. - Report Petrology 1977/25 (unpubl.) (GS1977/304).
- Binns, R. A. and Appleyard, E. C. 1986: Wallrock alteration at the Western System of the CSA Mine, Cobar, New South Wales, Australia. Applied Geochemistry 1 :211 - 225.
- Bone, Y., and Griffin, B. J. 1984: Qualitative analysis of the fluid in fluid inclusions, using the electron micro-probe. Geol. Soc. Aust. Abs. 12. 7th Aust. Geol. Conv. Sydney.
- Bouma, A. H. 1962: Sedimentology of some flysch deposits. Amsterdam, Elsevier 168p.
- Braithwaite, R. L. 1975: Final report on E. L. 569, E. L. 576 and E. L. 580. Mount Hope N. S. W. Newmont Pty. Ltd. - Report (unpubl.) (GS1975/050).
- Carmichael, I. S. E., Turner, F. J., and Verhoogen, J. 1974: Igneous Petrology. McGraw Hill. New York: 739p.
- Claypool, G. E., Holster, W. T., Kaplan, I. R., Sakai, H., and Zak, I. 1980: The age curves of sulphur and oxygen isotopes in marine sulphate and their mutual interpretation. Chem. Geol. 28: 199 - 260.
- Crawford, M. L. 1981: Phase equilibria in aqueous fluid inclusions. In: Hollister, L. S., and Crawford, M. L. Short course in fluid inclusions: Applications to petrology. Miner. Assoc. Canada. Short Course Handbook Vol. 6 May 1981 Calgary: 75-100.
- Eldridge, C. S., Barton, P. B. and Ohmoto, H. 1983: Mineral textures and their bearing on formation of the Kuroko orebodies. Econ. Geol. Mon. 5: 241 - 281.
- Gilligan, L. B., 1974: Cobar and Mineral Hill synclinal zones. In: The Mineral Deposits of New South Wales. Geol. Surv. N. S. W. : 148 - 171.
- Glen, R. A. 1982: The amphitheatre group, Cobar, New South Wales: Preliminary results of new mapping and implications for ore search. N. S. W. Geol. Survey - Quarterly Notes. 49: 1 - 14.
- Glen, R. A. 1985: Basement control of the deformation of cover basins: An example from the Cobar district in the Lachlan Fold Belt, Australia. Jour. Struct. Geol. 7: 301 - 315.
- Glen, R. A., MacRae, G. P., Pogson, D. J., Scheibner, E., Agostini, A., and Sherwin, L., 1985: Summary of the geology and controls of mineralization in the Cobar Region: Cobar Field Conference. N. S. W. Geol. Survey Report GS1985/203. Dept of Mineral Resources: 91p.
- Glen, R. A. 1987: Copper- and gold - rich deposits in deformed

- turbidites at Cobar, Australia. Their structural and hydrothermal origin. *Econ. Geol.* 82: 124 - 140.
- Guilbert, J.M. and Park, C.F. 1986: *The Geology of Ore Deposits*. Freeman and Co. New York: 985 p.
- Haas, J.L. 1971: The effect of salinity on the maximum thermal gradient of a hydrothermal system at hydrostatic pressure. *Econ. Geol.* 66: 940 - 946.
- Homestake, 1987: Homestake Gold of Australia Limited, Prospectus - 17th Sept 1987 to 16th March 1988: 128p.
- Krauskopf, K.B. 1967: *Introduction to Geochemistry*. McGraw Hill, New York: 721p.
- Kuno, H. 1969: Differentiation of basalt magmas. In: Hess, H.H., and Poldervaart, A. (Eds.). *Basalts; The Poldervaart Treatise on Rocks of Basaltic Composition*. 2 :623 - 688.
- Large, R.R. 1987: Some thoughts on the hydrothermal fluid chemistry of Gold - Copper - Iron oxide systems. In: *Geology and Geochemistry of Gold - Copper - Iron Oxide Systems: Tennant Creek and Starra Districts*. Workshop Manual 1: 235 - 248.
- Metzger, F.W., Kelly, W.C., Nesbitt, B.E., and Essene, E.J. 1977: Scanning electron microscopy of daughter minerals in fluid inclusions. *Econ. Geol.* 72 No. 2: 141 - 152.
- O'Connor, D.P.H. 1980: Evidence for an exhalative origin for the Cobar District, New South Wales. *B.M.R. Jour. Aust. Geol. Geophysics* 5: 70 - 72.
- Ohmoto, H., and Rye, R.O. 1979: Isotopes of sulphur and carbon. In: Barnes, H.L. (Ed) *Geochemistry of Hydrothermal Ore Deposits*: 509 - 567.
- Ohmoto, H., Mizukama, M., Drummond, S.E., Eldridge, C.S., Pisutha - Arnond, V., and Lenagh, T.C. 1983: Chemical processes of Kuroko formation. *Econ. Geol. Mon.* 5: 570 - 604.
- Pisutha - Arnond, V., and Ohmoto, H. 1983: History, and chemical and isotopic compositions of the ore-forming fluids responsible for the Kuroko massive sulphide deposits in the Hokuroku District of Japan. *Econ. Geol. Mon.* 5: 523-558.
- Pogson, D.J. 1983: Tectonic evolution of the Cobar - Mount Hope - Mineral Hill Region, and economic implication. *Geol. Soc. Aust. - Abstract* 9: 301 - 302.
- Pogson, D.J., and Felton, E.A. 1978: Reappraisal of geology, Cobar - Canbelego - Mineral Hill Region, Central Western New South Wales. *N.S.W. Geol. Surv. - Quarterly Notes* 33: 1 - 4.
- Potter, R.W., Clyne, M.A., and Brown D.L., 1978: Freezing point depression of aqueous sodium chloride solutions. *Econ. Geol.* 73 no. 2: 284 - 285.
- Rabone, G. 1987: Homestake - Cyprus joint venture Cobar - Mount

Hope project, exploration report, proposed programme and budget and expenditure statements. Report by Homestake Australia Ltd. to March 1987, (unpublished).

- Rayner, E. O. 1969: The copper ores of the Cobar region, New South Wales. N. S. W Geol. Surv. - Memoir Geology 10: 131p.
- Robinson, B. W. and Kusakabe, M. 1975: Quantitative preparation of sulphur dioxide, for $^{34}\text{S}/^{32}\text{S}$ analyses, from sulphides by combustion with cuprous oxide. Analytical Chem. 47: 1179 - 1181.
- Roedder, E. 1984: Fluid inclusions. Reviews in Mineralogy. 12. Mineralogical Society of America. 644 p.
- Russel, R. T., and Lewis, B. R. 1965: Gold and copper deposits of the Cobar District. In: Geology of Australian Ore Deposits, 2nd edn. Commonwealth Mining and Metallurgy Congress, Aust. and N. Z., 8th - publication 1: 411 - 419.
- Sangster, D. F. 1968: Relative sulphur isotope abundances in ancient seas and strata-bound sulphide deposits. Geol. Assoc. Canada, Proc. Vol. 19: 79 - 91.
- Sangster, D. F. 1979: Evidence of an exhalative origin for deposits of the Cobar District, New South Wales. B. M. R. Jour. Geol. Geophysics 4: 15 - 24.
- Scheibner, E., and Barron, L. 1982: The Mount Hope Group and co-magmatic granites in the Mount Hope area, New South Wales. In: Sutherland, F. C., Franklin, B. J., and Waltho, A. E., (Eds.) 1985: Volcanism in Eastern Australia. Geol. Soc. Aust. N. S. W. Div Pub 1, Symp. Nov. 1982, Sydney.
- Scheibner, E. 1987: Geology of the Mount Allen 1:100,000 Sheet 8032, New South Wales Geological Survey, Sydney.
- Scott, S. D. 1983: Basalt and sedimentary hosted seafloor polymetallic sulphide deposits and their ancient analogues. Invited papers from M. T. S. - I. E. E. E. Conference. "Oceans 83". San Francisco.
- Seward, T. M. 1982: The transport and deposition of gold in hydrothermal systems. In: Foster, R. P. (ed) Gold 1982: 99 - 81.
- Shepherd, T. J., Rankin, A. H., Alderton, D. H. M. 1985: A Practical Guide to Fluid Inclusion Studies. Glasgow. Blackie: 239 p.
- Styrt, M. M., Brackmann, A. J., Holland, H. D., Clark, B. C., Pisutha - Arnond, V., Eldridge, C. S., and Ohmoto, H. 1981: The mineralogy and the isotopic composition of sulphur in hydrothermal sulphide / sulphate deposits on the East Pacific Rise, 21^oN latitude. Earth Plan. Sci. Letters. 53: 382 - 390.
- Suppel, D. W., 1982: The geology and mineral deposits of the Mount Hope area, New South Wales. Dept. Miner. Resources. Geol. Surv. Rep. No. GS1982/476.

- Walshe , J.L. 1986: A six - component chlorite solid solution model and the conditions of chlorite formation in hydrothermal and geothermal systems. Econ. Geol. 81 No. 3: 681 -703.
- Winchester, J. A., and Floyd. P. A. 1977: Geochemical discrimination of different magma series and their differentiation products using immobile elements. Chem. Geol. 20: 325-343.
- Winkler, H. J. F. 1979: Petrogenesis of metamorphic rocks. Fifth Edition. Springer - Verlag, New York: 348 p.
- Ypma, P. J. M., 1979: Water soluble - CO₂ systems. In: Workshop Manual on Fluid Inclusions. La Trobe University, Melbourne, Australia.

APPENDIX 1

SELECTED THIN SECTION DESCRIPTIONS

-HOST ROCKS-

Sample 886-06

Hand specimen

A brown silicified massive coarse grained sandstone cross-cut by at least two phases of quartz veining.

Thin section

The quartz clasts are of two types; either medium grained (1mm) slightly strained, rounded quartz displaying polygonal contacts and dissolution along grain boundaries or polycrystalline aggregates (2mm) of amoeboid interlocking grains.

Other clasts consist of quartz siltstone, sericitized formerly micaceous siltstone or fine grained quartz sandstone with a sericitized matrix. Rare primary muscovite occurs in the interstices.

The matrix consists of sericite with extensive hematite staining. Zircon occurs as an accessory.

quartz grains	65%
siltstone fragments	15%
quartz aggregates	10%
sericite	10%
zircon	tr
primary muscovite	tr

Interpretation

A fluviatile or deltaic coarse grained sandstone with some clasts being derived from a metamorphic terrain.

Sample 886-07

Hand specimen

A purple \ brown massive quartz arenite.

Thin section

The section displays small scale graded bedding. The coarse fraction consists of rounded strained quartz grains (0.5-1mm)

exhibiting undulose extinction and micro-fracturing, and minor labile fragments in a hematite stained micaceous matrix. The coarser fraction grades into opaque rich, fine grained (0.2mm) quartz sandstone with interstitial muscovite and biotite aligned to form a weak sedimentary fabric. Aggregates of fine grained quartz represent incipient recrystallization. Extensive fracturing occurs throughout.

quartz grains	50%
muscovite/biotite	25%
opaques	20%
labile clasts	5%

Interpretation

A medium to fine grained submature arenite from a fluvial environment.

Sample 886-08

Hand specimen

A white massive very fine grained sandstone with minor hematitic staining along fractures.

Thin section

Very fine grained (<0.125mm) corroded equant polygonal to interlobate quartz containing abundant inclusions in a sericite matrix. Minor primary muscovite grains, zircons and opaques occur.

quartz	70%
sericite	25%
opaques	3%
primary muscovite	2%
zircon	tr

Interpretation

A very fine grained sericitized silty sandstone.

Sample 886-09

Hand specimen

A weathered light purple crystal tuff with a spotted appearance produced by small (0.5mm) altered white phenocrysts. A weak sericite fabric is evident on the weathered surface.

Thin section

The only primary mineral remaining in the section is quartz, which occurs as embayed medium grained (1-2mm) equant phenocrysts (15%) displaying shadowy extinction and deformation lamellae.

The rest of the section is composed of 1-2mm completely sericitized relict grains (50%) and flattened pumice fragments (10%) in a very fine grained sericite, sutured quartz and hematite stained groundmass. Elliptical relict phenocrysts contain abundant opaques clustered around the diffuse boundaries and may have been original mafic minerals or lithic fragments. Minor subhedral lath shaped (1-2mm) sericite pseudomorphs of inferred feldspar occur.

sericite	50%
quartz groundmass	25%
quartz phenocrysts	15%
opaques	10%

Interpretation

A crystal or lithic-crystal tuff of rhyolitic or dacitic composition that has been subjected to low grade metamorphism.

Sample 886-16

Hand specimen

A massive generally aphanitic siliceous dark grey acid volcanic with sporadic (5%) clear quartz phenocrysts to 2 mm. Weathering

surfaces display a convoluted fabric presumed to be flow banding.

Thin section

A partial alteration mineral assemblage of chlorite and sericite hosting quartz and remnant k-feldspar and plagioclase phenocrysts.

K-feldspar and plagioclase occur as minor remnant laths (3mm) altered by pervasive sericitization, particularly in the cores. A sodium cobalti-nitrite test revealed abundant k-feldspar in the groundmass. Occasional equant quartz phenocrysts displaying shadowy extinction occur to 2mm.

Decussate lepidoblastic chlorite after probable biotite, and sericite make up the groundmass mineralogy along with k-feldspar and acicular plagioclase. Minor disseminated opaques occur throughout.

Secondary quartz, carbonate and opaques occur as fracture fill.

sericite	25%
chlorite	25%
k-feldspar - phenocrysts	10%
- groundmass	10%
plagioclase	10%
quartz - phenocrysts	5%
- vein	5%
opaques - vein	3%
- disseminated	2%
carbonate - vein	5%

Interpretation

A flow banded rhyolite subjected to greenschist facies metamorphism.

Sample 886-43

Hand specimen

A weathered red amygdaloidal lava flow sample. The quartz filled amygdales (1 to 20mm) are elipsoidal to rod like with an X Y Z axis ratio of up to 1:1:12.

Thin section

The amygdales consist of radially oriented inward pointing prismatic quartz crystals that increase in size (<0.1 to 1mm) towards the core. Some cores posses voids filled with an acicular hematite network. Fractures penetrating the amygdales also contain hematite.

The groundmass consists of small (0.2mm) corroded quartz grains and intensely hematite stained, indistinguishable mineralogy.

groundmass	60%
Amygdales	40%

Interpretation

The relatively unstrained nature of the prismatic quartz and the hollow voids suggests later quartz infilling of oblate to rod like vesicles rather than the solid state deformation of spherical amygdales. The rock is representative of an acid lava flow that erupted with a high volatile content. The lava may have been extruded onto a wet surface resulting in the formation of pipe amygdales during devolatilization.

Sample 886-11

Hand specimen

A fine grained pink tuff hosting small (0.5mm) grains of quartz and possessing a weak planar fabric.

Thin section

The quartz occurs as small (0.2 - 1mm) aggregates of fine polygonal grains displaying shadowy extinction and embayed

boundaries.

The groundmass is composed of fine grained strained and corroded quartz (20%) and pervasive fine grained sericite aligned to form a planar fabric. Opaques are disseminated throughout the groundmass, including cubic hematite pseudomorphs of pyrite.

quartz	60%
sericite	30%
opaques	10%

Interpretation

A crystal tuff altered by low grade metamorphism.

Sample 886-12

Hand specimen

A light purple aphanitic acid tuff containing numerous iron stained spherical voids (1-5mm) resulting from the weathering of sulphide blebs.

Thin section

The rock is composed almost entirely of flattened sericitized pumice fragments (to 10mm) randomly oriented in a sericite groundmass.

Rare small (0.5mm) phenoclasts of quartz, and fine grained sutured quartz aggregates (2mm) occur. Minor relict inferred feldspar laths to 2mm are found as phenoclasts interstitial to the pumice fragments. Sericitization and hematite staining are pervasive.

sericite	60%
hematite	20%
quartz	15%
voids	5%

Interpretation

An altered pumice-lithic tuff originally containing sulphides.

Sample 886-2

Hand specimen

A light grey silicified siltstone displaying a prominent fabric of parallel discontinuous purple lensoidal banding 2-6cm long by 0.5-2mm thick and 5-10mm apart. The bands tend to follow a specific plane. Veins of the same apparent lithology cross-cut at high angle. Small (1mm) round light purple blebs occur in the lighter siltstone.

Thin section

In this section, fine grained quartz, feldspar, muscovite and opaque clasts comprise the siltstone fraction. A weak nemato - blastic fine muscovite preferred orientaton probably represents a weak metamorphic, rather than a sedimentary fabric as it cross-cuts the fine grained bands at thirty degrees.

The purple bands consist of a slightly coarser detrital component and a higher concentration of opaques than the rest of the sample. Due to the bifurcation of some bands their interpretation as a sedimentary fabric is tentative.

Quartz and hematite veins cross-cut both the "bedding" and muscovite fabrics. Dark blebs scattered throughout the sample are spherical zones of Fe staining probably indicative of weathered fine grained sulphides.

quartz	60%
muscovite/sericite	20%
feldspar	10%
opaques	10%

Interpretation

A deep water distal, probably turbiditic siltstone with a possible volcanic input (euhedral feldspar).

Sample 886-101

Hand specimen

A drill - core specimen displaying subrounded lithic clasts to 20mm of grey tuff scattered through a light greenish, grey tuffaceous matrix.

Thin section

The lithic clasts (15%) are composed of sericitic siltstone, unwelded vitric - crystal tuff, polycrystalline quartz aggregates and granophyre. The bulk of the section consists of anhedral to euhedral phenocrasts of sericitized and chloritized K - feldspar (probably orthoclase) (15%), and quartz (10%), ranging from 0.2 to 3mm in size.

The matrix (60% of sample) is composed of unwelded, formerly vitric, cusped shards about 0.1 to 0.5mm in size, that are silicified and rimmed by fine sericite. Much of the matrix has devitrified to fine K - feldspar, sericite and minor chlorite.

Equant phenocrysts of inferred ilmenite to 0.25mm in size, have been pseudomorphed by aggregates of fine rutile. Zircon is accessory.

Irregular veins (2mm in thickness) contain toothy quartz, subhedral pyrite, anhedral translucent brown sphalerite and galena.

sericite	45%
K - feldspar	25%
quartz	15%
chlorite	5%
rutile	2%
zircon	tr
pyrite/sphalerite/galena	8%

Interpretation

A vitric - lithic - crystal tuff of rhyolitic composition.

Sample 886-05

Hand specimen

An iron stained highly silicified conglomerate with angular to subrounded siltstone and fine silicified sandstone clasts set in a massive quartz and hematite stained cement. Clasts range from grit sized to 40mm in size. Extensive quartz filled fractures occur.

Thin section

The section displays subrounded clasts of fine silicified quartz - feldspar sandstone (20%) and silicified siltstone (60%) set in a hematite stained, quartz cemented silty matrix (20%) containing both well rounded and angular fine quartz grains. The angular quartz grains display bipyramidal refraction patterns indicative of low pressure crystallization and may represent a volcanic input.

At least two phases of quartz veining are present. Small (1mm) voids after inferred sulphides occur.

Sample 886-54

Hand specimen

A coarse grained holocrystalline dark green granite dominated by anhedral white k-feldspar phenocrysts to 1.5cm.

Thin section

The feldspar occurs as large (to 15mm) interlobate anhedral phenocrysts of sericitized k-feldspar and medium grained (2mm) subhedral plagioclase. Sericitization is prevalent in both feldspars, with remnants usually confined to the cores. Quartz occurs as equant fractured grains up to 4mm displaying shadowy extinction and complexly intergrown corroded boundaries,

especially when adjacent to feldspar. Granophyric texture is common.

Intense chloritic and sericitic alteration, and minor carbonate, occurs throughout. Opaques are intimately associated with chlorite.

Zircon, sphene and rutile are accessory.

sericite	30%
quartz	20%
granophyre	15%
k-feldspar	10%
chlorite	10%
opaques	6%
plagioclase	5%
sphene	2%
zircon	1%
carbonate	1%
rutile	tr

Interpretation

An altered plutonic rock of granitic composition.

Sample 886-77

Hand specimen

The drill core specimen is a dark pelitic rock of alternating medium grey and dark grey planar laminated bedding 3 to 12mm thick. The dark grey beds display very small scale load structures and pass gradationally into the lighter lithology.

Thin section

A tectonic foliation defined by an alignment of sericite and wisps of carbonaceous material or graphite cut the planar bedding

at about 45°.

The dark beds are composed of silt fraction quartz, sericite and carbonaceous material. Lenses of framboidal pyrite (1 - 5mm) which lie parallel to bedding are seen as spherical aggregates (0.01 - 0.04mm) of 1 - 2 micron sized euhedral, octahedral pyrite crystals. Framboidal pyrite is confined to the darker layers.

The light grey beds are composed almost entirely of sericite lesser quartz and some fine disseminated octahedral and cubic pyrite. Carbonaceous material is far less abundant in the lighter beds.

Small grains of carbonate (0.1mm) and minor detrital muscovite are distributed throughout both light and dark beds. Rutile occurs as an accessory.

sericite	60%
quartz	15%
carbonaceous material	10%
framboidal pyrite	6%
detrital muscovite	5%
carbonate	2%
disseminated pyrite	1%
rutile	1%

Interpretation

A distal turbidite deposited in deep water in which syn-sedimentary sulphides were precipitating.

Sample 886-32

Hand specimen

A dark grey carbonaceous slate cut by a 0.5mm thick quartz vein.

Thin section

The vague bedding is cut at a low angle by a pervasive tectonic fabric defined by fine acicular sericite and wisps of carbonaceous material or graphite.

Bedding is defined by variations in the abundance of fine quartz in the 10mm thick layers. Elipsoidal grains of carbonate (0.2mm) with the long axis parallel to the fabric suggests that either the carbonate was pre-tectonic or a post tectonic replacement of strained clasts.

1 to 4mm long lenses of framboidal pyrite occur parallel to the bedding, but show a slight re-alignment towards the tectonic fabric.

A quartz and carbonate vein bisects the bedding at a high angle.

sericite	60%
quartz	20%
framboidal pyrite	10%
carbonaceous material	5%
carbonate	5%
rutile	tr

Interpretation

A distal turbidite deposited in deep water in which syn-sedimentary sulphides were precipitating.

Sample 886-64

Hand specimen

The sample was taken from the conformable contact between the volcanoclastic sequence and the siltstone -slate sequence.

The drill-core sample is a light grey pelitic rock containing planar bedded, darker grey silty sandstone horizons. Bedding ranges from 3 to 20mm in thickness. A pyrite vein cross-cuts the

bedding at high angles.

Thin section

A weak sericite fabric cuts the bedding at high angles.

The lighter grey beds are composed of sericitic quartz siltstone, opaques and minor primary mica.

The darker beds consist of coarser siltstone to fine grained quartz sandstone with minor feldspar, altered opaque rich fragments or grains of inferred lithics or mafic minerals (0.5mm) and aggregates of opaques (0.2mm). Anhedral phenoclasts/grains (0.5mm) of dark green translucent sphalerite are bordered by quartz filled pressure shadows in a sericitized matrix.

There is some grain size gradation between beds, and within beds of the fine silty sandstone fraction. Small scale load structures occur on the base of the coarser beds.

sericite	48%
quartz	30%
opaques	10%
feldspar	5%
primary mica	5%
sphalerite	2%

Interpretation

A turbidite containing a possible detrital volcanic component.

Sample 886-25

Hand specimen

A dark grey tuffaceous silty sandstone containing anhedral phenoclasts (1-5mm) of pink k-feldspar. The sample contains quartz veins hosting grains of pyrite and chalcopyrite (1mm).

Thin section

The most abundant clast is composed of quartz that commonly

occurs as subrounded aggregates (1mm) of strained polygonal grains. Altered mafic clasts consist of chlorite (50%), cubic pyrite and anhedral opaques (50%)(<0.2mm). Occasional sericitized and chloritized clasts are devoid of opaques.

Small (0.5mm) corroded anhedral phenoclasts of angular quartz displaying shadowy extinction and k-feldspar occur.

The matrix is composed of very fine grained chlorite and sericite. Sphene, rutile and detrital zircon are accessory.

quartz aggregates	20%
quartz phenoclasts	20%
chloritized and pyritic clasts	20%
interstitial sericite	20%
interstitial chlorite	10%
chloritized and sericitized clasts	5%
unidentified opaques	4%
Zircon	1%
sphene	tr
rutile	tr

Interpretation

A tuffaceous silty sandstone altered by low grade metamorphism.

Sample 886-48

Hand specimen

The sample is a drill-core specimen of dark grey carbonaceous knotted slate containing augen 1-4mm in diameter.

Thin section

The augen are asymmetric, elliptical zones of sericite and clay devoid of carbonaceous material, with cores containing equant prismatic clay pseudomorphs that were likely to have been andalusite porphyroblasts.

A carbonaceous material and sericite defined fabric wrap around the augen with the foliation direction parallel to the augen long axis. An apparent weakly defined second fabric is probably bedding. Fine disseminated pyrite cubes (0.01 to 0.03mm), traces of rutile, and chlorite occur between the augen.

sericite	65%
clay pseudomorphs	15%
carbonaceous material	10%
pyrite	8%
chlorite	2%
rutile	tr

Interpretation

A pyritic carbonaceous slate that appears to reflect a somewhat higher degree of metamorphism than revealed by the other pelitics. A degree of asymmetry of the augen indicates a shearing movement during deformation.

APPENDIX 2

WHOLE ROCK ANALYSIS

MAJOR AND TRACE ELEMENT COMPOSITIONS

MAJOR ELEMENT ANALYSIS

Sample 886-	43	09	10	11	16	33	54
	weight %						
SiO ₂	74.39	78.91	72.90	78.08	74.95	73.00	68.62
Al ₂ O ₃	11.16	11.87	13.24	12.24	12.80	14.51	14.60
Fe ₂ O ₃	9.65	4.54	3.38	2.08	2.07	1.72	5.68
FeO	0.35	0.19	0.09	0.18	0.11	0.21	0.16
MnO	0.03	0.02	0.03	0.00	0.02	0.01	0.09
MgO	0.46	0.53	0.60	0.53	0.67	0.65	2.11
CaO	0.06	0.02	0.01	0.03	0.10	0.80	1.29
Na ₂ O	0.03	0.04	0.17	0.09	1.92	3.05	1.95
K ₂ O	3.18	3.29	8.53	6.45	7.07	5.54	4.43
TiO ₂	0.28	0.27	0.30	0.28	0.26	0.19	0.94
P ₂ O ₅	0.04	0.03	0.07	0.02	0.08	0.30	0.21
Total	99.63	99.70	99.31	99.98	100.30	99.97	100.07

TRACE ELEMENT ANALYSIS

Sample 886-	43	09	10	11	16	33	54
	ppm						
Sr	6.1	7.1	38	39	74	118	150
Rb	173	189	318	246	209	249	191
Y	32	33	42	35	44	21.1	40
Zr	213	194	249	219	211	79	215
Nb	15.2	17.8	17.7	16.3	18.6	15.1	14.5
Ba	125	229	1083	579	745	523	668
Sc	5.1	5.6	4.9	5.2	4.8	5.6	16.1

V	24	19	23	22	17	13	110
Ga	15	16	17	13	16	20	20
Ce	73	43	98	71	83	34	89
Nd	23	9	36	23	40	11	36
Ni	3	2	4	3	4	6	20
La	38	25	53	37	48	15	85
Cu	126	35	71	31	5	6	19
Pb	12	14	9	14	6	12	27
Zn	41	13	22	13	5	6	69
As	3	1	1	4	1	1	6
Mo	4.0	3.5	3.2	4.1	1.2	4.0	1.2
Cr	9	7	5	8	5	13	59

METHODS FOR CHEMICAL ANALYSIS

Sample preparation

- (1) Samples were crushed using a jaw crusher.
- (2) Crushed samples were ground to a fine powder using a Siebtechnik tungsten carbide mill.
- (3) Powder for major element analysis was ignited overnight at 960°C and the loss on ignition recorded. 280mg of ignited sample, 20mg of sodium nitrate and 1.5g of flux were weighed out and mixed to produce a fused disc.
- (4) Approximately 5g of each unignited sample was used to make pressed pellets for trace element analysis.

Major element analysis

- (1) SiO₂, Al₂O₃, Fe₂O₂, MnO, MgO, CaO, Na₂O, K₂O, TiO₂ and P₂O₅ concentrations were determined using the programmable Siemens

X. R. F. Spectrometer.

- (2) Na_2O concentrations were determined by digesting 50-60 mg of ignited sample in a teflon beaker containing 2ml of 50% sulphuric acid and 10ml of 50% hydrofluoric acid at 110°C for twelve hours. Sample solutions were made up to 100ml with deionised water and the Na_2O concentrations determined using the Varian Techtron Atomic Spectrophotometer.
- (3) FeO concentrations were determined by digesting 150-400mg of sample in 10ml of 50% sulphuric acid and 5ml of 50% hydrofluoric acid in a platinum crucible at 300°C for twenty minutes. The solution filled crucible is then placed into a solution of 300ml of deionised water, 10ml of 50% sulphuric acid, 30ml of saturated boric acid and N-Phenyl Anthranilic Acid indicator. This solution is then titrated using 0.01N ceric sulphate solution where 1ml of titrate equals 0.7185mg of FeO .

Trace element analysis

- (1) Rb, Sr, Zr, Nb, Y, Cr, Ni, Cu, Pb, Zn, Ba, Sc, V, Ga, Ce, Nd, La, As, Cr and Mo abundances determined using a Siemens X. R. F. Spectrometer.

APPENDIX 3

SELECTED POLISHED THIN SECTION DESCRIPTIONS

-MINERALIZATION-

Sample 886-21

Hand specimen

Very coarse grain vein type sulphide devoid of gangue minerals except rare quartz. Contains pyrite, chalcopyrite, galena and sphalerite.

Polished thin section

In thin section the sulphides display crude banding up to 10mm in thickness.

Pyrite usually occurs as fractured anhedral grains from 0.1mm to 1mm completely enclosed within bands of chalcopyrite. The grains are angular but no sharp corners are found and the rims are usually slightly embayed. Euhedral pyrite occurs within large galena masses.

Chalcopyrite occurs as a large amorphous mass enclosing pyrite, and as inclusions (<0.05mm) in sphalerite. In transmitted light the anhedral inclusions of chalcopyrite occur within individual grains of sphalerite and show no affinity for cleavage traces. The inclusions appear to be a replacement feature of sphalerite by chalcopyrite rather than exsolution.

Galena occurs as large (10mm) anhedral enveloping grains and as small inclusions (0.01mm) in pyrite. Cleavage traces are commonly curved suggesting deformation of the sulphides.

Sphalerite occurs as large (20mm) anhedral amoeboid translucent brown grains closely associated with galena.

The gangue consists of strained quartz grains displaying undulose extinction, and chlorite.

chalcopyrite	30%
pyrite	25%
sphalerite	25%
galena	15%

quartz	3%
chlorite	2%

Sample 886-99

Hand specimen

Very fine grain massive sulphide displaying planar and colloform banding.

Polished thin section

The coarser sulphide grains that make up 15% of the sample are composed of euhedral to subhedral pyrite (0.25mm), amorphous sphalerite to 0.75mm, and minor anhedral chalcopyrite and galena (0.5mm).

Both pyrite and sphalerite exist predominantly as very fine grains forming extensive colloform banding.

The colloform texture consists of concentric bands (0.02 - 0.75mm thick) of alternating fine grained sphalerite, pyrite and gangue around a core of coarser grained pyrite, sphalerite, galena and gangue.

Gangue with minor fine grain euhedral pyrite and anhedral galena, sphalerite and chalcopyrite fill up the areas between the colloform structures.

The gangue is composed of fine to medium grained (0.05 - 0.75mm) strained quartz, sericite and chlorite.

The colloform texture is probably due to the precipitation of alternating sulphide phases and gangue on a coarser grained gangue and sulphide nucleus in an open void. Later stage silica rich fluids deposited quartz and sulphide fragments in the remaining spaces.

pyrite	25%
sphalerite	14%
galena	10%

chalcopyrite	1%
quartz	25%
chlorite	15%
sericite	10%

Sample 886-45

Hand specimen

A fine to medium grained porous crudely banded massive sulphide. The bands, which are about 5 to 30mm thick, display variations in the proportions of pyrite, sphalerite and galena and the abundance of voids.

Polished thin section

In thin section, bands of gangue containing euhedral and subhedral fractured pyrite (0.1 - 2mm) alternate with bands (to 8mm thick) of irregular galena grains enveloped in sphalerite. Some sphalerite grains exhibit a strong zonation, from a translucent pale yellow core to dark brown rim. Chalcopyrite, absent in the cores, gradually increases in abundance towards the rims. Minor chalcopyrite also occurs as small grains (<0.1mm) associated with pyrite and galena.

The gangue is composed of sericitized siltstone fragments, fine grain quartz, chlorite and minor carbonate grains.

pyrite	35%
sphalerite	25%
galena	8%
chalcopyrite	2%
sericite	15%
quartz	10%
chlorite	5%
carbonate	tr

Sample 886-81

Hand specimen

A green porous crudely banded fine grained massive sulphide.

Polished thin section

The banding is composed of very fine grained pyrite and gangue layers (5 - 10mm thick) alternating with coarser grained (to 1mm) sphalerite, galena and gangue.

The pyrite occurs as irregular aggregates (0.01 - 0.25mm) of very fine euhedral grains in a fine grain gangue matrix. Individual grains of coarser euhedral pyrite (0.05 - 0.25mm) with inclusions of galena and sphalerite appear to represent recrystallization of the fine pyrite aggregates, suggesting post mineralization annealing of the sulphides. Pressure shadows of galena, sphalerite and gangue are commonly associated with coarser pyrite and the aggregates.

Sphalerite occurs as long irregular grains enveloping euhedral pyrite and is closely associated with minor galena (0.1mm). Under transmitted light, the large grains are seen to be composed of sphalerite fragments displaying a cyclic zonation within an unzoned lighter sphalerite mass. This is interpreted as a hydrothermal brecciation feature, with fragments of early formed sphalerite enclosed by subsequent sphalerite precipitation. Fractures across the zonation are filled with the lighter sphalerite.

Minor chalcopyrite is found as inclusions (0.05mm) within sphalerite.

The gangue is composed of chlorite, sericite and carbonate.

pyrite	40%
sphalerite	15%
galena	5%

chalcopyrite	tr
sericite	20%
chlorite	10%
carbonate	10%

Sample 886-28

Hand specimen

Coarse grained pyrite, chalcopyrite, sphalerite and galena vein type mineralization hosted by massive quartz (50%).

Polished thin section

Large grains of pyrite, chalcopyrite, sphalerite and galena typically displaying irregular embayed interlocking boundaries.

Pyrite occurs as subhedral grains (0.25 - 1mm) and larger anhedral fractured grains with the interstices filled with chalcopyrite or galena. Pyrite contains abundant inclusions of galena, especially near grain boundaries, even when isolated within sphalerite or chalcopyrite. Pyrite grains in galena possess complex ragged irregular boundaries. This texture is indicative of pyrite replacement by galena.

Galena occurs as large irregular grains enveloping pyrite, chalcopyrite and sphalerite. Sphalerite - chalcopyrite contacts commonly contain small grains of galena. Galena displays curved cleavage traces indicative of post mineralization deformation.

Chalcopyrite occurs as large moderately fractured grains hosting euhedral pyrite, sphalerite and gangue. Irregular blebs of cubanite (exsolution) are found in the centres of chalcopyrite grains.

Sphalerite occurs as large grains hosting abundant inclusions of chalcopyrite. In transmitted light the anhedral inclusions of chalcopyrite occur within individual grains of sphalerite. The inclusions appear to represent a replacement feature of sphalerite

by chalcopyrite rather than exsolution.

Fractures in sphalerite are typically filled with chalcopyrite and gangue.

The gangue consists entirely of large (to 8mm) strained quartz grains.

galena	25%
sphalerite	24%
chalcopyrite	20%
pyrite	10%
cubanite	1%
quartz	20%

Sample 886-88

Hand specimen

Coarse grained vein type sulphide containing only dark brown to black sphalerite in a vuggy quartz host.

Polished thin section

The sphalerite occurs as large (up to 30mm) irregular masses with fine intricate amoeboid contacts with the quartz gangue.

Patches of chalcopyrite inclusions (0.05mm) occur sporadically throughout the sphalerite. Occasional inclusions of anhedral pyrrhotite (0.01 - 0.05mm) occur throughout the sphalerite.

Minor pyrite inclusions are usually associated with the quartz gangue interstitial to the sphalerite. Rare small galena inclusions occur in sphalerite.

Large grains of strained quartz is the only gangue mineral except for fine grained chlorite filled fractures cross-cutting the gangue and sphalerite.

sphalerite	54%
chalcopyrite	2%
pyrrhotite	1%

pyrite	1%
galena	tr
quartz	40%
chlorite	2%

APPENDIX 4

X. R. D. ANALYSIS

ARGILLIC ALTERATION ZONE

X. R. D. ANALYSIS = ARGILLIC ALTERATION ZONE

Sample no / Drill hole / Depth	Q u a r t z	M/I u l s l c i o t v e i t e	K a o l i n i t e	C h l o r i t e	P y r i t e	G a l e n a	H i d a l g o i t e	J a r o s i t e	G o e t h i t e	S i d e r i t e	T a l c
88683 surface gossan	*	*					*	*	*		
88690 HD 2 28 m	*	*	*				*				
88697 HD 4 44 m	*	*	*				*				
88692 HD 9 131.3 m	*	*	*								
88658 HD 11 169 m		*	*	*			*				
88686 HD 11 169.1 m	*	*	*		*						
88665 HD 14 173.7 m	*		*	*	*	*	*				
88666 HD 14 176 m			*	*	*						
88671 HD 13 205.3 m	*	*		*	*		*				
88672 HD 13 213.2 m		*	*		*						
88694 HD 15 234 m	*	*		*	*		*			*	*
88644 HD 16 151.5 m			*	*	*		*				

APPENDIX 5

FLUID INCLUSION ANALYSIS

RESULTS OF FLUID INCLUSION ANALYSIS

Sample no. / Location	T _{fm} °C	T _m °C	Salinity wt% equivalent NaCl / CaCl ₂		T _h °C
886-27 HD13 241.4m Quartz primary	-25	-3.4	5.6	6.8	211.0
	-12	-2.8	4.6	5.7	234.7
	-26	-3.4	5.6	6.8	201.6
	-20	-2.6	4.3	5.1	194.4
	-20	-2.6	4.3	5.1	190.8
	-20	-2.4	4.0	4.8	190.1
	-15	-3.5	5.7	6.9	181.5
	-22	-2.6	4.3	5.1	187.5
	-12	-2.8	4.6	5.7	191.0
	-25	-3.2	5.2	6.3	163.3
	-24	-3.6	5.8	7.0	189.1
	886-22 HD12 230.7m Quartz primary	-15	-3.5	5.7	6.9
-15		-4.2	6.7	7.8	195.4
-13		-4.5	7.2	8.3	197.8
-23		-5.0	7.9	8.9	199.8
-20		-4.7	7.4	8.5	174.8
-20		-5.2	8.1	9.1	194.4
886-26 HD12 260.0m Quartz primary	-30	-1.3	2.2	2.5	203.4
	-30	-2.3	3.9	4.7	223.0
	-30	-1.9	3.2	3.9	196.4
	-30	-2.5	4.2	5.0	192.2
	-28	-2.6	4.3	5.1	193.6
	-32	-3.1	5.1	6.2	195.6
	-30	-1.8	3.1	3.8	199.4
886-49 HD10 401.0m Quartz primary					248.2
					297.3
					288.9
					290.6
	-20	-2.8	4.6	5.7	291.0
	-20	-3.2	5.2	6.3	299.5
					285.0
					262.4
					276.2
	-10	-5.5	8.5	9.5	266.0
	-5.4	8.4	9.4	252.2	
886-73 HD13 244.3m Sphalerite primary		-3.4	5.6	6.8	
		-2.7	4.5	5.3	170.9
		-2.1	3.5	4.3	
		-3.1	5.1	6.2	187.8
		-2.6	4.3	5.1	172.3
		-5.4	8.4	9.4	162.8

					190.8
					182.5
					189.5
					174.6
					164.0
					182.7
					179.1
	-23	-2.6	4.3	5.1	
	-31	-3.7	6.0	7.1	
	-27	-2.5	4.2	5.0	168.3
		-2.3	3.9	4.7	
		-1.4	2.4	3.0	164.8
	-18	-5.4	8.4	9.4	167.5
		-2.8	4.6	5.7	175.5
886-73 HD13 244.3m					137.3
Sphalerite secondary					136.4
					140.3
		-2.3	3.9	4.7	136.6
					132.5
					139.1
					141.2
886-73 HD13 244.3m	-18	-3.6	5.8	7.0	158.9
Quartz primary	-15	-2.6	4.3	5.1	160.0
		-3.2	5.2	6.3	168.8
					169.5
					204.5
					173.7
					186.6
					163.2
886-68 HD14 217.3m	-15	-3.7	6.0	7.1	179.4
Quartz primary	-16	-4.0	6.4	7.6	181.0
					182.4
					184.0
					188.7
886-67 HD14 191.1m	-15	-2.6	4.3	5.1	
Quartz primary					322.4
					321.8
					356.9
					223.6
					240.4
					242.5
					257.2
886-76 HD12 221.9m	-11	-3.8	6.1	7.3	
Quartz primary	-12	-4.2	6.7	7.8	
		-3.9	6.3	7.5	207.3
					204.7
					218.5
					258.0
					246.2
					211.6

886-62 HD10 400.0m	-20	-3.5	5.7	6.9	323.8
Quartz primary	-16	-3.9	6.3	7.5	350.8
					317.5
					346.0
					372.0
996-69 HD14 222.9m	-21	-4.2	6.7	7.8	205.2
Quartz primary					213.3
					200.1
					199.1
					188.0
		-3.7	6.0	7.1	203.0
					197.4

Tfm = First melt temperature

Tm = Final melt temperature

Th = Homogenization temperature.

FLUID INCLUSION ANALYSIS - APPARATUS AND METHOD

Doubly polished thin sections 0.2mm thick were prepared from suitable hand specimens and cemented onto glass slides. Fluid inclusions suitable for geothermometry were located using a Leitz Ortholux Pol-BK binocular microscope at 100x to 400x magnification. Selected inclusions were marked using a microscope mounted diamond cutter. The mineral sections were then removed from the glass slide by immersion in acetone for eight hours. The section was then broken into portions capable of being received by the heating - freezing stage.

A Reynolds heating - freezing stage made by Fluid Inc. USA, attached to a Leitz SM LUX-POL binocular microscope with a 100x to 320x magnification capability was used for microthermometry. Temperature values to one tenth of a degree celsius were recorded on a Fluid Inc. 410A Trendicator. The cooling capability is produced by liquid nitrogen stored in a large pressurized dewar containing a copper heat exchange coil linked to the stage by an insulated flexible conduit.

During the freezing run, a sample was cooled rapidly by passing chilled nitrogen gas, or liquid nitrogen through the stage until the fluid phase of the inclusion was completely frozen. The inclusion was then warmed at a rate controlled by the flow of cold nitrogen and an electrical heating element. A heating rate of about 0.5°C or less per minute was maintained close to the first melt temperature until after final melting to allow for thermal equilibration of the stage, sample and temperature sensor. In most cases at least two freezing runs were performed in order to check experimental precision.

The samples were allowed to equilibrate to approximately room temperature after freezing. Heating was achieved by passing air

across an integral electrical element in the stage into the sample chamber. Heating rates were reduced to about 1°C per minute close to the homogenization temperature. At least two runs on each fluid inclusion were made. All inclusions were observed as they cooled after homogenization. Results of any fluid inclusions that did not recover a vapour phase on cooling were rejected.

The calculation of wt% NaCl equivalent from the final melting temperature was carried out using the least squares regression method described by Robert et al. (1978).

$$W_s = 0.00 + 1.76958\theta - 4.2384 \times 10^{-2}\theta^2 + 5.2778 \times 10^{-4}\theta^3 \quad +/- \quad 0.028$$

W_s = weight % NaCl equivalent

θ = final melting point

The wt% CaCl₂ equivalent value was calculated using the graph from Crawford (1981).

APPENDIX 6

SULPHUR ISOTOPE ANALYSIS

SULPHUR ISOTOPE ANALYSIS RESULTS

Sample/type 886-	Co-existing Mineral Pairs			
	Sphalerite	/ Galena	/ Pyrite	/ Chalco.
$\delta^{34}\text{S}$ per mil				
28 v	11.7			
69 m	12.0	11.2	10.9	
103 m	9.9		6.7	
21 v	12.0	9.9	11.8	11.5
70 m	10.5			
88 v	10.8			
45 m	11.8		10.1	
46 v	11.4	9.9	12.0	
82 m			2.2	
47 v	11.3	9.7	11.9	
79 v		7.7		
83 C			-11.1	
83 B			-20.9	
68 v	9.9	8.1		

v = Vein type sulphide

m = massive type sulphide

C = pyrite concretion from siltstone - slate beds

B = pyrite band from siltstone - slate beds

SULPHUR ISOTOPE ANALYSIS - PROCEDURE

Vein type sulphide drill-core samples were selected which contained sulphides coarse enough to be extracted with a dental drill. Only minerals which display common grain boundaries were sampled.

The fine grained massive type sulphide minerals were crushed and then separated using a Superpanner and a Frantz Isodynamic Magnetic Separator.

The mineral sample concentrates were used to obtain a sample of pure SO₂ from which the S isotope ratios were measured on a Micromass 602E Mass Spectrometer. The SO₂ was obtained according to the method of Robinson and Kusakabe (1975) by burning the accurately weighed out sample with Cu₂O in a ceramic boat at 950°C for 12 minutes under vacuum. Non-condensables were removed by freezing the gas in liquid nitrogen. H₂O and CO₂ were removed by selective freezing of the gases with an acetone / liquid nitrogen and a n-pentane / liquid nitrogen slurry trap respectively.

The ratio of ³⁴S / ³²S measured on the mass spectrometer is then compared to that of the international standard - the Canyon Diablo troilite. The results are expressed in per mil (‰) values.

$$\delta^{34}\text{S} (\text{‰}) = \frac{{}^{34}\text{S} / {}^{32}\text{S} \text{ sample} - {}^{34}\text{S} / {}^{32}\text{S} \text{ standard}}{{}^{34}\text{S} / {}^{32}\text{S} \text{ standard}} \times 1000$$

mineral	sample weight
pyrite	10mg
chalcopyrite	15mg
sphalerite	15mg
galena	40mg

APPENDIX 7

CHLORITE DATA

ELECTRON MICROPROBE ANALYSIS - CHLORITE

Sample no. 886-	Oxide wt%								Total
	SiO ₂	TiO ₂	Al ₂ O ₃	FeO	MnO	MgO	Na ₂ O	K ₂ O	
74	24.33	-	20.48	25.79	0.30	14.66	-	-	85.56
	24.60	-	20.86	28.52	0.19	12.84	-	-	87.07
	24.61	-	20.35	28.11	0.27	13.37	0.18	-	87.16
	23.99	-	20.71	29.03	0.30	12.29	-	-	86.31
81	24.81	-	20.01	21.63	0.31	16.92	-	-	83.68
	25.51	-	20.61	21.72	0.38	17.23	-	-	85.46
99	24.28	0.13	20.51	30.89	0.29	10.14	-	-	86.38
	23.78	-	20.02	32.01	0.28	10.84	-	-	86.93
45	23.67	-	20.95	28.86	0.14	12.10	-	-	85.72
	25.23	-	21.25	27.44	-	10.80	0.27	0.92	85.91
	23.83	-	20.32	32.69	-	10.13	-	-	86.97

CHLORITE SOLID SOLUTION MODEL - RESULTS

Sample no.	Temperature °C	Log fO ₂	Log fS ₂
886-74	299.6	-31.9	-10.08
	288.9	-33.6	-10.97
	290.1	-33.4	-10.87
	298.1	-32.7	-10.53
886-81	283.5	-32.8	-10.44
886-99	228.3	-42.5	-15.88
	298.4	-33.4	-10.89
886-45	302.6	-32.2	-10.28
	243.4	-39.7	-14.05
	235.1	-41.9	-15.63

APPENDIX 8

ELECTRON MICROPROBE ANALYSIS

-SPHALERITE-

ELECTRON MICROPROBE ANALYSES OF SPHALERITE

Sample no.	Element	wt%	atom fraction	mole % FeS	
886-					
28 v	Fe	4.68	0.041	8.5	
	S	32.64	0.484		
	Zn	62.48	0.464		
	As	0.21	0.001		
	total	99.91	1.000		
28 v	Fe	4.79	0.041	8.3	
	S	32.78	0.493		
	Zn	62.83	0.464		
	As	0.30	0.002		
	total	99.89	1.000		
28 v	Fe	5.42	0.047	9.5	
	S	32.59	0.494		
	Zn	61.83	0.459		
	total	99.84	1.000		
45 m	Fe	7.19	0.062	12.5	
	S	32.74	0.494		
rim 1	Zn	59.64	0.442		
	Cu	0.15	0.001		
	Co	0.13	0.001		
	total	99.85	1.000		
t r a v e r s e	2	Fe	7.17	0.062	12.5
		S	32.85	0.495	
		Zn	59.84	0.442	
		Co	0.14	0.001	
		total	100.00	1.000	
	3	Fe	7.02	0.060	12.0
		S	33.05	0.498	
		Zn	59.94	0.442	
		total	100.01	1.000	
	4	Fe	5.93	0.051	10.3
		S	32.77	0.495	
		Zn	61.30	0.454	
		total	100.00	1.000	
core 5	Fe	3.70	0.031	6.2	
	S	33.71	0.504		
	Zn	63.42	0.465		
	total	100.83	1.000		

t r a v e r s e	45 m	Fe	7.12	0.062	12.5
	rim 1	S	32.89	0.495	
		Zn	59.99	0.446	
		total	100.00	1.000	
	2	Fe	6.46	0.056	11.2
		S	33.09	0.498	
		Zn	60.45	0.446	
		total	100.00	1.000	
	3	Fe	6.44	0.056	11.3
		S	32.84	0.495	
	Zn	60.71	0.449		
	total	99.99	1.000		
core 4	Fe	4.02	0.035	7.0	
	S	32.81	0.497		
	Zn	63.07	0.468		
	total	99.90	1.000		
88 v	Fe	7.00	0.061	12.4	
	S	32.72	0.493		
	Zn	60.28	0.446		
	total	100.00	1.000		
88 v	Fe	6.99	0.061	12.4	
	S	32.59	0.492		
	Zn	60.03	0.447		
	total	99.88	1.000		
88 v	Fe	7.44	0.064	13.1	
	S	32.42	0.489		
	Zn	60.35	0.447		
	total	100.21	1.000		
99 m	Fe	8.31	0.072	14.7	
rim 1	S	32.50	0.491		
	Zn	59.07	0.437		
	total	99.88	1.000		
t r a v e r s e	2	Fe	6.56	0.057	11.6
		S	32.46	0.491	
		Zn	60.99	0.452	
		total	100.01	1.000	
	3	Fe	3.41	0.030	6.2

	S	32.13	0.488	
	Zn	64.67	0.482	
	total	100.21	1.000	
core 4	Fe	1.34	0.012	2.4
	S	32.14	0.490	
	Zn	66.36	0.497	
	Co	0.16	0.001	
	total	100.00	1.000	
81 m	Fe	5.42	0.047	9.5
	S	32.38	0.491	
	Zn	61.93	0.461	
	Co	0.13	0.001	
	total	99.86	1.000	
73 v	Fe	1.45	0.013	2.6
	S	32.35	0.492	
	Zn	65.82	0.494	
	Cu	0.21	0.002	
		99.83	1.000	

v = vein type sulphide

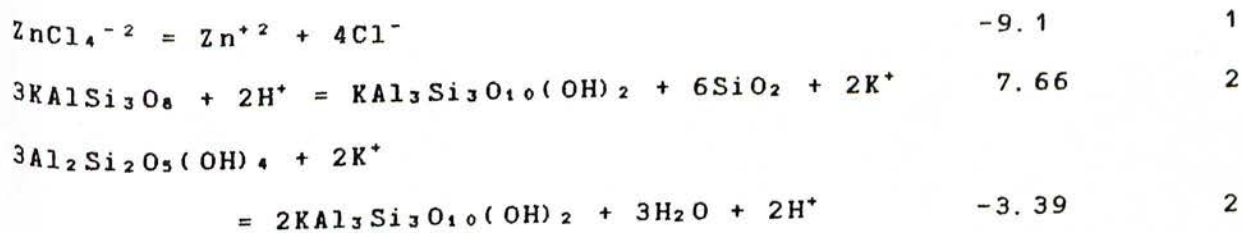
m = massive type sulphide

APPENDIX 9

THERMODYNAMIC EQUATIONS

LOG EQUILIBRIUM CONSTANTS USED IN FIGURES 15, 16 AND 17.

Reaction Equation	Log K (325°C)	Ref
$H_2S = H^+ + HS^-$	-8.61	1
$HS^- = H^+ + S^{-2}$	-11.91	1
$H_2S + 2O_2 = HSO_4^- + H^+$	49.71	1
$HSO_4^- = H^+ + SO_4^{-2}$	-6.08	1
$H_2S + 2O_{2g} = 2H^+ + SO_4^{-2}$	43.64	1
$H_2S + 2O_{2g} = 0.5S_{2g} + H_2O$	12.87	1
$2FeS + S_{2g} = 2FeS_2$	9.93	1
$4FeS + 3H_2S + 2H^+ + SO_4^{-2} = 4FeS_2 + 4H_2O$	27.70	1
$4Fe_3O_4 + O_{2g} = 6Fe_2O_3$	28.23	1
$8Fe_3O_4 + 2H^+ + SO_4^{-2} = 12Fe_2O_3 + H_2S$	12.82	1
$3Fe_3O_4 + S_{2g} = FeS_2 + 4Fe_2O_3$	7.89	
$6Fe_3O_4 + 3H_2S + 2H^+ + SO_4^{-2} = 2FeS_2 + 8Fe_2O_3 + 4H_2O$	23.63	1
$4Fe_2O_3 + 15H_2S + SO_4^{-2} + 2H^+ = 8FeS_2 + 16H_2O$	56.07	1
$2Fe_3O_4 + 11H_2S + 2H^+ + SO_4^{-2} = 6FeS_2 + 12H_2O$	45.21	1
$5CuFeS_2 + S_{2g} = Cu_5FeS_4 + 4FeS_2$	5.98	1
$10CuFeS_2 + 3H_2S + 2H^+ + SO_4^{-2}$ $= 2Cu_5FeS_4 + 8FeS_2 + 4H_2O$	19.84	1
$CuCl = Cu^+ + Cl^-$	-2.45	1
$CuFeS_2 + H^+ + 0.5O_{2g} = FeS_2 + Cu^+ + 0.5H_2O$	5.25	1
$8CuFeS_2 + 10H^+ + SO_4^{-2}$ $= 8FeS_2 + H_2S + 8Cu^+ + 4H_2O$	-1.65	1
$8Cu_5FeS_4 + 42H^+ + SO_4^{-2}$ $= 8FeS_2 + 17H_2S + 40Cu^+ + 4H_2O$	-87.5	1
$ZnCl^+ = Zn^{+2} + Cl^-$	-6.5	1
$ZnCl_2 = Zn^{+2} + 2Cl^-$	-7.5	1
$ZnCl_3^- = Zn^{+2} + 3Cl^-$	-8.4	1



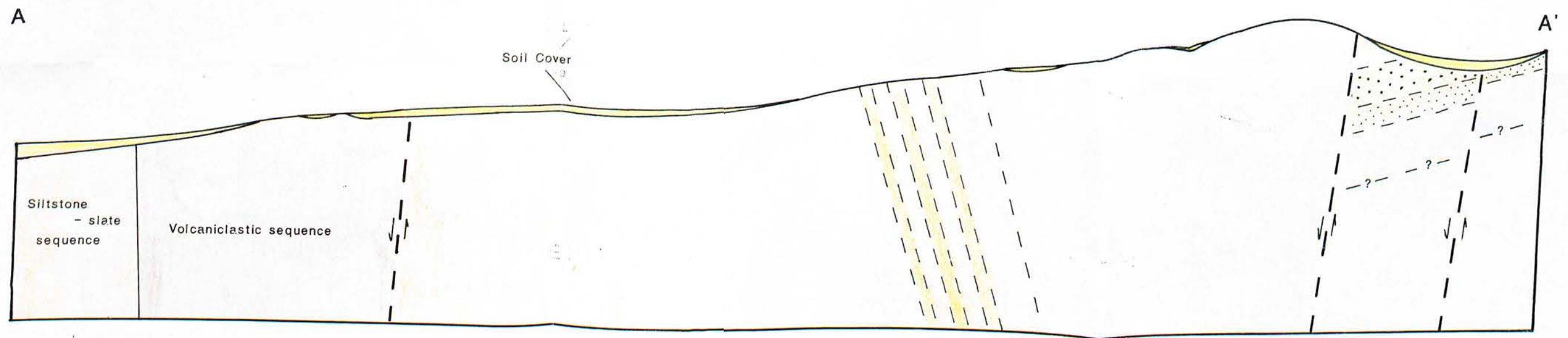
Ref

1 = Ohmoto et al., 1983

2 = Pisutha - Arnon and Ohmoto., 1983

FIGURE 4

INTERPRETIVE CROSS - SECTIONS (GEOLOGICAL MAP - FIGURE 3)



(Legend - as for figure 3)

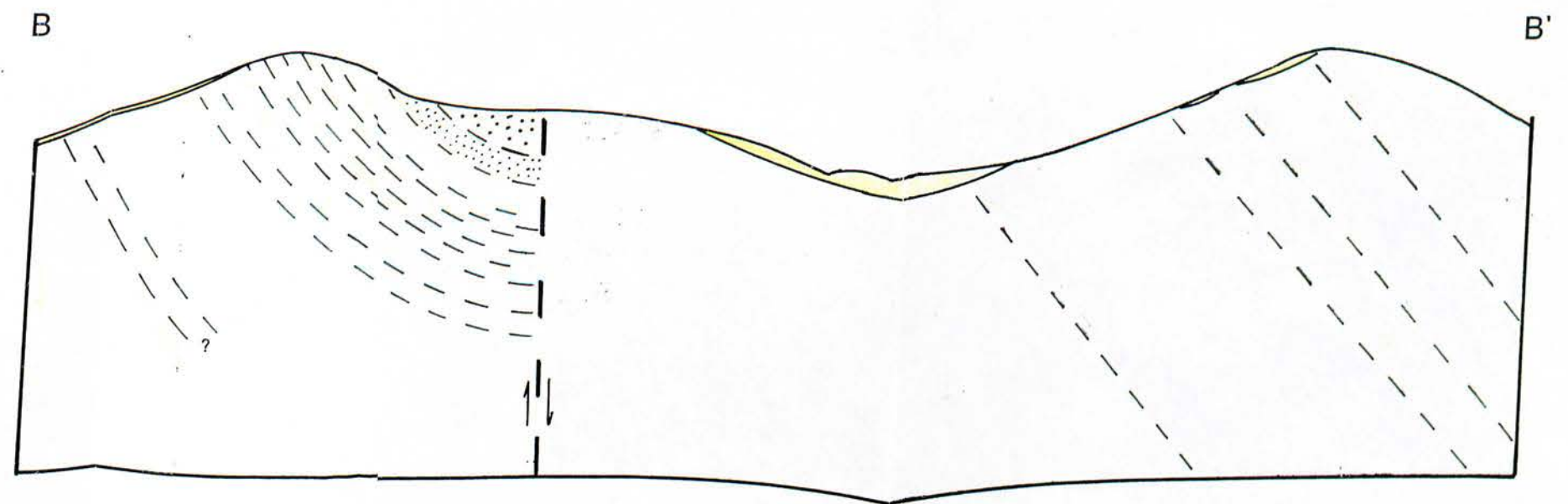
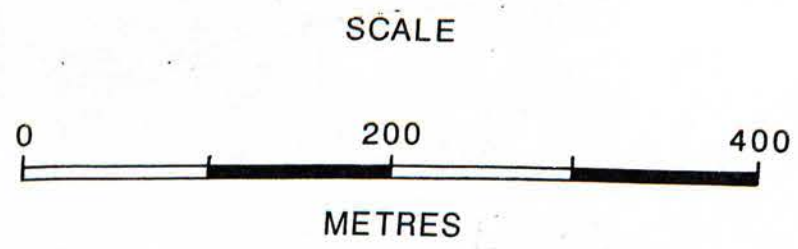
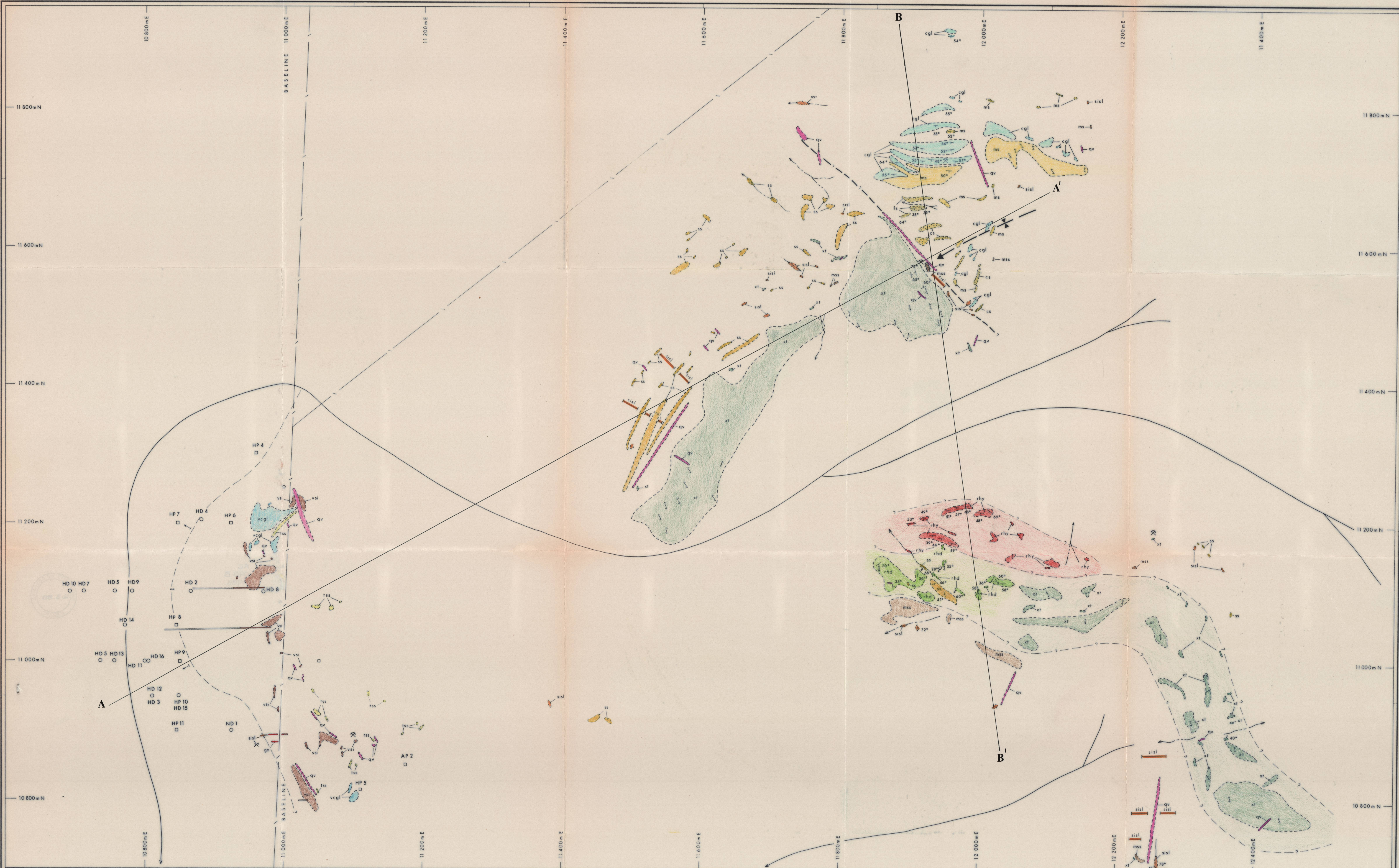


FIGURE 4



MOUNT HOPE GROUP
MOUNT KENNAN VOLCANICS

SILTSTONE SLATE SEQUENCE

- Thinly laminated siltstone and slate
- Massive silicified siltstone
- Sandstone

VOLCANICLASTIC SEQUENCE

- Sericitized and silicified siltstone containing feldspar phenoclasts
- Conglomerate. Clasts of siltstone and fine sandstone to 40mm in a silicified silty matrix
- Tuffaceous sandstone. Poorly sorted quartz sandstone, phenoclasts of quartz and feldspar

LOWER DEVONIAN LOCHKOVIAN

- GOSSAN
- QUARTZ VEIN

PYROCLASTICS

- Crystal and lithic crystal tuff of rhyolitic to rhyodacitic composition

AMYGDALOIDAL RHYODACITE

- Contains interbeds of flow banded rhyolite

FLOW BANDED RHYOLITE

CONGLOMERATIC SANDSTONE SEQUENCE

- Fine grained sandstone
- Medium grained sandstone
- Coarse grained sandstone
- Polymict conglomerate. Predominantly massive quartz clasts and lesser fine sandstone and siltstone clasts to 150mm in a muddy lithic arenite matrix. Graded bedding.

LOWER DEVONIAN LOCHKOVIAN

Outcrop boundary
 Established boundary
 Established boundary - position approx.
 Inferred boundary
 Bedding - strike and dip, vertical
 Schistosity - strike and dip
 Flow lineation - direction and plunge
 Flow banding - strike and plunge
 Surface rubble
 Fold axis - anticline, syncline, plunge
 Fault - inferred
 Facing direction
 Trench
 Pit

DRILLING

- HP □ Percussion drill hole - Homestake
- HD ○ Diamond drill hole - Homestake
- ND ○ Diamond drill hole - Newmont

TOPOGRAPHIC

- Fence
- Drainage channel

TW MN
 GN
 31.5°

HOMESTAKE AUSTRALIA LIMITED

MOUNT HOPE PROJECT
 NEW SOUTH WALES

WAGGA TANK PROSPECT
GEOLOGICAL INTERPRETATION

Revised	Date	Author	Date	Sheet No	Drawing No
		S. Ryan	Sept. 1987		MH 165
Plan Index	Drawn	Geodrafting	Scale	FIGURE 3	
			1:2500		